DETERMINATION OF PRESSURE LOSS AND DISCHARGE COEFFICIENTS FOR NON-NEWTONIAN FLUIDS IN LONG SQUARE-EDGED ORIFICES

by

M.R.CHOWDHURY
BTech: Chemical Engineering

Dissertation submitted in fulfilment of requirements for the degree
MTech: Chemical Engineering

in the FACULTY OF ENGINEERING

at the CAPE PENINSULA UNIVERSITY OF TECHNOLOGY

Supervisor: Dr V.G. Fester

Cape Town Campus
July 2010

DECLARATION

I, M.R.Chowdhury, declare that the contents of this thesis represent my own unaided work, and that the thesis has not previously been submitted for academic examination towards any qualification. Furthermore, it represents my own opinions and not necessarily those of the Cape Peninsula University of Technology.

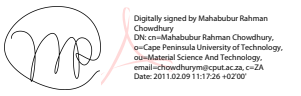

Signed Date

Determination of pressure loss and discharge coefficients for non-Newtonian fluids in long square-edged orifices

M.R.Chowdhury

ABSTRACT

Loss characteristics of three sharp square-edged orifices are studied in laminar to turbulent flow régime ($1 \leq Re_{MR} \leq 100000$) to meet the scarcity of experimental data in the open literature. Experiments were conducted at CPUT on orifices having β ratios of 0.36, 0.5 and 0.7 with varying aspect ratios. Water was used to calibrate the test rig to ensure measurement accuracy and also to acquire turbulent régime pressure drop data. Carboxymethyl cellulose (CMC) and kaolin of different concentrations were used to obtain non-Newtonian laminar flow loss coefficient data. A tube viscometer with three different pipe diameters was used to determine the rheological properties of the fluids. The hydraulic grade line method was used to evaluate pressure drop data. Flange tapping methods were used to measure C_d data. Sufficient pipe length was given for the flow to be fully developed before measuring pressure drop. An average K_{or} value of 76, 17.7 and 2.33 were found for 0.36, 0.5 and 0.7 diameter ratio orifices respectively in the turbulent régime. The results obtained may be reliably extrapolated to higher Reynolds numbers. The laminar flow loss coefficient, C_{or}, data is presented as a function of Re_{MR} and is $3300Re_{MR}^{-1}$, $1500Re_{MR}^{-1}$ and $800Re_{MR}^{-1}$for β ratio of 0.36, 0.5 and 0.7 orifices respectively. Presentation of orifice loss coefficients against Re_{MR} indicates that as the beta ratio decreases orifice laminar loss coefficient increases. Discharge coefficient value of 0.79 and 0.8 was found for 0.5 and 0.7 diameter ratio orifice in turbulent flow régime which agrees well with a model published by Hall. An empirical correlation for predicting pressure loss coefficients in laminar – turbulent flow régime was derived using 500 data points. This correlation can be successfully used by design engineers to design fluid flow loops in several hydraulic applications. In addition, this work provided reliable experimental loss coefficient data that showed the models published by Ward – Smith (1971) and Idel'chik et al.,(1994) can be extended to turbulent flow Reynolds number ranges less than 10000 depending on β and aspect ratios.

DEDICATION

To my Father: - For all the love you gave me in the short time before you left for eternity
To my Mother: - The pillar of my strength; for always being supportive, understanding and all the unconditional love you have given me
To my eldest sister: - For all your support through the rough times in my life
To my brother in law: - For all your financial support
To my younger brothers: - This work might encourage you to pursue higher studies

With love to all of you

"Do not acquire knowledge in order to vie with scholars, and to wrangle with the foolish, and to sit in the best seats: Whoever does that, his abode will be the Fire, the Fire"- ***Prophet Mohammed S.A.A.W (P.B.U).***

"We must not forget that when radium was discovered no one knew that it would prove useful in hospitals. The work was one of pure science. And this is a proof that scientific work must not be considered from the point of view of the direct usefulness of it. It must be done for itself, for the beauty of science, and then there is always the chance that a scientific discovery may become like the radium a benefit for mankind"- ***Marie Curie***

*"Wealth can be earned by lot of people but very few people are lucky enough to earn knowledge, so always try to make yourself one of those lucky persons"-****My Mother***

ACKNOWLEDGEMENTS

The All Mighty ALLAH - For giving me the strength and courage to pursue higher degree

Dr.Veruscha Fester - For her excellent supervisory role and her support throughout the process of completing the dissertation

A. Kabwe Mume - For his wise advice in various situations

Prof. Rainer Haldenwang - For always encouraging me and being supportive

Richard du Toit - For his splendid laboratory supervisor role

Alwyn Bester - For his technical assistance throughout the project

Elizma Alberts - For always going an extra mile to help me with official matters

Angelo Opperman - For his assistance with IT related matter

Butteur Mulumba - For being an excellent colleague with whom to work

All other staff of the Material Science and Technology group who somehow contributed to this work

Dr. Ntwampe - For his advice and inspiration for science and research

The financial assistance of the Cape Peninsula University of Technology towards the research is acknowledged. Opinions expressed in this thesis and the conclusions arrived at are those of the author and not necessarily attributable to the Cape Peninsula University of Technology

TERMS AND CONCEPTS CITED

β **Ratio:**	This term is used to describe the ratio between the orifice bore and pipe diameter.
Orifice plate:	Is a device used to measure the flow rates of fluids or to restrict flow. It is basically a thin plate with a hole in the middle.
Short orifice:	Defined as a category of orifice plate in which flow reattachment on the orifice wall does not occur.
Long orifice:	An orifice in which, the jet formed downstream of the orifice entry tends to re attach to the orifice wall is defined as a long or thick orifice.
Velocity profile:	The velocity y profile represents an instantaneous velocity distribution across the pipe diameter.
Entry length:	Is the length required for the fluid to develop a steady distance-independent velocity profile inside a contraction or die or conduit.
Vena contracta:	Is the point in a fluid stream where the cross sectional area is the least.
Laminar flow:	Nonturbulent streamline flow in parallel layers.
Turbulent flow:	Flow in which the velocity at any point varies erratically.
Transition:	The region or process acting between the laminar and turbulent flow regimes.
Newtonian fluid:	Any fluid that has a directly proportional relationship between shear stress and shear rate. Water is an example of a Newtonian fluid.
Reynolds number:	The ratio between viscous and inertial forces is proportional to the Reynolds number. The number is expressed in terms of the density, velocity, characteristic length and the viscosity of the fluid. This number is also used to define whether a fluid is laminar or turbulent.
Viscosity:	A measure of the resistance to flow of a fluid under an applied force.

Transducer: A device that converts one type of energy to another, or responds to a physical parameter. A transducer is, in its fundamental form, a passive component. If the component is electrical, it generally has two electrical terminals.

Friction factor: Is a dimensionless number usually used in fluid flow calculations.

Shear Stress: Shear stress is a stress state where the shape of a material tends to change (usually by "sliding" forces – torque by transversely-acting forces) without particular volume change.

Loss coefficient: Is defined as the non-dimensionalized difference in total pressure between the extreme ends of two long straight pipes when there is a zero loss component between the two pipes and when the real fitting is installed.

Discharge coefficient: Discharge coefficient for an orifice plate can be defined as the ratio between the actual and theoretical volumetric flow rate

TABLE OF CONTENTS

LIST OF FIGURES

LIST OF TABLES

LIST OF SYMBOLS

Notation	Description	Unit
A	Length from upstream fitting to orifice plate	m
A_1	Pipe cross sectional area	m^2
A_2	Orifice cross sectional area	m^2
A_{vc}	Area of *vena contracta*	m
a	Diameter of a single tapping or width of annular slot	m
b	Internal diameter of carrier ring	m
C	Length from straightening vanes to orifice plate	m
C'	Length from upstream fitting to straightening vanes	m
C_c	Contraction coefficient	-
C_d	Discharge coefficient	-
C_{or}	Orifice laminar flow loss coefficient	-
C_v	Velocity coefficient	-
D	Pipe diameter	m
d	Orifice bore diameter	m
E	Total energy per unit mass	J/kg
E	Error function equation 2.25	-
E_u	Euler function	-
e_{cl}	Longitudinal eccentricity	-
e_{cn}	Perpendicular eccentricity	-
f	Friction loss coefficient	-
G	Elasticity modulus	-
g	Gravitational constant	m/s^2
H	Total head loss of the system	m
k	Pipe roughness	-
K_{or}	Orifice loss coefficient	-
K	Fluid consistency index	$Pa.s^n$
K'	Apparent fluid consistency index	$Pa.s^n$
L	Length of the pipe	m
L_e	Equivalent length	m
L_{s2x}	Downstream reattachment length	m
l_e	Edge chamfer length	m

l_1	Distance between upstream pressure tap Centreline and upstream orifice face	m
l_2	Distance between downstream pressure tap centre line and upstream orifice face	m
l_2'	Distance between downstream pressure tap centre line and downstream orifice face	m
M_w	Mass of water	kg
m	Mass	kg
m_1	Upstream slope of the fitting	-
m_2	Downstream slope of the fitting	-
n	Flow behaviour index	-
n'	Apparent flow behaviour index	-
P	Pressure	Pa
P_v	Vapour Pressure	Pa
Q	Volumetric flow rate	m^3/s
R	Pipe radius	m
RD	Relative density	-
Re	Reynolds number	-
Re_D	Pipe Reynolds number	-
Re_d	Orifice Reynolds number	-
Re_{ge}	Generalized Reynolds number	-
Re_{MR}	Metzner & Reeds Reynolds number	-
Re_s	Slatter Reynolds number	-
r	Plug radius	m
T	Time	s
t	Orifice plate bore thickness	m
t*	Orifice plate thickness	m
t/d	Aspect ratio	-
U	Axial local fluid velocity	m/s
U_{cl}	Axial local centreline velocity	m/s
U_{max}	Maximum velocity	m/s
U_{plug}	Plug velocity	m/s
V_{mean}	Fluid mean velocity	m/s
V_*	Kinematic viscosity	m^2/s

X	Data point in a population	-
Z	Height of the pie centre-line above datum	m

GREEK SYMBOLS

Notation	Description	Unit
α	Porosity	-
β	Diameter ratio	-
$\dot{\gamma}$	Shear rate	1/s
ΔP	Measured pressure drop	Pa
δ	Boundary layer thickness	m
δ^*	Boundary layer displacement thickness	m
μ	Dynamic viscosity	Pa.s
μ_{ge}	Generalized viscosity	Pa.s
μ_{re}	Relative viscosity	-
μ_n	Newtonian viscosity	Pa.s
μ_r	Ratio of actual to reference viscosity	-
ν	Fluid kinematic viscosity	m^2/s
ρ	Fluid density	Kg/m^3
σ	Standard deviation	-
τ	Empirical constant	-
τ	Shear stress	Pa
τ_y	Yield stress	Pa
ϕ	Edge chamfer angle	Degree
φ	Back bevel angle	Degree

CHAPTER 1

1.1 Introduction

Use of an orifice meter as a flow metering device is part of traditional hydraulics. The effect of macroscopic local disturbances in pipe flow because of orifices and pipe fittings has received the attention of several researchers (Lakshmana Rao & Sridharan, 1972). The main momentum to the problem arose from the needs of flow metering, choking etc. Beside the metering characteristic, knowledge of the excess loss caused by disturbances and the settling length downstream became of considerable engineering interest (Lakshmana Rao & Sridharan, 1972). Experimental and numerical methods have been used to study flow through orifices in various engineering applications, such as cooling holes, fuel lines, hydraulic systems, air conditioning systems, and water pipe systems in more recent years (Coulson & Richardson, 1990). Although data on pressure loss and discharge coefficients are still actively generated in these areas, there remains a lack of loss coefficient data for design engineers in the open literature.

Accurate non-Newtonian loss coefficient data has great importance in predicting energy loss during the design of pipe lines and process plants, where fluids involved may exhibit non-Newtonian behaviour. Sharp-edged cylindrical orifices are used for metering flows and also to inject liquid fuels into combustion chambers at high velocity. Sharp-edged orifices are preferred over other shaped orifices for different applications (Ramamurthi & Nandakumar, 1999). Most pressure loss data found for long square-edged orifices in the open literature is based on Newtonian fluids. In this work the characteristics of long square-edged orifices are investigated.

1.2 Problem statement

Deficiencies for certain orifice geometry and flow condition ranges remain, although considerable research has been under taken in the area. Experimentally determined pressure loss and discharge coefficient data for long square-edged orifices are scarce in the public domain, especially in the laminar flow régime. Data available in open literature is typically for the turbulent flow régime. The majority of experimental work was conducted using Newtonian fluids with little work executed on long square-edged orifice

plates using non-Newtonian fluids. A correlation for predicting pressure loss coefficients in laminar to turbulent régime is non-existent to engineers involved in hydraulic application design purposes. Hence, there is a need for accurate non-Newtonian pressure loss coefficient data and a correlation applicable from laminar to turbulent flow régimes for energy efficient process plants and in the design of hydraulic applications.

1.3 Aim and objectives

The objectives of this project were:

- To provide both discharge coefficient and pressure loss coefficient data for long square-edged orifices with β ratios of 0.36, 0.5 and 0.7 and aspect ratios of 4, 5 and 5 respectively.
- To develop a correlation to predict pressure losses through long square-edged orifices in the laminar to turbulent flow régime.

1.4 Methodology

Experiments were conducted on a test rig in the slurry laboratory at the Cape Peninsula University of Technology (Cape Town campus) using a 46 mm (ID) straight, clear pipe. Long square-edged orifices with different β and aspect ratios were used and pressure losses and discharge coefficients associated with such orifices were measured.

The hydraulic gradient line method was used to determine pressure drop across the orifice. The flange tapping arrangement was used to measure the discharge coefficient. Tube viscometry was employed to determine the rheological parameters of the non-Newtonian fluids; three pipe sizes were used to evaluate the possible existence of wall slip.

A Newtonian fluid (water) was used to calibrate the test rig. Pressure drop measurements were conducted using 11 pressure tappings ranging from 0.5D to 110D upstream and 0.5D to 200D downstream of the orifice plate. The non-Newtonian fluids tested were carboxymethyl cellulose and kaolin at different concentrations. Carboxymethyl cellulose was prepared at concentrations of 4, 5, 7 and 8% (w/w) with rheological parameters

ranging from 0.436 ≤ K' ≤ 8.3 and 0.746 ≥ n' ≥ 0.6. Kaolin was prepared at concentrations of 8, 14 and 20% (v/v) with rheological parameters ranging from 0.06 ≤ K' ≤ 16 and 0.15 ≤ n' ≤ 0.5. The range of concentrations of CMC tested in this work was sufficiently low to exclude time-dependant effects.

Results were expressed in terms of loss coefficient (k_{or}) against Reynolds number in the range of laminar to turbulent flow. The same method was used in presenting discharge coefficient data. Turbulence data was compared with the correlations available in literature. A new correlation was presented to predict pressure loss coefficient for long square-edged orifices from laminar to turbulent flow régimes.

1.5 Delineation of the study

This research was based on Newtonian and non-Newtonian fluids or slurries flowing through long square-edged orifice in the turbulent, transitional and laminar flow régimes. Only time independent non-Newtonian fluid behaviour was investigated in this research. The following areas were excluded from this study:

- Time dependent non-Newtonian fluid behaviour
- Thin or short orifices
- β < 0.3 and β > 0.75

1.6 Significance of research

This study has reported experimental pressure loss coefficient and discharge coefficient data for long square-edged orifices (β = 0.36, 0.5 and 0.7 and t/d = 4, 5 and 5 respectively) using non-Newtonian fluids to open literature for the first time. The correlation developed can be used for designing fluid flow loops for hydraulic applications.

CHAPTER 2

2.1 Introduction

The theory and literature on orifice head loss, flow through orifice and rheology are presented in Chapter 2. The definition, description of different types of orifices and purposes are outlined. Different rheological models are discussed. Flow through a straight pipe is reviewed. Correlations published by several researchers to predict head loss for flow through orifices are discussed. An overview of the methodology used to measure the discharge coefficient is also presented in this chapter.

2.2 Orifice

"Orifice plates are differential pressure producing devices which can be inserted into a pipeline of any shape and size and orientation of conduit" (Swamee, 2005). The characteristics of the flow through orifice plates depend mainly on the following parameters (ESDU, 2007):

- Orifice edge geometry;
- β ratio (orifice bore to pipe diameter ratio);
- Orifice thickness to bore diameter ratio and,
- Reynolds number.

A schematic diagram of a long square-edged orifice is presented in Figure 2.1

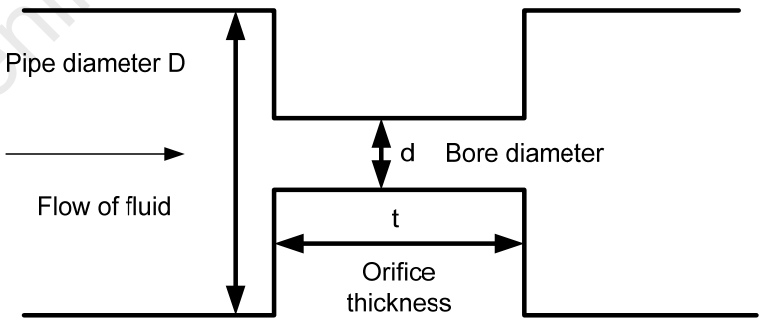

Figure 2.1 Schematic diagram of a long square-edged orifice

2.2.1 Application of orifice plates

Orifice plates have been used for many years as accepted devices for bulk flow measurement in a variety of industries (Morrison et al., 1990). Besides flow metering applications, orifice plates can be used in varying ways. Some of the orifice applications are presented (Nally, 2010):

- Creation of false head for centrifugal pump to operate close to the pumps best efficiency point or BEP;
- increase line pressure;
- decrease the flow through a line;
- increase fluid velocity in line;
- large orifice plates are used as an energy dissipater in flood conduits (Zhang & Chai, 1999) and,
- energy dissipater in slurry flow applications.

2.2.2 Advantages of orifice plates

Orifice plates possess several features. Some features are presented (Morrison et al., 1990):

- Reliable performance;
- low installation cost;
- wide regulatory acceptance;
- simplicity;
- suit different applications;
- well documented and,
- low maintenance cost.

2.2.3 Different orifice plate geometries

It is an experimentally proven fact that orifice geometry affects wall pressure distributions. An orifice installed as an energy dissipater is required to do so at a designed discharge. Sharp-edged and streamlined orifices can meet different energy dissipation requirements, but a large pressure drop can be expected. A compromise between the contraction ratio and the abruptness of transition helps to minimize the pressure drop (Zhang & Chai, 1999). There are many geometrically different types of

orifices. The different geometry of an orifice plate is mainly defined by using the following parameters (ESDU, 2007):

- Orifice plate bore diameter, d;
- orifice plate bore thickness, t;
- orifice plate thickness, t^*;
- porosity, α;
- back bevel angle, φ;
- orifice thickness to diameter ratio;
- entry edge profile such as square-edged, knife edged, bevelled, quadrant, chamfered, rounded with edge radius, r, chamfered edge with chamfer length, l_e and chamfer angle, ϕ and,
- exit edge profile such as square-edged, square back cut or back bevel with back bevel angle, φ.

Standard orifice plates typically have the following dimensions (ESDU, 2007):

- Back bevel angle, $\varphi = 45^\circ \pm 15^\circ$;
- high β ratios, 0.2 < β < 0.75;
- small t/d ratios for thin or short orifice, t/d < 0.01 and,
- edge radius of $r \leq 0.0004d$.

β ratio can be defined mathematically as:

$$\beta = \frac{d}{D} \qquad \text{Equation 2.1}$$

Porosity is expressed as:

$$\alpha = \frac{d^2}{D^2} \qquad \text{Equation 2.2}$$

According to IS0 5167, ASME MFC-3M and ANSI/API 2530 standard orifice plate bore thickness should be in the range:

- IS0 5167 and ASME MFC-3M $\longrightarrow$ $0.005D \leq t \leq 0.02d$ and,
- ANSI/API 2530 Largest $\longrightarrow$ $t \geq 0.01d$ or $t > 0.127$ mm

Smallest $\longrightarrow$ $t \le 0.02D$ or $t \le 0.125d$.

Standard plate thickness is specified by 1SO 5167 and ASME MFC-3M and it should be in the range of, $t \le t* \le 0.05D$. For a $50\ mm \le D \le 64\ mm$ pipe, an orifice plate thickness, t^*, of 3.2 mm is acceptable.

Figure 2.2 presents a schematic diagram of different orifice geometries.

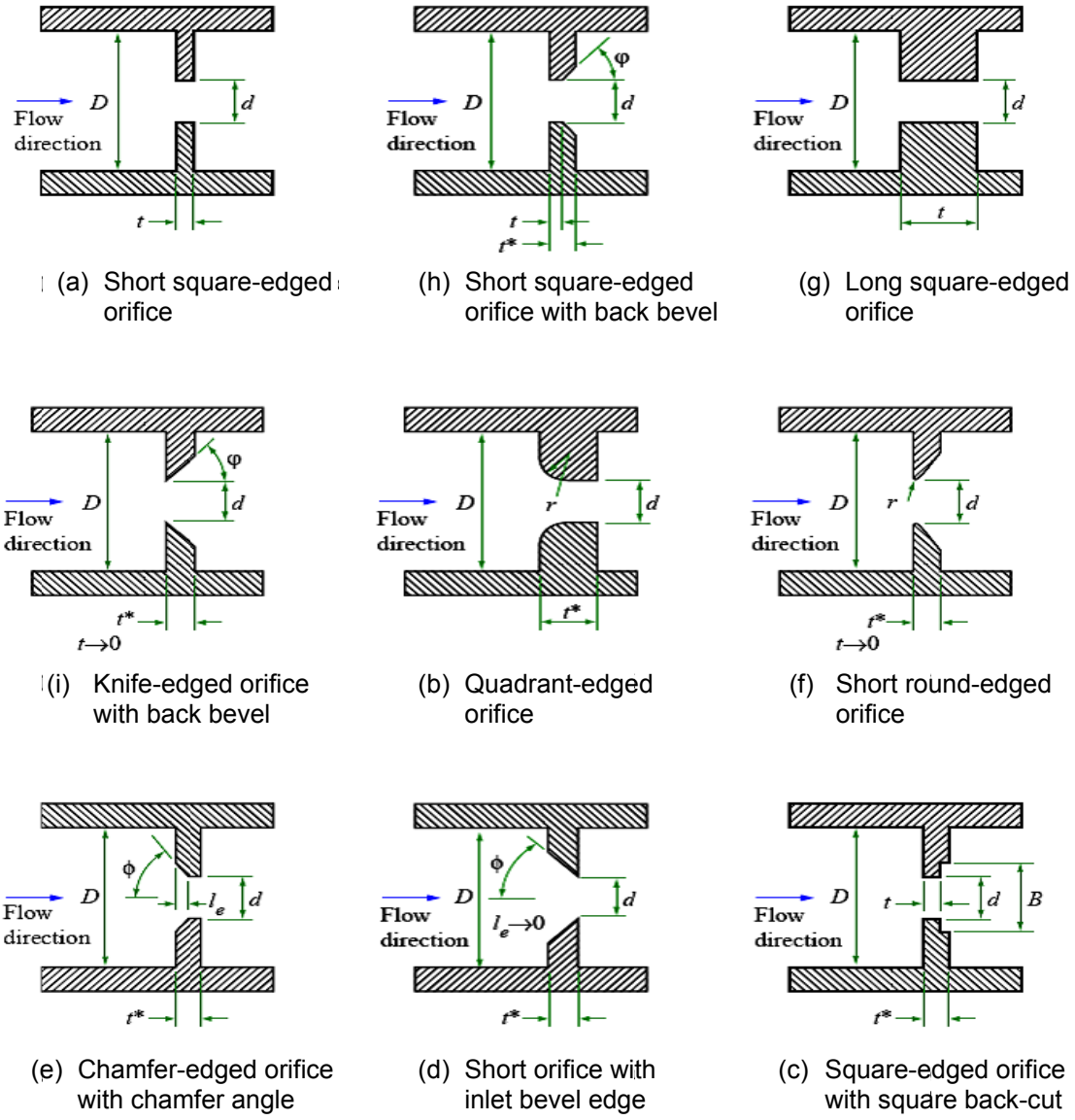

(a) Short square-edged orifice

(h) Short square-edged orifice with back bevel

(g) Long square-edged orifice

(i) Knife-edged orifice with back bevel

(b) Quadrant-edged orifice

(f) Short round-edged orifice

(e) Chamfer-edged orifice with chamfer angle

(d) Short orifice with inlet bevel edge

(c) Square-edged orifice with square back-cut

Figure 2.2 Different orifice plate geometry (ESDU, 2007)

2.2.4 Ideal flow condition

To ensure accurate flow rate data, discharge coefficient data and the pressure loss coefficient data an orifice plate must be operated under ideal conditions. This ideal flow condition is also known as the reference condition. The reference condition is intricate to achieve since different fittings are used in the pipe line upstream and downstream of the orifice plate. Distortions of the flow velocity profile are produced by fittings used in a pipe line which affects the pressure gradient upstream of the orifice plate, downstream of the orifice plate to a smaller extent and flow characteristics through the orifice plate. Flow through an orifice is recognized as ideal if the flow has the following features (ESDU, 2007):

- Axisymmetric;
- fully developed;
- swirl free;
- steady flow with no cross-flow upstream and downstream of the orifice plate and,
- no interference with other components.

Such conditions are achieved by allowing sufficient length of pipe upstream and downstream of the orifice. The minimum length of pipe required for the flow to be fully developed depends on the β ratio, as the required pipe length increases with the increase in β ratio (ANSI/API 2530, 1995). Normally a 50D length is considered sufficient for the flow to be fully developed (Samanta et al., 1999). It was suggested that for a β ratio of 0.75 at least 22D pipe length is required for turbulent flow even while no upstream disturbances were present (Prabu et al., 1995). Figure 2.3 represents graphically the minimum length required for the flow from a valve to orifice and from orifice to a valve. A is the length from a partly closed valve to the orifice upstream face without a flow conditioner, A' is the length from a partly closed valve to the orifice with a flow conditioner (flow straightening vanes) and B is the length from the orifice downstream face to a partly closed valve (ANSI/API 2530).

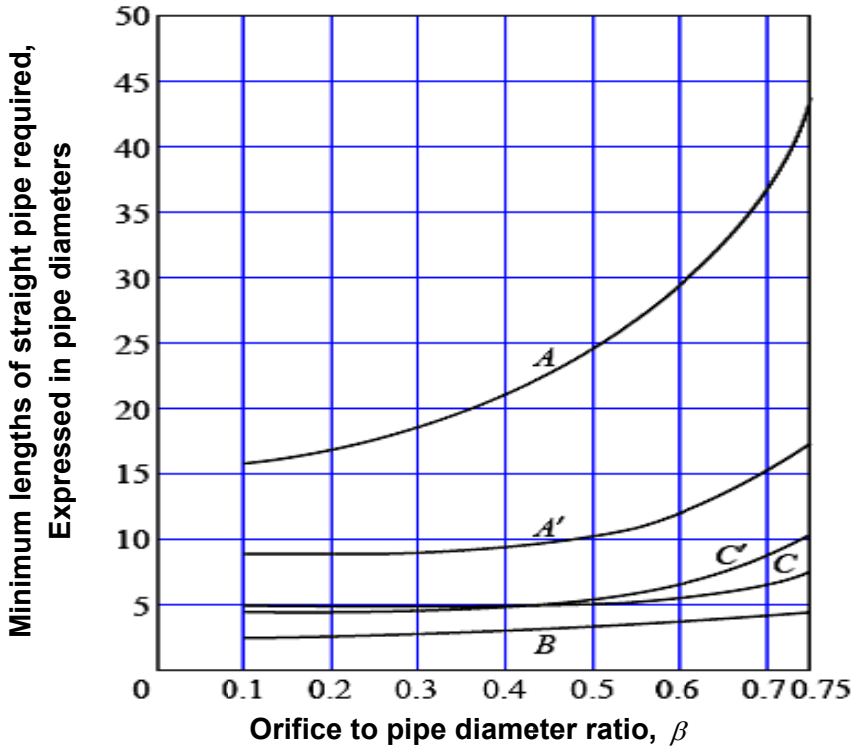

Figure 2.3 Upstream and downstream length required from a partly closed valve (ANSI/API 2530)

2.2.5 Flow through orifice

Fluid flowing through a pipe possesses a certain velocity and pressure. When a fluid flowing through a pipe approaches an orifice plate, flow accelerates as the fluid converges through the opening of the orifice plate which leads to a formation of a jet downstream of the orifice plate (ESDU, 2007). A flow velocity gradient occurs as the cross-sectional area changes. And hence a pressure gradient occurs. At the downstream of the orifice entry edge, contraction to a minimum-cross sectional area of the jet occurs because of the inward radial velocity component. This minimum cross-sectional area is also known as the *vena contracta*. Normally, the *vena contracta* plane occurs at an axial distance of 0.5D from the orifice upstream face (ESDU, 2007). Fluid entrainment caused by the jet continues downstream of the *vena contracta*. Gradual expansion of the jet takes place until the flow re-attaches downstream. The entrainment process drives a recirculation zone immediately behind the orifice with some fluid moving counter to the main flow. As the flow expands, an intensive mixing occurs in the flow which results in an irrecoverable energy loss and a flatter velocity profile with high

turbulence level (ESDU, 2007). A graphical presentation of fluid flowing through a square-edged orifice plate is given in Figure 2.4. The pipe cross-sectional area, orifice cross-sectional area and flow area at the *vena contracta* plane are defined as A_1, A_2 and A_{vc}

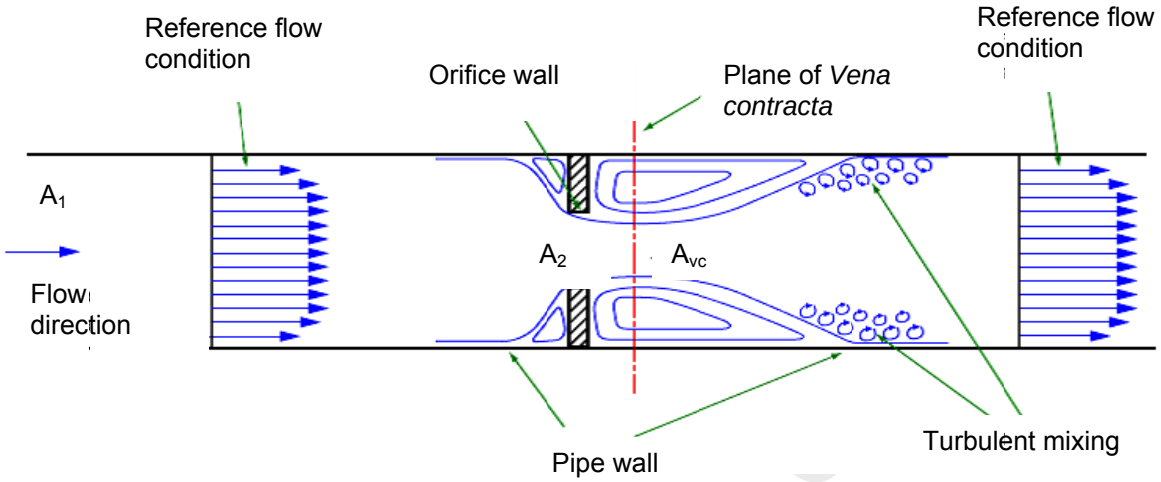

Figure 2.4 Schematic diagram of typical flow through orifice (ESDU, 2007)

Flow separation and reattachment occurs at the entry edge of the orifice depending on orifice geometry. Re-attachment of the flow on the orifice wall does not occur in the case of a short or a thin square-edged orifice. Different flow régimes are established depending on whether the jet formed downstream of the orifice plate entry remains separated from the orifice wall and re-attaches to the pipe wall, or whether the flow re-attaches to the orifice wall and on the pipe wall. When the flow remains separated from the orifice wall it is known as a fully separated flow régime. This condition normally occurs typically in the range of $0 < t/d < 0.75$ and where the C_c is increasing monotonically from $C_c = 0.61$ at $t/d = 0$ to $C_c = 0.8$ at $t/d = 0.75$ (Ward-Smith, 1979). If the thickness of the orifice plate is increased, the jet formed downstream of the orifice entry tends to converge on the inner wall of the orifice. This is known as marginally separated flow régime and normally occurs over a small, but finite range around $t/d = 0.75$. If the thickness of the orifice increases further, the jet just re-attaches to the orifice wall and instantaneously separates again from the orifice wall. This is known as a marginally-reattached flow régime. For $t/d > 0.75$ where C_c is constant $C_c \approx 0.61$ the flow tends to re-attach to the orifice wall in the form of a turbulent boundary layer. This régime is known as the fully reattached flow régime (Ward-Smith, 1979). The two intermediate stages of marginally-separated and marginally-reattached flow régimes are

still not fully understood. These stages remain uncertain regions where either reattached or separate flow might occur (ESDU, 2007). A schematic diagram of different flow régimes is presented in Figure 2.5, where, L_{s2x} represents the downstream reattachment length.

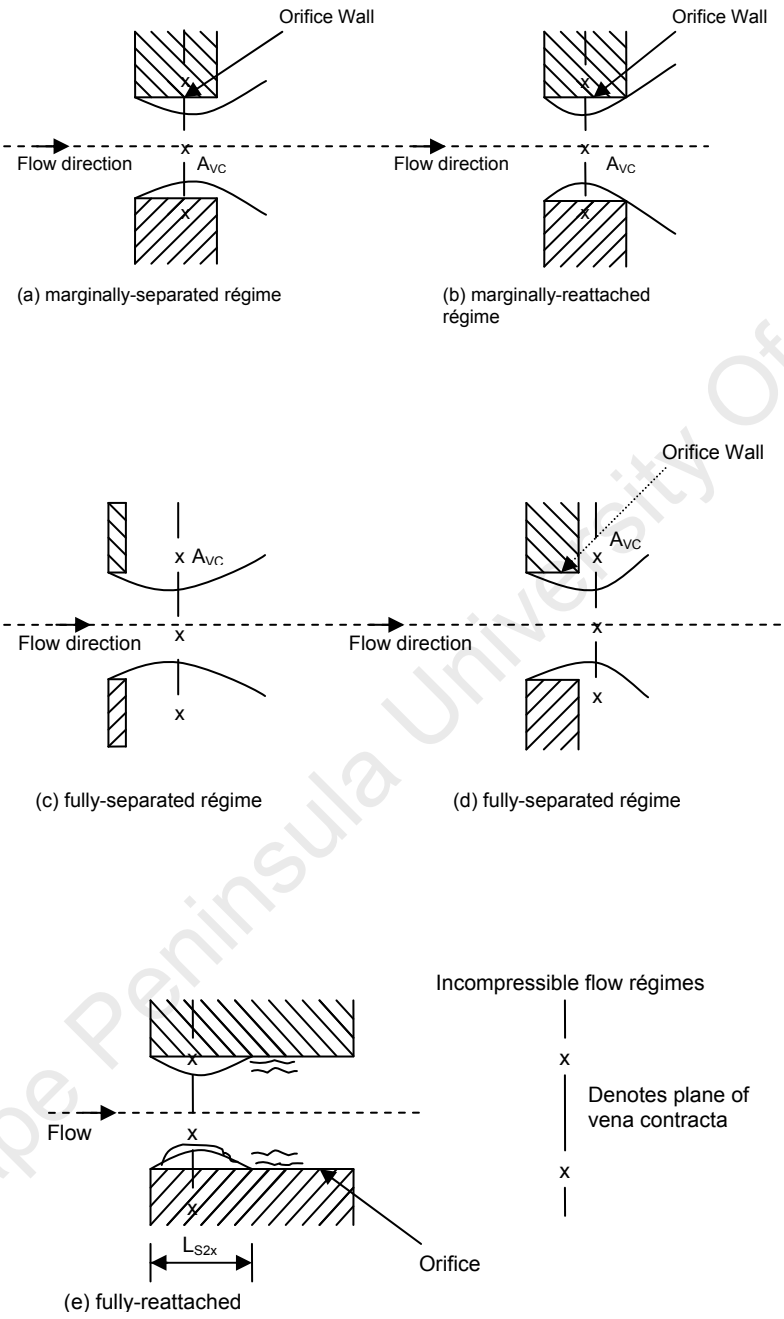

Figure 2.5 Schematic diagram of different flow régimes with varying orifice thickness (ESDU, 2007)

2.2.6 Effect of Reynolds number

Osborne Reynolds established the relationship between the ratio of inertial force and viscous force which is called the Reynolds number for the first time in 1883. A Reynolds number less than 2000 indicates laminar flow and a Reynolds number above 4000 indicates turbulent flow in straight pipes. The zone between a Reynolds number of 2000 to 4000 is an unstable zone known as a transitional zone. A Reynolds number can be presented by the following equation:

$$\mathrm{Re} = \frac{\rho V D}{\mu} \qquad \text{Equation 2.3}$$

A Reynolds number can be defined also in terms of orifice Reynolds number, $\mathrm{Re_d}$, with a slight alteration of Equation 2.3. The equation for orifice Reynolds number is presented as:

$$\mathrm{Re_d} = \frac{\mathrm{Re}}{\beta} \qquad \text{Equation 2.4}$$

For Reynolds numbers (Re) below 10, the flow remains attached to the orifice wall. The flow separates at the entry of the orifice wall to form a jet downstream of the orifice as Re increases. For high laminar flow, $\mathrm{Re} \approx 2000$ laminar to turbulent transition takes place in the jet, but re-laminarization may occur downstream of the orifice plate depending on the β. The transition to turbulent zone is well established at higher Re and the nature and geometry of the flow are then largely intensive to further increases in Re. A Reynolds number of $1x10^4$ can be taken as the lower limit for a single hole orifice plate for practical purposes. In the case of long orifices, where the reattachment loss is dominant no significant variation has been found for Re greater than $1x10^4$. For long orifices where the reattached flow loss is dominant, no significant variation has been observed for $\mathrm{Re_d}$ greater than $1x10^4$ (ESDU, 2007).

2.3 Classification of fluids

Fluids can be classified into two major categories. Firstly, according to the response from a fluid experiencing by externally applied pressure and secondly, by the effect a fluid produces under the action of a shear stress (Chhabra & Richardson, 2008). Compressible and incompressible fluids are also encountered. The flow characteristics of single phase liquids, solutions and pseudo-homogeneous mixtures which may be

treated as a continuum if stable in the absence of turbulent eddies, are considered in this thesis, depending on their response to externally imposed shearing action. All fluids tested in this thesis were assumed to be incompressible. In general a fluid belongs to one of the two main categories - Newtonian fluids and non-Newtonian fluids.

2.3.1 Newtonian fluid

In rheology one of the fundamental concept is the idea of a Newtonian liquid or Newton-Stokes liquid. A Newtonian fluid is the simplest linear fluid, where a linear relationship between components of stress and rate of deformation tensors exist (Malkin,1994). The coefficient of this linear relationship is known as viscosity or Newtonian viscosity. Thus the complete definition of a Newtonian fluid is it possesses not only a constant viscosity, but also when the shear stress is plotted against shear rate it always represents a straight line passing through the origin of the co-ordinates (Chhabra & Richardson, 2008). A plot of shear stress against shear rate is named a rheogram. A typical rheogram of a Newtonian fluid is presented in Figure 2.6. Liu (2003) stated that physically the shear rate is the velocity gradient or the rate of angular deformation of the fluid. Newtonian fluids can be expressed mathematically by the following relationship;

$$\tau = \mu_n \dot{\gamma} \qquad \text{Equation 2.5}$$

where, τ the shear stress, μ_n is the viscosity and $\dot{\gamma}$ the shear rate.

In any rheogram the slope of the straight line represents the viscosity or more specifically the dynamic viscosity of the fluid; the steepness of the slope depends on the viscosity of the fluid. The higher the viscosity of the fluid the steeper the slope becomes. Table 2.1 represents some typical viscosity values at room temperatures (Chhabra & Richardson, 2008).

Table 2.1 Various viscosity data at room temperature

Substance	**μ (mPa.S)**
Air	0.1
Benzene	0.65
Water	1
Molten sodium chloride (1173K)	1.01
Ethyl alcohol	1.20
Mercury (293 k)	1.55
Honey	100000

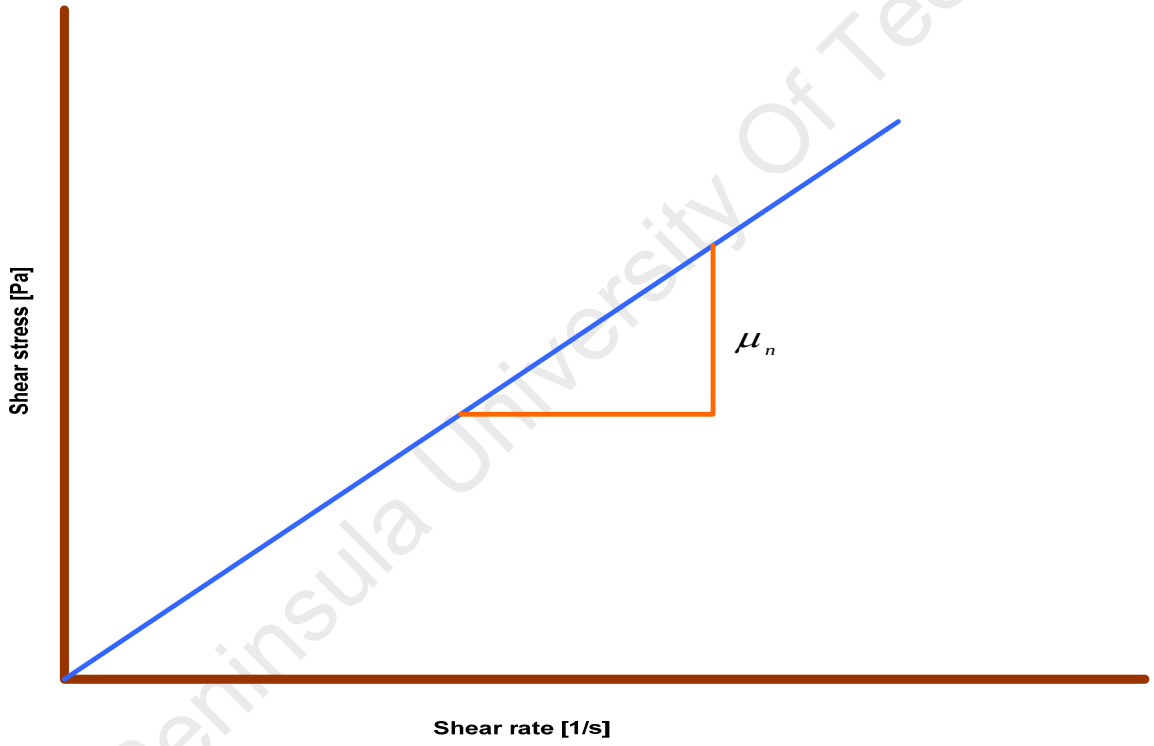

Figure 2.6 A typical rheogram of Newtonian fluid

Figure 2.7 presents graphically the change in steepness with the change in dynamic viscosity

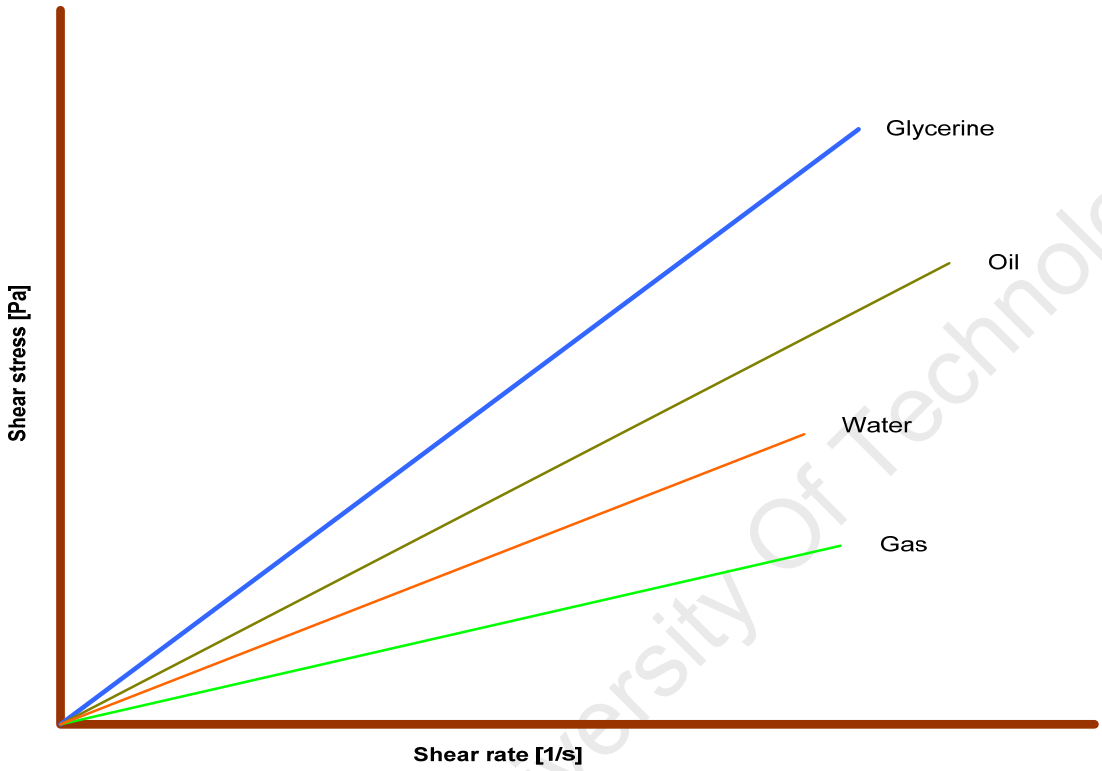

Figure 2.7 Rheogram of various Newtonian fluids

2.3.2 Non-Newtonian fluid

A non-Newtonian fluid can be defined as a fluid whose rheogram is non linear or does not pass through the origin. Malkin (1994) states the apparent viscosity i.e. shear stress divided by shear rate of a non-Newtonian fluid depends on condition of flow. It means that the apparent viscosity is inconstant at a given temperature and pressure, but depends on flow geometry, shear rate etc. and sometime even on the kinematics history of the fluid element under consideration.

2.3.3 Classification of non-Newtonian fluids

Non-Newtonian fluids may be conveniently grouped into three general classes. Although in those, most real materials, often exhibit a combination of two or even all the three types of non-Newtonian features. Generally, it is, however, possible to identify the

dominant non-Newtonian characteristics and to take it as a basis for subsequent process calculation (Chhabra & Richardson, 2008). In this thesis, only the time-independent non-Newtonian fluids are presented, but brief explanations will be presented for the time-dependent fluids and the visco-elastic fluids.

2.3.4 Time-independent non-Newtonian fluid

These are fluids of which the shear rate at any point is determined only by the shear stress at that point at that instant. The flow behaviour of these types of fluids may be described by using the constitutive relation (Chhabra & Richardson, 2008):

$$\dot{\gamma}_{yx} = f(\tau_{yx}) \qquad \text{Equation 2.6}$$

it may also be written inversely

$$\tau_{yx} = f_1(\dot{\gamma}_{yx}) \qquad \text{Equation 2.7}$$

Time-independent non-Newtonian fluids can also be divided in the following three types:

2.3.4.1 Shear thinning or pseudoplastic fluid

According to Chhabra and Richardson (2008) the most common type of time independent non-Newtonian fluid behaviour observed is shear thinning or pseudo plasticity. This type of fluid is characterised by an apparent viscosity which decreases with an increase in shear rate.

2.3.4.2 Shear thickening or dilatant fluid

Dilatant fluids are similar to pseudoplastic fluids in that they show no yield stress, but their apparent viscosity increases with any rise in shear rate; dilatant fluid behaviour was originally found in concentrated suspensions. The phenomenon of their dilatant behaviour is because at high shear rates the material expands or dilates slightly so that there is insufficient liquid to fill the increased void space and facilitate direct solid-solid contact resulting in increased friction and higher shear stress. This mechanism causes the apparent viscosity to rise rapidly, with an increasing shear rate (Chhabra & Richardson, 2008).

2.3.4.3 Viscoplastic fluid behaviour

Viscoplastic fluid behaviour is characterized by the existence of a yield stress which must be exceeded before the fluid will flow or deform. But if the externally applied stress is smaller than the yield stress, then such a material deforms elastically. Strictly speaking, it is almost impossible to establish if any real material possesses a true yield stress or not. Nevertheless, the concept of a yield stress has proved convenient in practice. Viscoplastic fluids also display an apparent viscosity which decreases as the shear rate increases. It is vital to note that a viscoplastic material also displays an apparent viscosity, which decreases with increasing shear rate for yield pseudoplastic fluids only, but is constant for Bingham plastic fluids. The flow curve may be linear or not, but will not pass through the origin.

2.3.4.3.1 Bingham plastic fluid

This is a fluid with a linear flow curve and with a yield stress. It is also characterised by a constant plastic viscosity (the slope of the shear stress versus the shear rate curve) and a yield stress (Chhabra & Richardson, 2008).

2.3.4.3.2 Yield pseudoplastic fluid

This type of fluid represents a non-linear flow curve on linear co-ordinates; yield pseudoplastic fluids possess a yield stress.

2.3.5 Time-dependent non-Newtonian fluid

Apparent viscosity for time dependent non-Newtonian fluids not only depends on the shear rate, but also on the time for which the fluid is subjected to shear. When certain materials are sheared at a constant rate following a long period of rest their apparent viscosities gradually reduce as the internal structure of the material is progressively broken down. Time-dependent non-Newtonian fluids can be divided further in two different groups (Chhabra & Richardson, 2008).

2.3.5.1 Thixotropic Fluid

When a material is sheared at a constant rate and the fluid's apparent viscosity decreases with the time of shearing, this fluid is described as a thixotropic fluid (Chhabra & Richardson, 2008).

2.3.5.2 Rheopectic fluid

This type of fluid is referred to as a negative thixotropic fluid; the rheopectic fluids are related to those for which apparent viscosity increases with time of shearing (Chhabra & Richardson, 2008).

2.3.5.3 Visco-elastic fluid

Many materials demonstrate both elastic and viscous effects under appropriate circumstances. In the absence of time dependent behaviour such materials are said to be visco-elastic. At the other extreme, when a perfect solid is deformed elastically, it regains its original form on removal of the stress. In the classical theory of elasticity, the stress in a sheared body is directly proportional to the strain. For tension, Hooke's Law applies and the coefficient of proportionality is known as Young's Modulus, G (Chhabra & Richardson, 2008):

$$G(\gamma_{yx}) = \tau_{yx} = G\frac{dx}{dy} \qquad \text{Equation 2.8}$$

Where, dx is the shear displacement of two elements separated by a distance dy.

Figure 2.8 represents different non-Newtonian flow curves for easy comparison.

2.3.6 Settling slurries

Settling slurries are basically solutions or pseudo-homogeneous mixtures in which the suspended particles settle rapidly relative to their residence time in a pipeline (Heywood & Brown, 1991). Or in other words, a mixture in which solid and liquid phases are separated and liquid properties are normally unaltered by the presence of solids. Antiparticle collisions and turbulent mixing supports the solid particles (Paterson & Cooke, 1999).

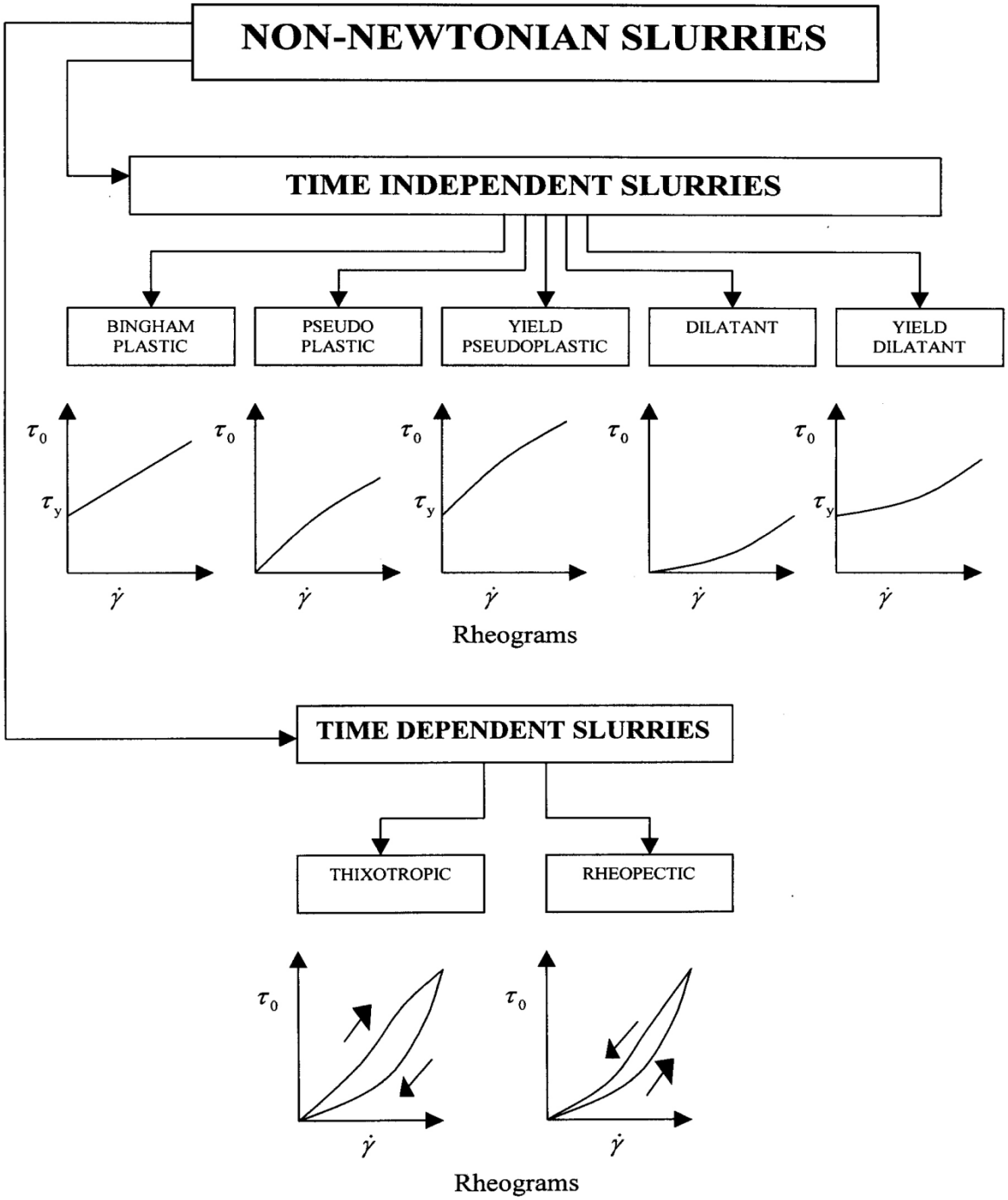

Figure 2.8 Various non-Newtonian fluids flow curve (Paterson & Cooke, 1999)

2.4 Flows in straight pipe

It is not always necessary to measure the losses separately since one is usually interested in measuring the combined pressure loss (Pienaar, 1998). To publish reliable and acceptable loss coefficient data, matters related to fluid flow in a straight pipe should be well understood.

2.4.1 Shear stress distribution in straight pipe

Massey (1990) stated that the flow of an incompressible fluid in a closed conduit, such as a pipe, is subjected to inertia and viscous forces. One is therefore able to distinguish between two different types of flow, i.e. laminar flow and turbulent flow. In many situations laminar flow may occur. It does so at velocities low enough for forces due to viscosity to predominate over inertia forces. Turbulent flow is subject to random fluctuating components that are superimposed on the main flow, and these haphazard movements are unpredictable (Massey, 1990). A graphical representation of the shear stress distribution in a straight pipe is given in Figure 2.9:

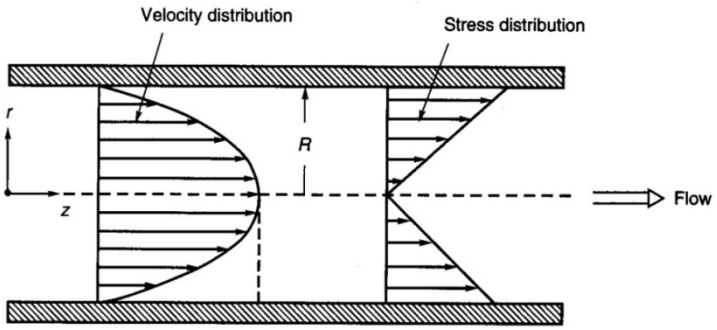

Figure 2.9 Velocity and shear stress distribution (Slatter, 1994)

The shear stress distribution in a straight pipe can be represented by Equation 2.9 (Chhabra & Richardson, 2008):

$$\tau = \frac{\Delta P R}{2L} \qquad \text{Equation 2.9}$$

where, ΔP is the pressure gradient in a straight pipe of length L and the radial distance R.

Equation 2.9 can be written in a different form at the pipe wall and which is given as:

$$\tau_o = \frac{D\Delta P}{4L} \qquad \text{Equation 2.10}$$

2.4.2 Energy loss in a straight pipe

Fluid passing through a pipe dissipates energy described as head loss. The Darcy-Weisbach equation can be used to calculate this head loss (Massey, 1990),

$$\Delta H = \frac{4fL}{D}\left(\frac{V^2}{2g}\right) \qquad \text{Equation 2.11}$$

where, f is the fanning friction factor and can be calculated by using the following equation (Massey, 1990):

$$f = \frac{\tau_o}{\frac{1}{2}\rho v^2} \qquad \text{Equation 2.12}$$

Where, V represents velocity of the fluid and can be calculated by the relation:

$$V = \frac{Q}{A} \qquad \text{Equation 2.13}$$

The nature of the fluid or nature of the flow does not affect Equations 2.9-2.13. They depend on the homogeneity of the fluid and on the development of the flow (Massey, 1990).

2.4.3 Newtonian laminar flow velocity distribution in straight pipe

In the case of no-slip or hold-up effect, the velocity distribution in a straight pipe in laminar flow can be presented by the following equation (Massey, 1990):

$$U = \frac{\tau_o}{2R\mu}(R^2 - r^2) \qquad \text{Equation 2.14}$$

The velocity of the fluid is maximum when r = 0. So, Equation 2.14 can be written as:

$$U_{max} = \frac{\tau_o R}{2\mu}$$ Equation 2.15

Equation 2.15 can be rewritten in terms of mean fluid velocity V, which is the following:

$$U_{max} = V_{mean} \times 2$$ Equation 2.16

Substituting Equation 2.16 in 2.15 the following equation is achieved:

$$V_{mean} = \frac{\tau_o R}{4\mu}$$ Equation 2.17

For laminar flow the shape of the velocity profile is parabolic. A typical laminar velocity profile is presented in Figure 2.10.

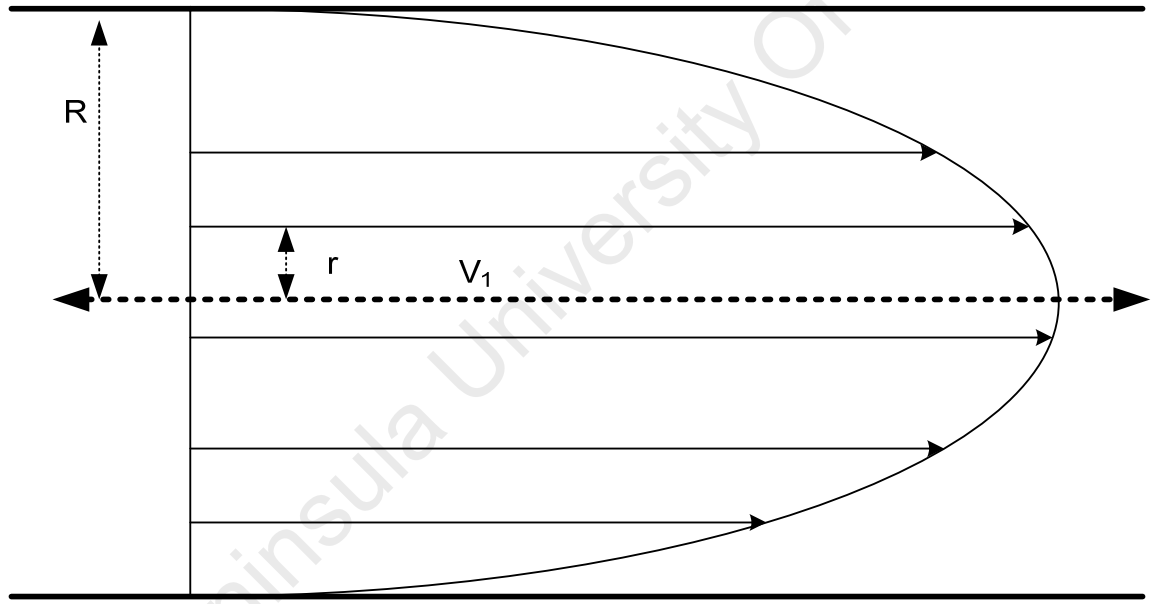

Figure 2.10 Typical laminar velocity profile

2.4.3.1 Friction factor

The friction factor is a function of both the Reynolds number and the pipe wall roughness. The friction factor is normally calculated by using Equation 2.12. In Newtonian laminar flow the pipe wall roughness does not play any role on the friction factor. For Newtonian laminar flow the friction factor is given by the following equation (Massey, 1990):

$$f = \frac{16}{\mathrm{Re}}$$ Equation 2.18

2.4.4 Newtonian turbulent flow in straight pipe

Losses caused by turbulence have greater magnitude compared to the losses in laminar flow. To prevent rapid decaying of turbulence it needs a continuous supply of energy (Miller, 1990). This energy is generated from the shear flow at the expense of the flow's total energy. Turbulence in internal flow is a phenomenon which is considered desirable in one condition, yet undesirable in another condition. Turbulence is responsible for the majority of pressure loss, but it also provides much heat transfer, mass transfer and combustion to make processes economically feasible. Turbulent dissipation is minimum in a smooth straight pipe or passage, but can be enhanced by roughening a pipe wall or turning or diffusing the flow or changing the pipe's diameter. Part of the energy transferred into turbulence is immediately dissipated - partly in regions close to boundaries and along the edges of discontinuities in velocity associated with flow separation. The remaining energy is transferred into large eddies and cascaded down to smaller and smaller eddies, to be eventually converted into internal energy by viscous shear (Miller, 1990). A typical example of both laminar and turbulent flow can be observed in the smoke from a cigarette as shown in Figure 2.11.

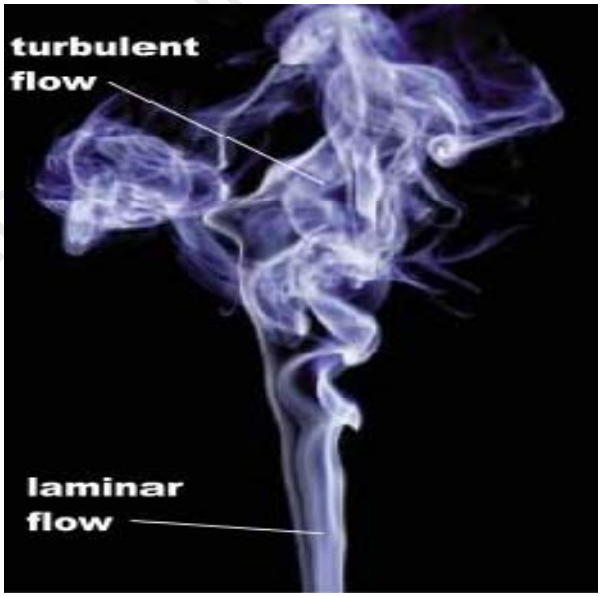

Figure 2.11 Example of turbulent and laminar flow (Bechtold, 2006)

Turbulent flow is complex and consistent mathematical analysis has not yet been achieved. Predictions are obtained empirically from experiments. In turbulent flow the friction factor is a function of the Reynolds number and pipe roughness k.
Equation 2.19, well known as the Colebrook and White equation, can be used to calculate the friction factor (Massey, 1990).

$$\frac{1}{\sqrt{f}} = -4\log\left[\frac{\mathrm{k}}{3.7\,\mathrm{D}} + \frac{1.26}{\mathrm{Re}\sqrt{f}}\right] \qquad \text{Equation 2.19}$$

Equation 2.20, the Blasius equation, can be used in the case of a smooth wall pipe and Reynolds number between 3000 and 100000, to determine the friction factor.

$$f = \frac{0.079}{(\mathrm{Re})^{0.25}} \qquad \text{Equation 2.20}$$

Friction factors can also be determined from a Moody diagram. A Moody diagram is a graphical presentation of pipe Reynolds number against friction factor. If the pipe Reynolds number and the pipe roughness, k/D value is known, the friction factor can easily be read off the Moody diagram. Figure 2.12 represents a Moody diagram.

2.4.5 Rheology

The word Rheology is derived from a Greek word “rheos” which is flow and “logos” meaning knowledge. Rheology is the science of flow phenomena; or in other words, rheology is defined as the science of deformation and flow of matter (Mezger, 2002). According to Malkin (1994) rheology is a science dealing with materials having properties not described by Newton-Stokes and Hooke. Rheology is also defined as a branch of science dealing with relationships between the shear stress and the resulting shear rate of a fluid in a laminar flow region and any variable influencing such relationships (Metzner & Reeds, 1955). Within the context of this thesis rheology is defined as the viscous characteristics of a fluid or homogeneous solid-liquid mixture.

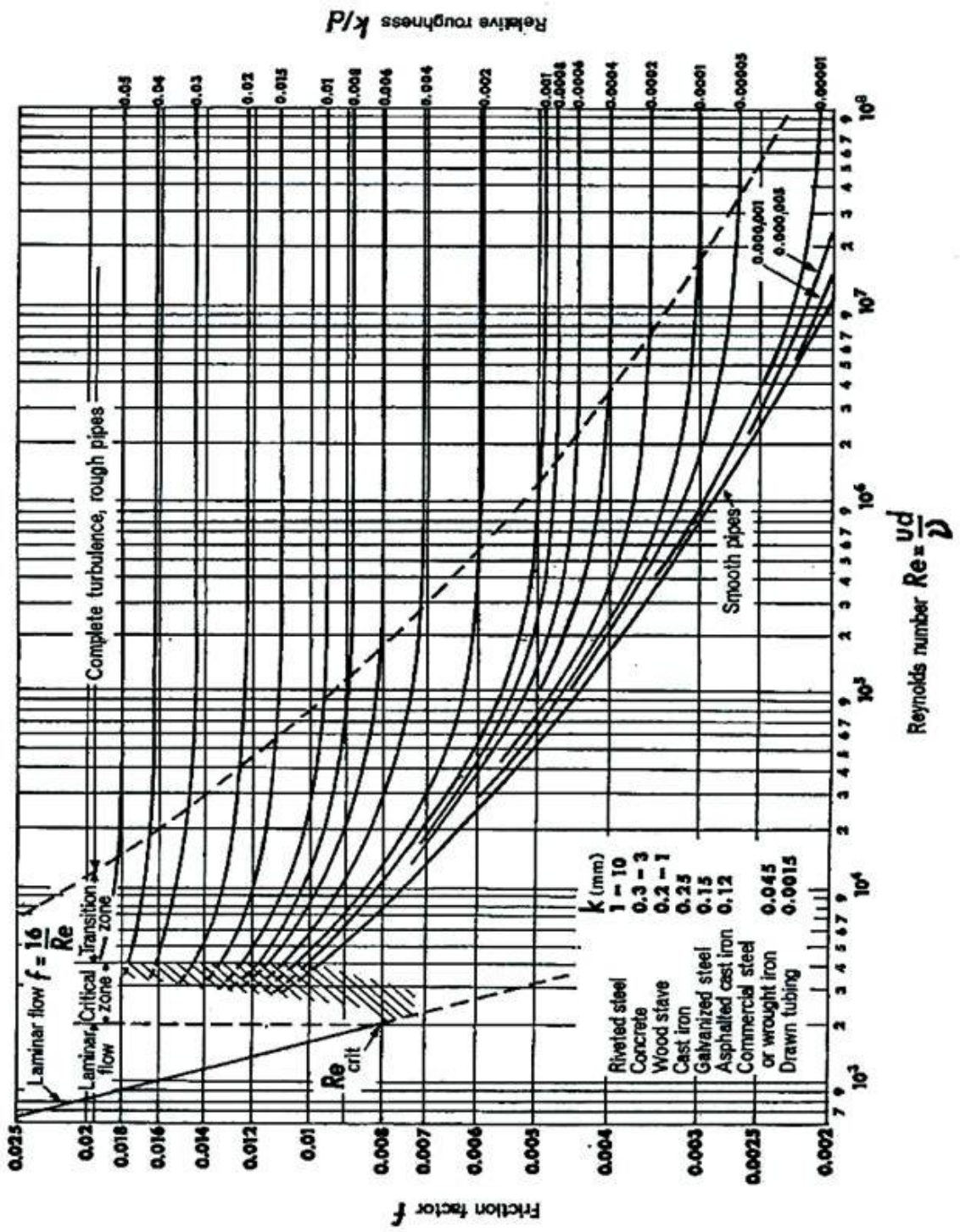

Figure 2.12 Moody diagram (Massey, 1990)

2.4.5.1 Rheological properties and laws of non-Newtonian fluids

Newtonian fluids have only one rheological parameter which is defined by Newton's Law of viscosity. However, non-Newtonian fluids have two or three rheological parameters, defined by the following laws.

2.4.5.1.1 Power-law fluids

For certain non-Newtonian fluids the relationship between shear stress and the velocity gradient can be expressed satisfactorily by using the following relationships:

$$\tau = K\left(\frac{du}{dy}\right)^n \qquad \text{Equation 2.21}$$

Equation 2.21 can also be written in the following way:

$$\mu = K\left(\frac{du}{dy}\right)^{n-1} \qquad \text{Equation 2.22}$$

Equation 2.21 is applicable to pseudoplastic fluids when $n<1$, dilatant fluids when $n>1$, and Newtonian fluids when n = 1. From Equation 2.21, the two rheological properties of pseudoplastic and dilatant fluids that can be represented by the equation are the fluid consistency index and the flow behaviour index. The constant μ in Equation 2.22 is the apparent viscosity, which reduces to the dynamic viscosity when a fluid is Newtonian $n=1$ (Liu, 2003).

2.4.5.1.2 Bingham fluids

The following law is applicable for any Bingham plastic fluid;

$$\tau = \tau_y + K\frac{du}{dy} \qquad \text{Equation 2.23}$$

where τ_y is the yield stress and K is the coefficient of rigidity - simply the rigidity of the fluid.

2.4.5.1.3 Yield stress fluids

For yield pseudoplastic fluids and yield dilatant fluids Equation 2.24 is applicable.

$$\tau = \tau_y + K\left(\frac{du}{dy}\right)^n \qquad \text{Equation 2.24}$$

Equation 2.24 is a combination of Equation 2.21 and 2.23. The exponent n in Equation 2.22 is greater than one for yield dilatant fluids and less than one for yield pseudoplastic fluids. When $n=1$ Equation 2.24 reduces to Equation 2.23, which is applicable for Bingham fluids.

2.4.5.1.4 Other non-Newtonian fluids

Many rheological models are found in the literature for various types of non-Newtonian fluids. Not all models are discussed in the thesis, but some are presented in Table 2.2.

Table 2.2 Various rheological models (Chhabra & Richardson, 2008)

Fluid model	Constitutive equation	Number of parameter	Parameters
Carreau	$\frac{\mu_0-\mu_\infty}{\mu_0\mu_\infty}=\left[1+\left(\lambda\left(-\frac{du}{dy}\right)\right)^2\right]^{\frac{n-1}{2}}$	4	μ_∞, μ_o, λ and n
Casson	$\sqrt{\tau}=\sqrt{\tau_y}+\sqrt{\mu_c\left(-\frac{du}{dy}\right)}$	2	τ_y and μ_c
Cross	$\frac{\mu_0-\mu_\infty}{\mu_0\mu_\infty}=\left[1+\left(\lambda\left(-\frac{du}{dy}\right)\right)\right]^{\frac{n-1}{2}}$	4	μ_∞, μ_o, λ and n
E-function	$\mu=\mu_0\exp\left[m\left(-\frac{du}{dy}\right)\right]$	2	μ_o and m
Ellis	$\mu=\frac{\mu_0}{1+\left(\frac{\tau}{\tau_{\frac{1}{2}}}\right)^{\alpha-1}}$	3	μ_o, α and $\tau_{1/2}$

2.4.5.1.5 Choice of rheological model

Many rheological models have been published to be used to model the laminar flow of non-Newtonian fluids. The choice of the model is extremely important, not only for

characterization in laminar flow, but also more importantly, for turbulent flow predictions (Hanks & Ricks, 1975). According to Chhabra and Richardson (2008) it is difficult to characterise non-Newtonian fluids. It can be achieved by using a rotary viscometer or a tube viscometer. In the context of this thesis, tube viscometry was used as the experimental loop also served as a tube viscometer.

2.4.6 Viscometry

Rheometry or viscometry deals with the establishment of a relationship between the shear stress and shear rate of a specific fluid (Chhabra & Richardson, 2008). An instrument used to measure the shear stress at various rates is a viscometer.

2.4.6.1 Rotational viscometer

In 1890 Maurice Couette was the first to construct and test a rotational viscometer based on the principle of coaxial cylinders (Macosko,1993). A rotational rheometer usually consists of a concentric bob and cup, one of which is rotated to produce shear in the test fluid located in the gap between bob and cup. The shear stress is determined by measuring the applied torque on one of the elements. Other measuring geometries apart from the cup-and-bob, includes concentric cylinders, cone and plate and parallel disks. The main measurements are angular velocity and applied torque. Software connected to these instruments converts these signals into shear rate and shear stress (Chhabra & Richardson, 2008). Figure 2.13 represents two different types of rotational viscometer. The rheometer is a sophisticated instrument capable of measuring a full range of rheological phenomena.

2.4.6.2 Tube viscometer

Test fluid flows through a tube viscometer at a controlled, measured rate. The tube diameter is known and the pressure drop over a known length of tube is measured. Data gathered from tube viscometers yields a series of co-ordinates of pseudo shear rate and wall shear stresses. This data must be processed to give the required rheology (Chhabra & Richardson, 2008).

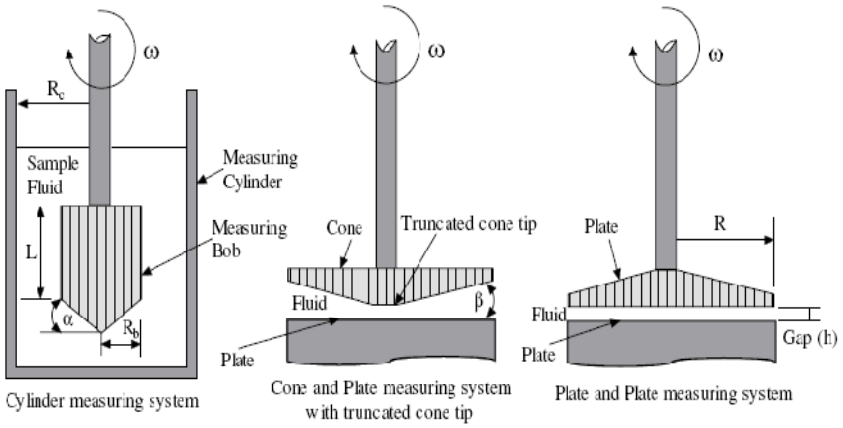

Figure 2.13 Different measuring systems of rotational rheometer (Chhabra & Richardson, 2008)

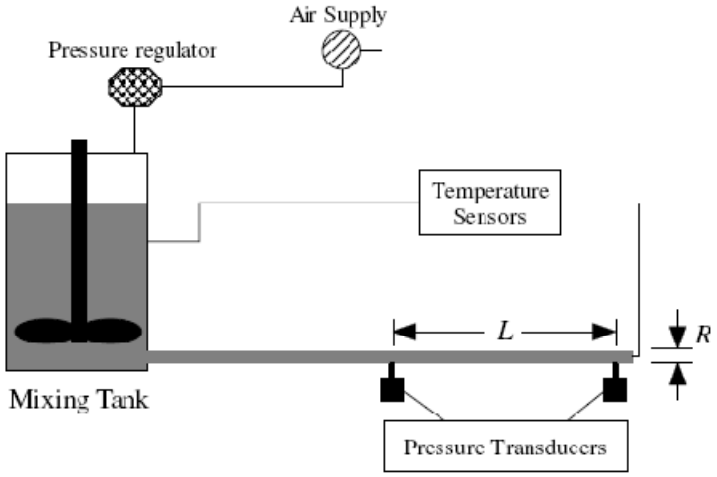

Figure 2.14 Air driven pipe viscometer (Kotzé, 2007)

Figure 2.14 shows how a pump or gas system may be used to create a driving force in pipe viscometers. Interpretation of tube viscometer data was achieved in the following manner:

- Data $\left(\frac{8V}{D}\right)$ and $\left(\frac{D\Delta P}{4L}\right)$ obtained from the tube viscometer was plotted on a log-log scale in the X axis and Y axis respectively;
- data points in laminar flow were used only;
- different mathematical function was used to fit the data point; the best curve was fitted to the data and,

- a realistic value of τ_y was then adjusted until the error function was minimal.

The error function E is the root square difference between observed data and can be calculated as (Slatter, 1994):

$$E = \sqrt{\frac{\sum_{i=1}^{N}\left[\left(\frac{8V}{D}\right)_{iobs} - \left(\frac{8V}{D}\right)_{icalc}\right]^2}{N-1}} \qquad \text{Equation 2.25}$$

K value for minimum error K_{min} is given by the following equation:

$$K_{min} = \frac{1}{\left[\frac{2\sum_{1}^{N}\left(\frac{8V}{D}\right)_i / 8}{n\sum_{i=1}^{N}\left(\tau_0-\tau_y\right)^{\frac{1+n}{n}}\left[\frac{\left(\tau_0-\tau_y\right)^2}{1+3n}+\frac{2\tau_y\left(\tau_0-\tau_y\right)}{1+2n}+\frac{\tau_y{}^2}{1+n}\right]}\right]} \qquad \text{Equation 2.26}$$

The main error sources in tube viscometry arise from wall slip and entrance or exit losses (Chhabra & Richardson, 2008).

1. According to Heywood and Brown (1991) wall slip occurs when layers of particles near a wall are more diluted than the bulk flow. As a consequence, viscosity near the wall is reduced and apparent slip occurs. Chhabra and Richardson (2008) warn that serious errors might occur when the wall slip is not accounted for. Pipes of varying diameters should be tested to check for the wall slip. The laminar flow data should coincide for all pipe diameters if there is no wall slip. If they do not coincide, the slip velocity must be calculated for each tube then deducted from the measured mean velocity (Heywood & Brown, 1991).
2. It is important the entrance and exit losses in tubes used are minimized. This can be achieved by ensuring the flow is fully developed before differential pressure readings are taken; usually at least 50 pipe diameters is allowed.

2.4.7 Non-Newtonian laminar flow in straight pipe

In laminar flow the velocity distribution of a yield pseudoplastic fluid can be found by using the following equation (Slatter, 1994):

$$u = \frac{R}{\frac{1}{K^{\frac{1}{n}}\tau_o}} \frac{n}{n+1}\left[\left(\tau_o - \tau_y\right)^{\frac{n+1}{n}} - \left(\tau - \tau_y\right)^{\frac{n+1}{n}}\right] \qquad \text{Equation 2.27}$$

Equation 2.27 is valid for $R > r > r_{plug}$

If, $0 < r < r_{plug}$ the fluid moves as a plug at a uniform plug velocity $U_{plug.}$

The volumetric discharge is the sum of the flow through the sheared region $R > r > r_{plug}$ and the plug $r < r_{plug}$ and can be found by the following relation:

$$Q = \left[2\pi \int_{r_{plug}}^{R} u.r.dr\right] + \left(\pi {r_{plug}}^2 u_{plug}\right) \qquad \text{Equation 2.28}$$

Equation 2.28 can be written in the following form after integration:

$$\frac{32Q}{\pi D^3} = \frac{8V}{D} = \frac{4n}{\frac{1}{K^{\frac{1}{n}}\tau_o^{\,3}}}\left(\tau_0 - \tau_y\right)^{\frac{1+n}{n}}\left[\frac{\left(\tau_0 - \tau_y\right)^2}{1+3n} + 2\tau_y\frac{\left(\tau_0 - \tau_y\right)}{1+2n} + \frac{\tau^2{}_y}{1+n}\right] \qquad \text{Equation 2.29}$$

Where τ_0 and V is defined by using Equation 2.10 and 2.13 respectively.

Table 2.3 represents various rheological relationships which can be accommodated in the yield pseudoplastic model.

Table 2.3 Rheological Relationships (Chhabra & Richardson, 2008)

Fluid	τ_y	n
Yield dilatant	>0	>1
Bingham plastic	>0	=1
Yield pseudoplastic	>0	<1
Newtonian	=0	=1
Pseudoplastic	=0	<1
Dilatant	=0	>1

Equation 2.29 can be changed into the following equation for Newtonian liquid by substituting $\tau_y = 0$, $K = \mu$ and $n = 1$:

$$\tau_0 = \mu \frac{8V}{D} \qquad \text{Equation 2.30}$$

Equation 2.30 shows that the shear rate at the pipe wall for a Newtonian fluid is $8V/D$. For a non-Newtonian fluid, however this is not the case. A plot of τ_0 vs. $8V/D$ is described as a pseudo shear diagram. It is of great importance in non-Newtonian fluid flow in general and can be related to the true shear rate by the Rabinowitsch-Mooney relation (Chhabra & Richardson, 2008).

2.4.7.1 Rabinowitsch-Mooney relation

The Rabinowitsch-Mooney relation is used to obtain true shear rate from the pseudo shear rate as given in Equation 2.31 (Chhabra & Richardson, 2008):

$$\left[-\frac{du}{dr}\right]_0 = \frac{8V}{D}\left[\frac{3n'+1}{4n'}\right] \qquad \text{Equation 2.31}$$

An apparent fluid behaviour index can be found by using the equation:

$$n' = \frac{d\left(\text{Log}\tau_o\right)}{d\left(\text{Log}\frac{8V}{D}\right)} \qquad \text{Equation 2.32}$$

If, the rheological parameters of the fluid are known (τ_y, K and n), K' and n' can be obtained for pseudoplastic fluids directly by using the relations:

$$K' = K\left(\frac{3n+1}{4n}\right)^n \qquad \text{Equation 2.33}$$

and,

$$n = n' \qquad \text{Equation 2.34}$$

2.4.7.2 Metzner & Reed generalised Reynolds number

According to Metzner and Reed (1955) the true shear stress τ_0, for any time independent fluid can be established by using the equation:

$$\tau_0 = \frac{D\Delta P}{4L} = K'\left(\frac{8V}{D}\right)n' \qquad \text{Equation 2.35}$$

In general K' and n' are not constants, but vary with 8V/D. If τ_0 is plotted against 8V/D on a logarithmic scale Equation 2.35 is simply the equation of the tangent to the curve at a given value of 8V/D, n' being the slope of this tangent and K' is the intercept on the ordinate at 8V/D equal to unity (Skelland, 1967). Metzner & Reed (1955) developed a generalized Reynolds number applicable to the pseudoplastic model from such considerations above as:

$$Re_{MR} = \frac{8\rho V^2}{K'\left(\frac{8V}{D}\right)^{n'}} \qquad \text{Equation 2.36}$$

substituting Equation 2.33 and 2.34 in Equation 2.36 the following can be achieved:

$$Re_{MR} = \frac{8\rho V^2}{K\left(\frac{8V}{D}\right)^{n}\left[\frac{4n}{3n+1}\right]^n} \qquad \text{Equation 2.37}$$

Equation 2.36 can also be written after transformation as the following:

$$Re_{MR} = \frac{\rho V^{2-n'} D^{n'}}{8^{n'-1} K'} \qquad \text{Equation 2.38}$$

In practice it has been observed experimentally for many fluids that the apparent fluid consistency index, K' and apparent fluid behaviour index, n' are constant over any range of τ_o or 8V/D values for which the power law is valid. This is not the case in general (the log-log plot is not always a straight line) and care must be taken to ensure the range of application is narrow. The quantity n' characterises the degree of non-Newtonian behaviour for a given fluid. The greater the departure of n' from unity, the more non-Newtonian is the fluid. The quantity K' is a measure of the consistency of the fluid; the larger the value of K' the thicker or less mobile is the fluid (Metzner & Reed, 1955).

For a Bingham plastic fluid (Skelland, 1967):

$$n' = 1 - \frac{4\tau_y}{3\tau_0} \qquad \text{Equation 2.39}$$

2.4.7.3 Slatter Reynolds number

The Slatter Reynolds number is given by:

$$Re_S = \frac{8V_{ann}^2\rho}{\tau_y + K\left(\frac{8V_{ann}}{D_{shear}}\right)^n}$$ Equation 2.40

Equation 2.40 takes directly into account the yield stress of non-Newtonian fluids and seeks to express the ratio of inertial forces to viscous shear forces in the sheared portion of the flow (Chhabra & Richardson, 2008).

For a fluid with a yield stress there is a plug flow at the centre of the pipe in laminar flow, and the radius of the plug is:

$$r_{plug} = \frac{\tau_y}{\tau_0}R$$ Equation 2.41

The shear diameter is:

$$D_{shear} = D - D_{plug}$$ Equation 2.42

again,

$$D_{plug} = 2r_{plug}$$ Equation 2.43

The mean velocity of the annulus is:

$$V_{ann} = \frac{Q_{ann}}{A_{ann}}$$ Equation 2.44

Where, Q_{ann} is:

$$Q_{ann} = Q - Q_{plug}$$ Equation 2.45

$$Q_{plug} = U_{plug}.A_{plug}$$ Equation 2.46

And,

$$U_{plug} = \frac{R}{K\frac{1}{n}\tau_0}\frac{n}{n+1}\left(\tau_0 - \tau_y\right)\frac{n+1}{n}$$ Equation 2.47

The transitional value of the Slatter Reynolds number is 2100 in straight pipe (Lazarus & Slatter, 1988).

2.4.7.4 Friction factor for non-Newtonian fluids

According to Chhabra & Richardson (2008) for inelastic non-Newtonian fluids the Fanning friction factor in laminar flow is calculated by using the following equation:

$$f = \frac{16}{Re_{MR}}$$ Equation 2.48

But for fluids with a yield stress Slatter (1999) proposed a friction factor which is given below:

$$f_{ann} = \frac{2\tau_0}{\rho V^2_{ann}}$$ Equation 2.49

Transition is considered when f_{ann} is equal to 0.008.

But in the case of turbulent flow, the friction factor for a smooth wall pipe is calculated by using the following equation:

$$f = \frac{0.079}{Re_s^{0.25}}$$ Equation 2.50

2.5 Loss coefficient

Miller (1990) defines loss coefficient as: “The non-dimensionalized difference in total pressure between the extreme ends of two long straight pipes when there is a zero loss component between the two pipes and when the real fitting is installed”. In non-dimensionalizing the pressure loss, the convention is to use the fittings inlet velocity head, except when the fitting is an inlet from a large space when the pipe velocity head is used. The long pipe before the fitting ensures developed flow at the inlet and the long

pipe after the fitting ensures losses caused by flow re-development after the fitting are debited to the fitting. A graphical definition of loss coefficient is presented in Figure 2.15.

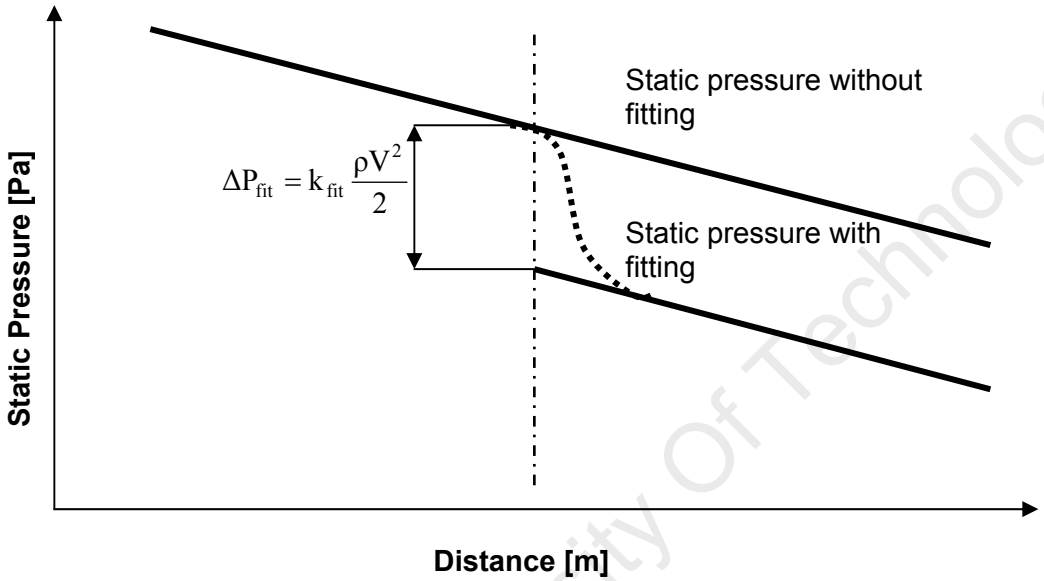

Figure 2.15 Definition of the loss coefficient (Miller, 1990)

2.5.1 Pressure loss coefficient

The energy equation gives the macroscopic mechanical energy balance for a pipe system, as well as the total head loss in the system and used in different systems to determine different losses. The formula for a system connected to two pipes in a series connected by a fitting can be expressed as:

$$Z_1 + \frac{\alpha_1 V_1^2}{2g} + \frac{P_1}{\rho g} = Z_2 + \frac{\alpha_2 V_2^2}{2g} + \frac{P_2}{\rho g} + H_1 + H_{fit} + H_2 \qquad \text{Equation 2.51}$$

Where, 1 and 2 refers to the upstream and downstream respectively. H_1 and H_2 represent the head loss upstream and downstream respectively. The head loss because of fittings, H_{fit} can be expressed mathematically as:

$$H_{fit} = K_{fit} \frac{V^2}{2g} \qquad \text{Equation 2.52}$$

where, K_{fit} is the fitting head loss coefficient.

After rearranging, Equation 2.52 can be written as:

$$K_{fit} = H_{fit}\frac{2g}{V^2} \qquad \text{Equation 2.53}$$

Equation 2.53 can be written in terms of a pressure drop as:

$$K_{fit} = \frac{\Delta P_{fit}}{\frac{1}{2}\rho V^2} \qquad \text{Equation 2.54}$$

Loss coefficients can be calculated, by including or excluding the length of the fitting. When the length of the fitting is excluded, K_{fit} is named K_{gross} and obtained by using the following equation (Turian et al., 1997):

$$K_{gross} = \frac{1}{\frac{\rho V^2}{2}}\left[-\Delta P - \frac{\rho V^2}{2}\frac{4f}{D}\left(L_u + L_d\right)\right] \qquad \text{Equation 2.55}$$

If the length of the fitting is included, K_{fit} is called K_{net} and is calculated by using Equation 2.56 (Turian et al., 1997):

$$K_{net} = \frac{1}{\frac{\rho V^2}{2}}\left[-\Delta P - \frac{\rho V^2}{2}\frac{4f}{D}\left(L_u + L_{fit} + L_d\right)\right] \qquad \text{Equation 2.56}$$

For orifices the pressure loss coefficient can be expressed as a function of the orifice bulk mean velocity, which is also referred to as the Euler number (ESDU, 2007):

$$Eu = \frac{\Delta P}{\frac{1}{2}\rho v_2^2} = \beta^4\frac{\Delta P}{\frac{1}{2}\rho v_1^2} = \beta^4 K_i \qquad \text{Equation 2.57}$$

where, V_1 and V_2 are pipe bulk velocity and orifice bulk velocity respectively.

2.5.2 Methodology to determine pressure loss coefficient

Two methods are preferred to determine fittings loss coefficients - the hydraulic grade line approach (HGL) and the total pressure method. Several researchers have used the HGL method to obtain pressure loss coefficients. As an example, Banerjee et al., (1994), Baudouin (2003) and Kazadi (2005) adopted the HGL approach to determine pressure

loss coefficients. The first two authors used it to determine the loss coefficients in valves, the latter for loss coefficients in sudden contractions. The hydraulic grade line approach consists of measuring and plotting static pressure gradients upstream and downstream of the orifice plate in the region of the fully developed flow far from the orifice plane, to avoid disturbance of the flow from the presence of the orifice plate.

U-tube manometers containing mercury beneath the water connected to pressure tappings were used by Banerjee et al., (1994) to measure the static pressure at different points upstream and downstream of the orifice plate. Point pressure transducers connected to pressure tappings were used by Baudouin (2003) and Kazadi (2005) to measure the static pressure drop. Figure 2.16 represents the HGL approach.

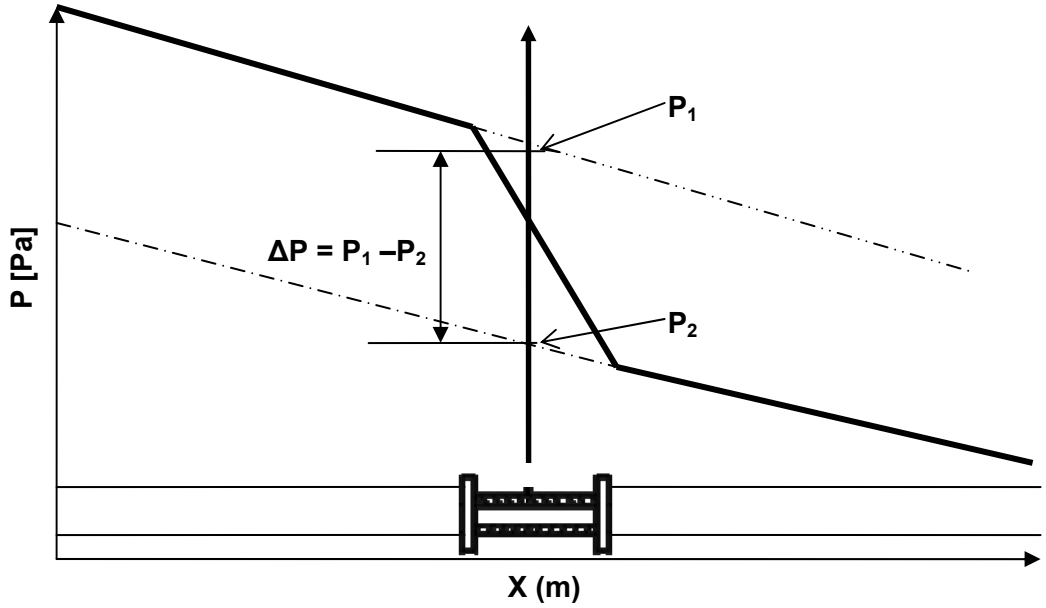

Figure 2.16 Diagram illustrating pressure loss coefficient calculation

The total pressure drop method was used by Turian et al., (1997) and Pienaar (1998) to determine the pressure loss coefficient for different fittings in slurry applications. The total pressure drop method consists of measuring the pressure drop between two points in the region of fully developed flow in straight pipes around the fitting. Thus, by knowing the straight pipe losses, one can deduct the fitting loss.

Static pressure (P) versus axial distance (X) points of co-ordinates (P_i,X_i) are plotted on a graph from the experimental data. Figure 2.16 shows that in pipes upstream and

downstream of the orifice plate, the curves of static pressure drop follow a linear law and are straight lines. The co-ordinates of the points upstream of the orifice plate plane, which is the y-axis in this case, are used to calculate the slope m_1 and intercept P_1 of the line upstream by linear regression. The slope m_2 and intercept P_2 of the line downstream of the orifice plate plane are also calculated by linear regression using the co-ordinates of the points downstream of the orifice plate. In the case of the orifice plate, the pipes upstream and downstream of the test valve have the same diameters, the two hydraulic grade lines upstream and downstream of the test orifice have identical slopes, m_1 and m_2 are equal and the pressure drop because of the orifice plate is given by:

$$\Delta P_{or} = P_1 - P_2 \qquad \text{Equation 2.58}$$

By using Equation 2.54 the following may be said:

$$K_{or} = \frac{(P_1 - P_2)}{\frac{1}{2}\rho V^2} \qquad \text{Equation 2.59}$$

A schematic of the pressure drop and recovery during flow separation and the subsequent re-attachment and frictional pressure drop in the attached portion of the orifice is presented in Figure 2.17. Orifices with two different aspect ratios are shown with the extended region of the larger aspect ratios shown by a dashed line. The pressure at the exit of the orifices in both cases is the ambient pressure and shown by A and A' for the small and larger aspect ratio orifice respectively. The larger pressure drop in the increased re-attached portion of the larger aspect ratio orifice is possible only for a higher pressure at the re-attachment point. This is shown by B' for the orifice of larger aspect ratio and is compared with the value B for the smaller aspect ratio orifice in Figure 2.17. The higher value of pressure B' for the larger aspect ratio orifice demands the upstream pressure be higher to drive the same flow. The corresponding upstream pressure is denoted by C' and C for the two orifice in Figure 2.17 with C' being higher than C. A higher dynamic head would be required to reduce the pressure corresponding to the higher pressure C' to the value of vapour pressure P_v (Ramamurthi & Nandakumar 1999).

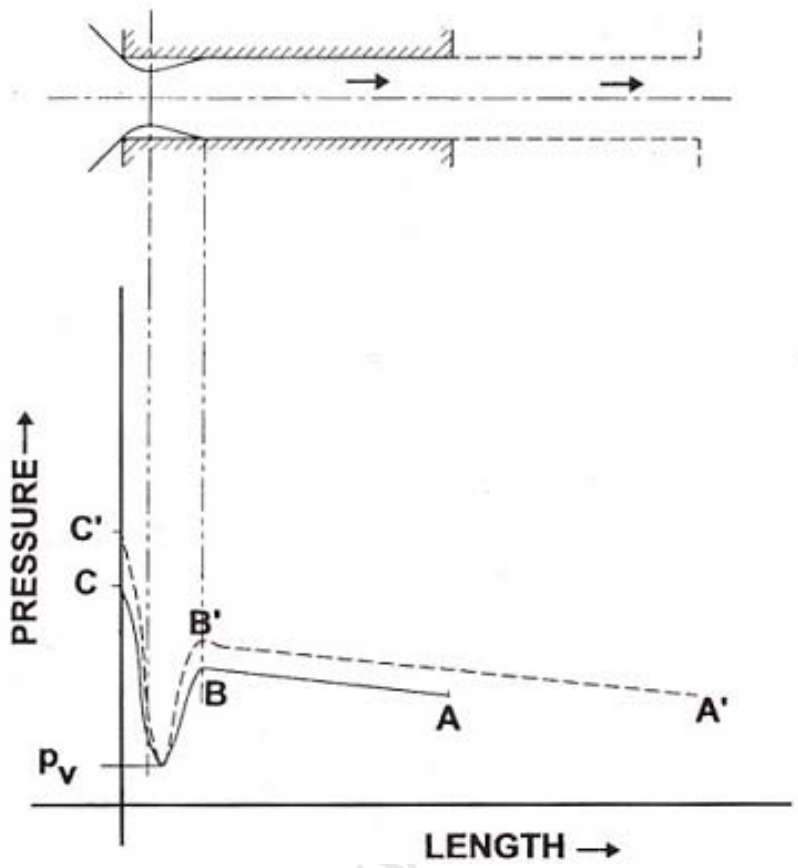

Figure 2.17 Pressure variation along the length of a short and long orifice (Ramamurthi & Nandakumar, 1999)

2.6 Discharge coefficient

The discharge coefficient for an orifice plate can be defined as the ratio between the actual and theoretical volumetric flow rate. Mathematical expression for discharge coefficient is given as:

$$C_d = \frac{Q_{actual}}{Q_{theo}} \qquad \text{Equation 2.60}$$

The theoretical volumetric flow rate can be calculated by using the Bernoulli equation if the followings are assumed:

- One dimensional axial flow;
- constant static pressure upstream of the orifice plate and,
- constant static pressure at the plane of *vena contracta*.

The discharge coefficient is a function of the orifice thickness to diameter ratio, β ratio and Reynolds number Re (Sahin et al., 2004):

$$C_d = f\left(Re, \beta, \frac{t}{d}\right) = f\left(\frac{\rho U_{avg} D}{\mu}, \frac{d}{D}, \frac{t}{d}\right) \quad \text{Equation 2.61}$$

For orifice flows Equation 2.51 is simplified as follows:

$$P_1 + \frac{1}{2}\rho V_1^2 = P_2 + \frac{1}{2}\rho V_2^2 \quad \text{Equation 2.62}$$

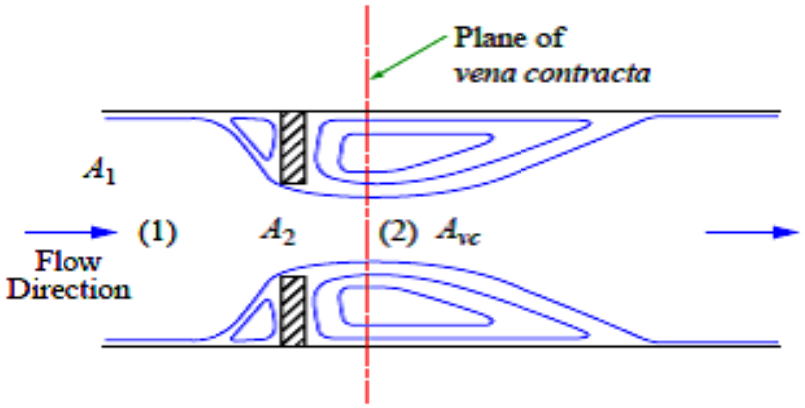

Figure 2.18 Definition of discharge coefficient (ESDU, 2007)

P_1 is the static pressure at section A_1 of Figure 2.18 and P_2 is the static pressure at section A_{vc} of Figure 2.18.

If Equation 2.62 is used to define theoretical volumetric flow rate, then the following can be said:

$$Q_{theo} = V_1 A_1 = V_2 A_2 \quad \text{Equation 2.63}$$

From Equation 2.62 and 2.63 it follows that:

$$Q_{theo} = \frac{\frac{\pi}{4} d^2 \sqrt{\frac{2\Delta P}{\rho}}}{\sqrt{1-\beta^4}} \quad \text{Equation 2.64}$$

where $\Delta P = P_1 - P_2$ and is the maximum static pressure drop across the orifice plate and $\sqrt{1-\beta^4}$ is known as the velocity approach factor.

Now by rearranging Equation 2.60 the following equation is achieved:

$$C_d = \frac{Q_{actual}}{\frac{\pi}{4} d^2 \sqrt{\frac{2\Delta P}{\rho}}} \sqrt{1-\beta^4} \qquad \text{Equation 2.65}$$

Discharge coefficient can also be defined as a function of the contraction coefficient, C_c and the velocity coefficient, C_v and can be calculated by using the following equation:

$$C_d = C_v . C_c \qquad \text{Equation 2.66}$$

where,

$$C_c = \frac{A_{vc}}{A_2} \qquad \text{Equation 2.67}$$

A_2 is the orifice area and A_{vc} is the flow area at the *vena contracta* and

$$C_v = \frac{V_{2\,actual}}{V_2} \qquad \text{Equation 2.68}$$

$V_{2actual}$ and V_2 are the actual mean velocity at the *vena contracta* plane and bulk orifice velocity respectively.

An equation for orifice discharge coefficients can be obtained by using the momentum and continuity equations to the orifice flow (Sahin et al., 2004):

$$C_d = \frac{1}{2\sqrt{2}} \left(\frac{1}{\beta}\right)^2 \left(1-\beta^4\right)^{\frac{1}{2}} \frac{1}{\sqrt{\Delta P}} \qquad \text{Equation 2.69}$$

Discharge coefficients are mainly determined empirically. Discharge coefficient data are dependent on a number of factors such as orifice geometry, pipe diameter, pipe Reynolds number, β ratio, tap location etc. Normally, the discharge coefficient has to be determined by iteration because of its dependence on a Reynolds number, itself dependant on the actual volumetric flow rate (ESDU, 2007).

2.7 Pressure tapping arrangement

The accuracy of pressure measurement in order to calculate the discharge coefficient depends profoundly on the location of pressure taps. Different tap arrangements are used and are:

- Flange pressure tappings;
- corner pressure tappings and,
- D and D/2 pressure tappings.

Flange and corner pressure tappings may produce errors in the measurements of pressure drop across the orifice plate. The reason for this is that these tapping arrangements do not take the variation of the orifice geometry into account and measurements may be taken at significant static pressure gradient locations. Figure 2.19 presents a typical schematic diagram of a pipe with flange and D and D/2 tapping arrangements. Where, l_1 and l_2 is the distance of the pressure tapping upstream and downstream of the orifice plate from the orifice upstream face. In all tap arrangements the tap edges are flush to the internal surface of the pipe wall and free from burrs; the edges of the tap holes may be rounded slightly. The pressure tap arrangements for the determination of the discharge coefficient are not appropriate for the determination of a pressure loss coefficient (ESDU, 2007). To determine the discharge coefficient, the largest pressure drop is measured without allowing sufficient length downstream of the orifice plate for pressure recovery occurring in the return of the flow to fully developed conditions (ESDU, 2007).

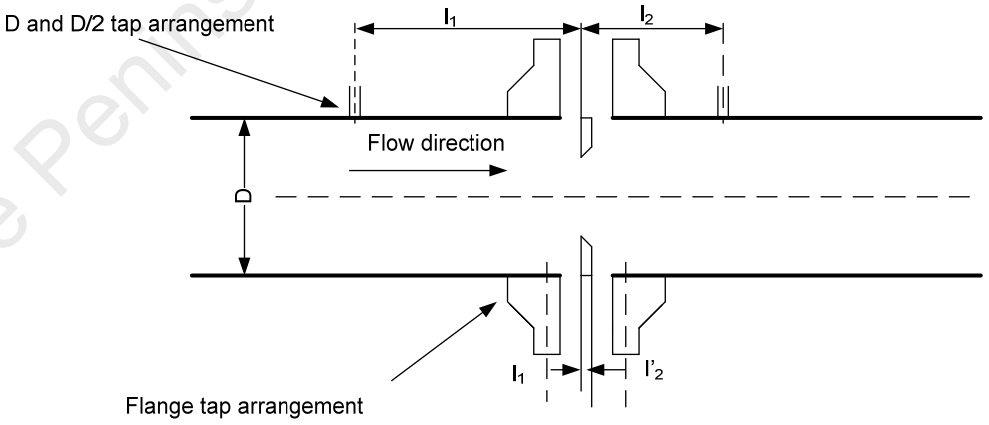

Figure 2.19 Different tap arrangements (ESDU, 2007)

For the corner tapping arrangement the pressure tappings should be either single taps or annular slots. Both types of tappings may be located either in the pipe or its flanges, or in carrier rings as shown in Figure 2.20:

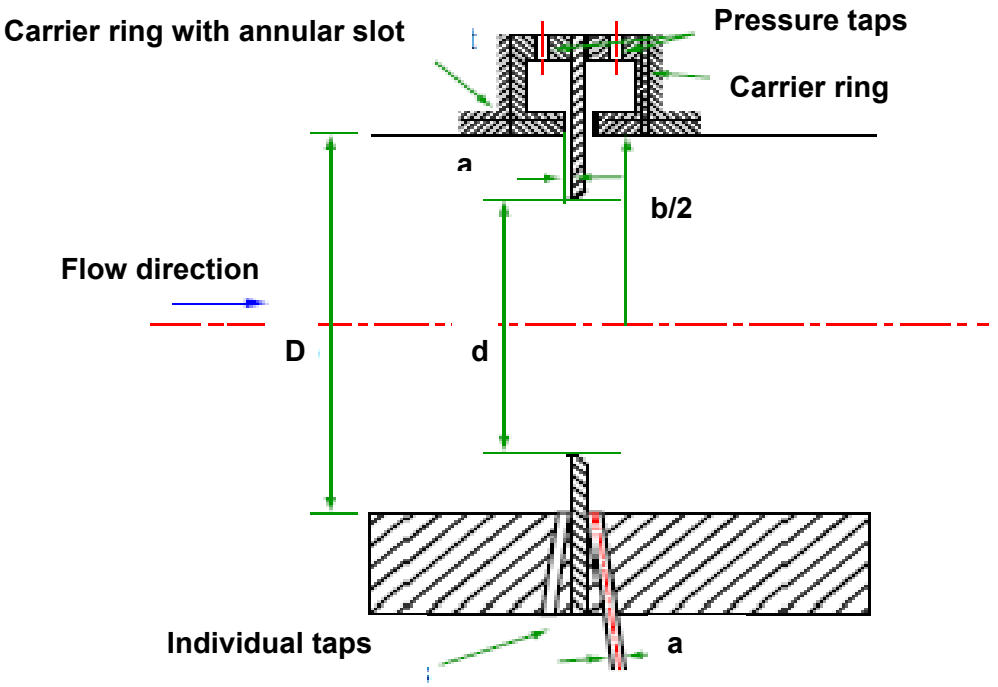

Figure 2.20 Corner tapping arrangement (ESDU, 2007)

The width of the annular slot, a, is specified and presented in Table 2.4 to prevent accidental blockage and give satisfactory dynamic performance. The internal diameter of the carrier ring, b, is to be such that no protrusion occurs in the pipe.

Table 2.4 Details of standard tap location

Tap arrangements	ISO 5167	ASME MFC-3M	ANSI/APi 2530
Flange	$l_1 = l'_2$ l'_2 = 25.4 mm ± 0.5 mm β > 0.6 and D < 150 mm l'_2 = 25.4 mm ± 1 mm (β <0.6 β)	$l_1 = l'_2$ l'_2 = 25.4 mm ± 0.5 mm β > 0.6 and D<150 mm l'_2 = 25.4mm ± 1 mm (β <0.6)	$l_1 = l'_2$ l'_2 = 25.4 mm ± 1.588 mm β ≤ 0.6 and D ≤ 101.6 mm l'_2 = 25.4 mm ± (5.956-6.951 β) for 0.4 < β ≤ 0.75
D and D/2	l_1 = D ± 0.1 D l_2 = 0.5 D ± 0.02 D for β ≤ 0.6 l_2 = 0.5 D ± 0.01 D for β > 0.6	l_1 = D ± 0.1 D l_2 = 0.5 D ± 0.02 D for β ≤ 0.6 l_2 = 0.5 D ± 0.01 D for β > 0.6	----------
Corner	Clean fluids - β ≤ 0.65: 0.005 D ≤ a ≤ 0.03 D - β > 0.65: 0.01 D ≤ a ≤ 0.02 D Any values of : – clean fluids: 1 mm ≤ a ≤ 10 mm vapours, liquefied gases, single tappings 4 mm ≤ a ≤ 10 mm D ≤ b ≤ 1.04 D	Clean fluids - β ≤ 0.65: 0.005 D ≤ a ≤ 0.03D - β > 0.65: 0.01 D ≤ a ≤ 0.02 D Any values of : – clean fluids: 1 mm ≤ a ≤10 mm vapours, liquefied gases, single tappings 4 mm ≤ a ≤10 mm D ≤ b ≤ 1.04 D	----------

2.8 Correlations for predicting different orifice coefficients

Different correlations for predicting pressure loss coefficient and discharge coefficients based on experimental data are given in the open literature for different orifice

geometries. This section of the thesis focuses only on available correlations for long square-edged orifices in the β ratio range of 0.3-0.75.

2.8.1 Correlations for pressure loss coefficient

In turbulent flow, the pressure loss through a long orifice is estimated by applying the Carnot-Borda formula to the losses because of an irreversible expansion process downstream of the *vena contracta* to the orifice wall (theoretical entry loss) and then to the pipe wall (theoretical exit loss). If the loss upstream of the *vena contracta* is assumed to be negligible, the Euler Number for a double expansion is given as (ESDU, 2007):

$$E_u = \left(\frac{1}{C_c} - 1\right) + \left(1 - \beta^2\right)^2 = \left(\frac{1}{C_c} - 1\right) + (1 - \alpha)^2 \qquad \text{Equation 2.70}$$

Dividing both side of Equation 2.70 by β^4 the pressure loss coefficient K_{or} can be achieved and is given as:

$$K_{or} = \left(\frac{1}{C_c \beta^2}\right)^2 - 1 - \frac{2}{\beta^4}\left(\frac{1}{C_C} - 1\right) - 2\left(\frac{1}{\beta^2} - 1\right) = \left(\frac{1}{C_{c\alpha}}\right)^2 - 1 - \frac{2}{\alpha^2}\left(\frac{1}{C_c} - 1\right) - 2\left(\frac{1}{\alpha} - 1\right)$$

Equation 2.71

where, C_c is the contraction coefficient and is defined by Equation 2.67.

Ward-Smith (1971) provides the following correlations which are applicable for a Reynolds number greater than 10000.

a) For 0 < β < 0.75 and t/d < 0.8

$$K_{or} = \left[\frac{1}{0.608\beta^2\left(1 - \beta^{5.2}\right)\left(1 + \left(\frac{t}{d}\right)^{3.5}\right) + \beta^{7.2}} - 1\right]^2 \qquad \text{Equation 2.72}$$

Equation 2.72 has a root mean square error of 9.5%

b) For 0 < β < 0.48 and 0.8 < t/d < 7.1

$$K_{or} = \left[\frac{1}{\beta^2\left(0.872 - 0.015\frac{t}{d} - 0.08\frac{d}{t}\right)\left(1-\beta^{6.6}\right) + \beta^{8.6}\left(1+0.134\left(\frac{t}{d}\right)^{\frac{1}{2}}\right)^{-1}} - 1 \right]^2 \quad \text{Equation 2.73}$$

Equation 2.73 has a root mean square error of 3.8%.

In 1994 Idel'chik et al., provided the following correlation to predict pressure loss coefficients for long square-edged orifice plates. This correlation is valid for Re ≥ 10^5 and 0.015 ≤ t/d ≤ 10, where τ is an empirical constant and range from 0 -1.35:

$$K_{or} = \left[\left(0.5 + \tau\sqrt{1-\beta^2}\right)\left(1-\beta^2\right)^2 + 0.02\frac{t}{d}\right]\left(\frac{1}{\beta^2}\right)^2 \quad \text{Equation 2.74}$$

A table of different K_{or} values in turbulent flow for different β ratios was obtained from the Engineering Science Data Unit and is presented in Table 2.5. The K_{or} values were calculated using Equation 2.74.

Table 2.5 Different K_{or} values using equation 2.74

	K_{or}		
t/d	**β = 0.3**	**β = 0.5**	**β = 0.7**
0.10	303	29.0	4.19
0.20	289	27.7	4.01
0.40	277	27.7	4.01
0.80	205	19.6	2.85
1.00	186	17.8	2.60
2.00	165	15.8	2.34
3.00	165	15.9	2.40
5.00	170	16.6	2.60

In 1997 Hasegawa and his co-workers developed a correlation for square-edged orifice plates. The correlation is valid for β = 0.1, 0 < t/d < 1.2 and in the range of Reynolds number, 1 < Re < 1000:

$$E_u = 2.2 + \frac{K''}{Re_D}$$ Equation 2.75

Bohra (2004) presented the following correlations to predict non-dimensional pressure drop across square-edged orifice plate while accounting for non-Newtonian behaviour. The correlations have a range of applicability:

- 0.32 < t/d < 5.72;
- 0.023 < β < 0.137;
- 0.09 < Re_{ge} < 9677;
- 0.019 < μ_{ge} < 9.589 (pa.s) and,
- 0.19 < μ_{re} < 95.89.

a) For Reynolds number ≥ 6

$$E_u = \left[\left\{ \left(\frac{1}{Re_{ge}^{0.882}} \right) \left(64 \times \left(\frac{t}{d} \right)^{1.159} \beta^{0.075} \mu_{re} - 0.334 + 17.16 \times \Pi \right) \right\}^3 + \left\{ \frac{1-\beta^4}{c^2 d} \right\}^3 \right]^{\frac{1}{3}}$$ Equation 2.76

b) For Reynolds number < 6

$$E_u = \left(\frac{1}{Re_{ge}^{1.203}} \right) \left(64 \times \left(\frac{t}{d} \right) \right)^{1.502} \mu_{re} - 0.470 + 36 \times \pi$$ Equation 2.77

Figures 2.21 and 2.22 illustrate the ranges of diameter ratio and pipe Reynolds number covered by experimental, numerical pressure loss coefficient data and correlations available in the literature.

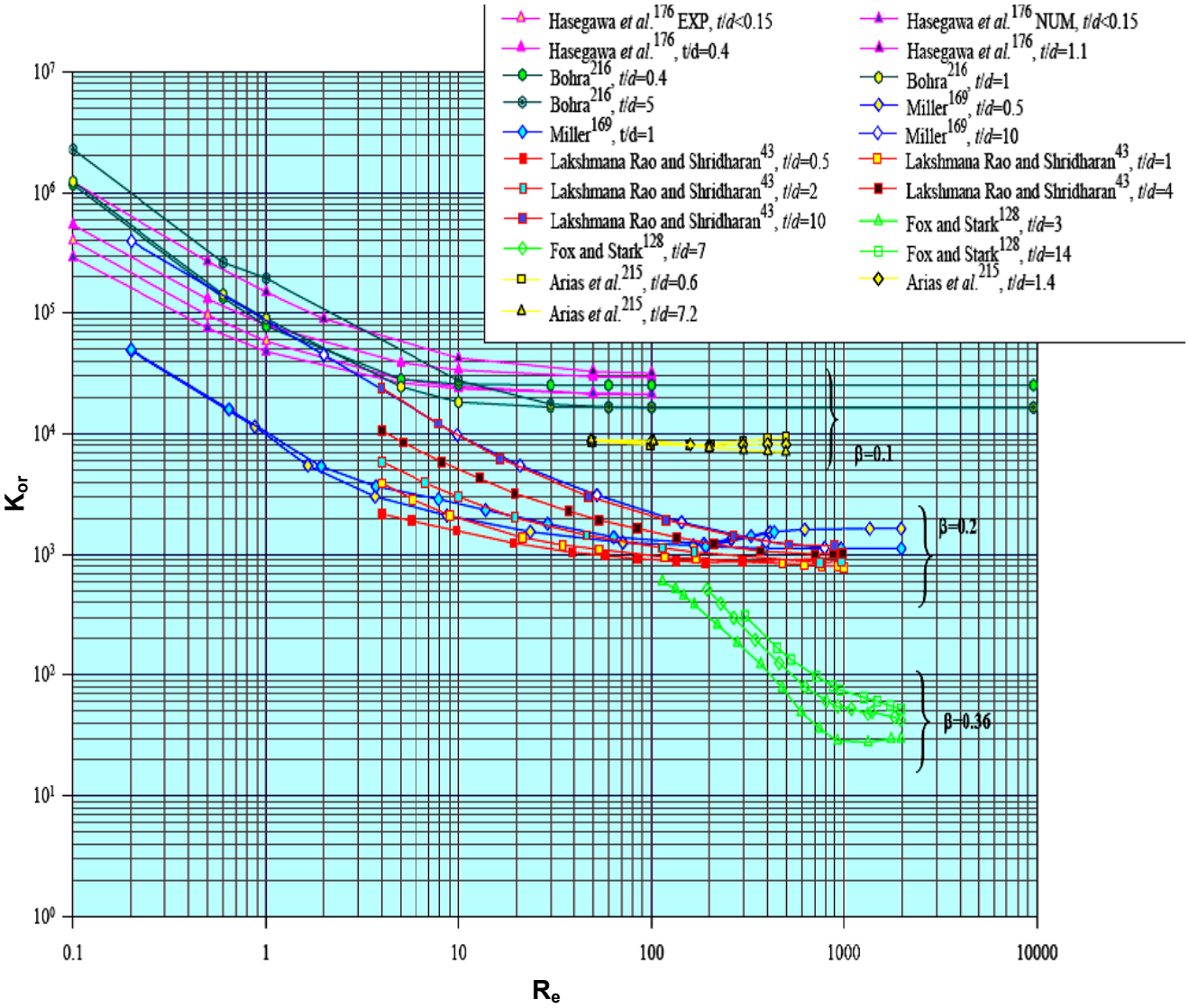

Figure 2.21 Availability of pressure loss coefficient data (ESDU, 2007)

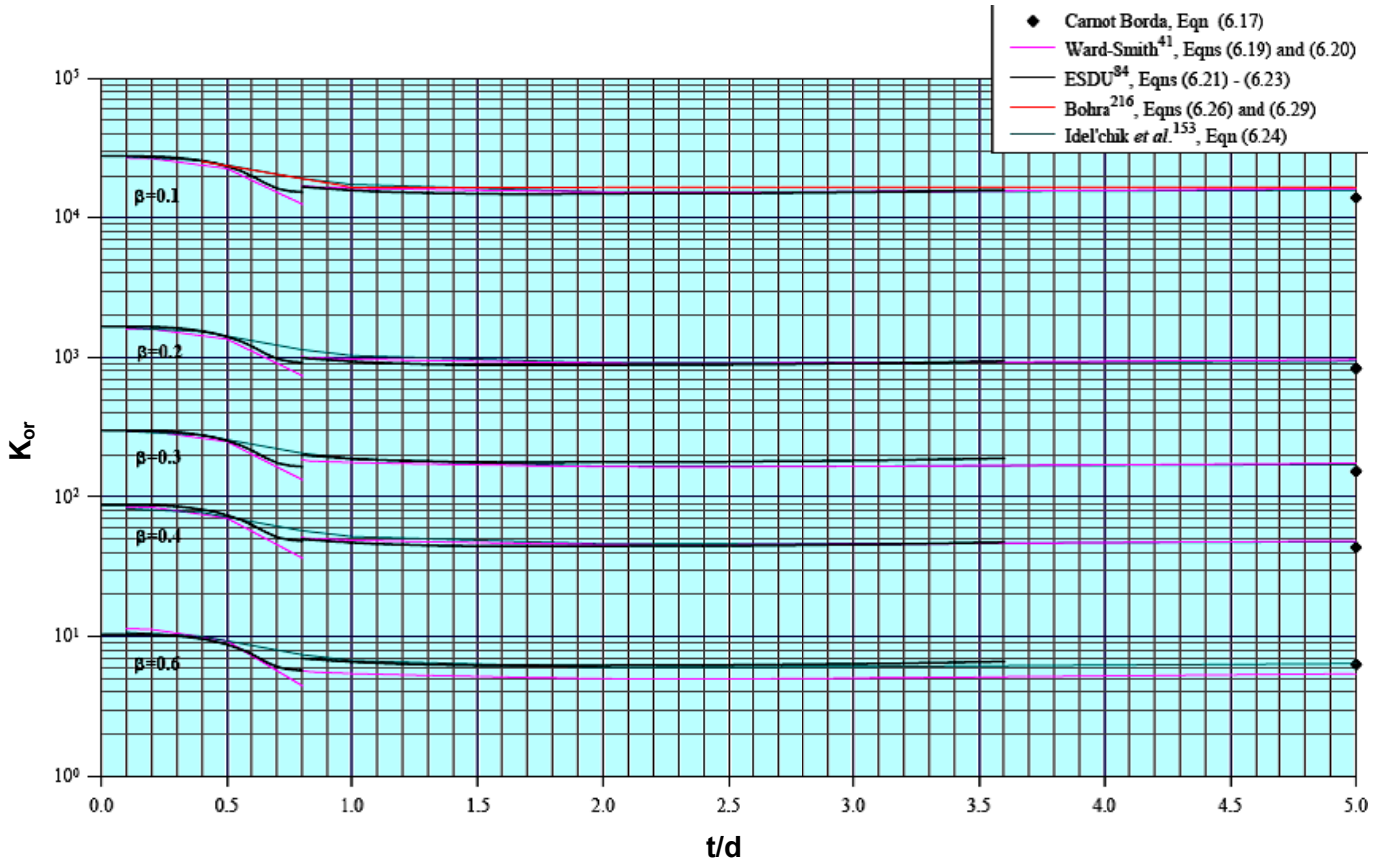

Figure 2.22 Pressure loss coefficient data obtained using correlations (ESDU, 2007)

2.8.2 Correlations for discharge coefficient

Hall (1963) derived semi-empirical correlation for predicting discharge coefficients in turbulent flow. The equation holds true for a thickness to diameter ratio range of $0 \leq t/d \geq 10$:

$$C_d = 1 - 0.184\left(\left(\frac{t}{d}\right) - 1 + k(\beta(Re_d{}^{0.25}\right)^{0.8} Re_d{}^{-0.2} \qquad \text{Equation 2.78}$$

The values of $k(\beta)$ varies with β. Table 2.6 presents the different $k(\beta)$ values.

Table 2.6 Value of $k(\beta)$ (Hall, 1963)

β	0.00	0.10	0.20	0.30	0.40	0.50	0.60	0.70	0.80	0.90
$k(\beta)$	1.11	1.11	1.09	1.06	1.03	0.99	0.919	0.83	0.71	0.52

Equation 2.78 is based on the following assumptions:

- One seventh power law of the turbulent velocity and,
- the discharge coefficient is related to the boundary layer displacement thickness, δ^*, defined as-

$$\delta^* = \int_0^{\delta} \left(1 - \left(\frac{u}{u_{cl}}\right)\right) dy \qquad \text{Equation 2.79}$$

From Equation 2.79 the following is derived:

$$C_d = \left(1 - 2\frac{\delta^*}{d}\right)^2 \qquad \text{Equation 2.80}$$

In the laminar flow régime ($1 < Re_d < 150$), β ratio of 0.5 and $0.0625 \leq t/d \leq 1$

Sahin and Ceyhan (1996) provides the following correlation for predicting discharge coefficient:

$$C_d = \frac{1}{2\sqrt{2}}\left(\frac{1}{\beta}\right)^2 \sqrt{1-\beta^4}\sqrt{\frac{\rho u^2_{cl}}{\Delta p}} \qquad \text{Equation 2.81}$$

Swamee (2005) derived an explicit correlation using a method of curve fitting which eliminates any iterative process:

$$C_d = 0.5 + 0.43\left(\frac{d}{D}\right)^2 + 0.25\left[1 + \left(\frac{d}{D}\right)^3\right] v_*^{0.145} \qquad \text{Equation 2.82}$$

Equation 2.82 is sufficiently accurate for all practical purposes. For flow with a high Reynolds number viscous effects are negligible and in such case Equation 2.82 reduces to:

$$C_d = 0.5 + 0.43\left(\frac{d}{D}\right)^2 \qquad \text{Equation 2.83}$$

Figures 2.23 and 2.24 illustrates the ranges of diameter ratio, aspect ratio and pipe Reynolds number covered by experimental discharge coefficient data and correlations available in the literature.

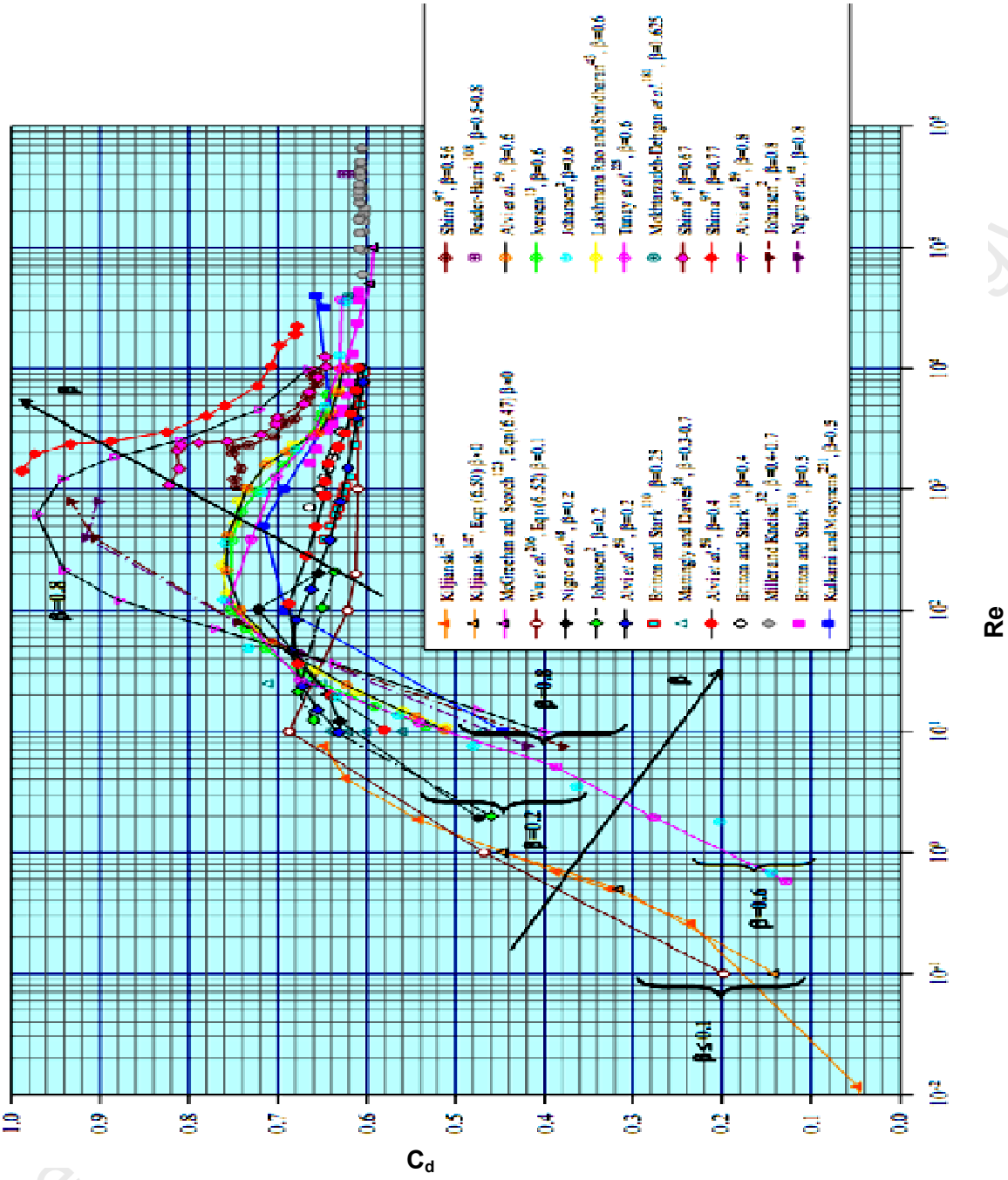

Figure 2.23 Available experimental discharge coefficient data against Reynolds number (ESDU, 2007)

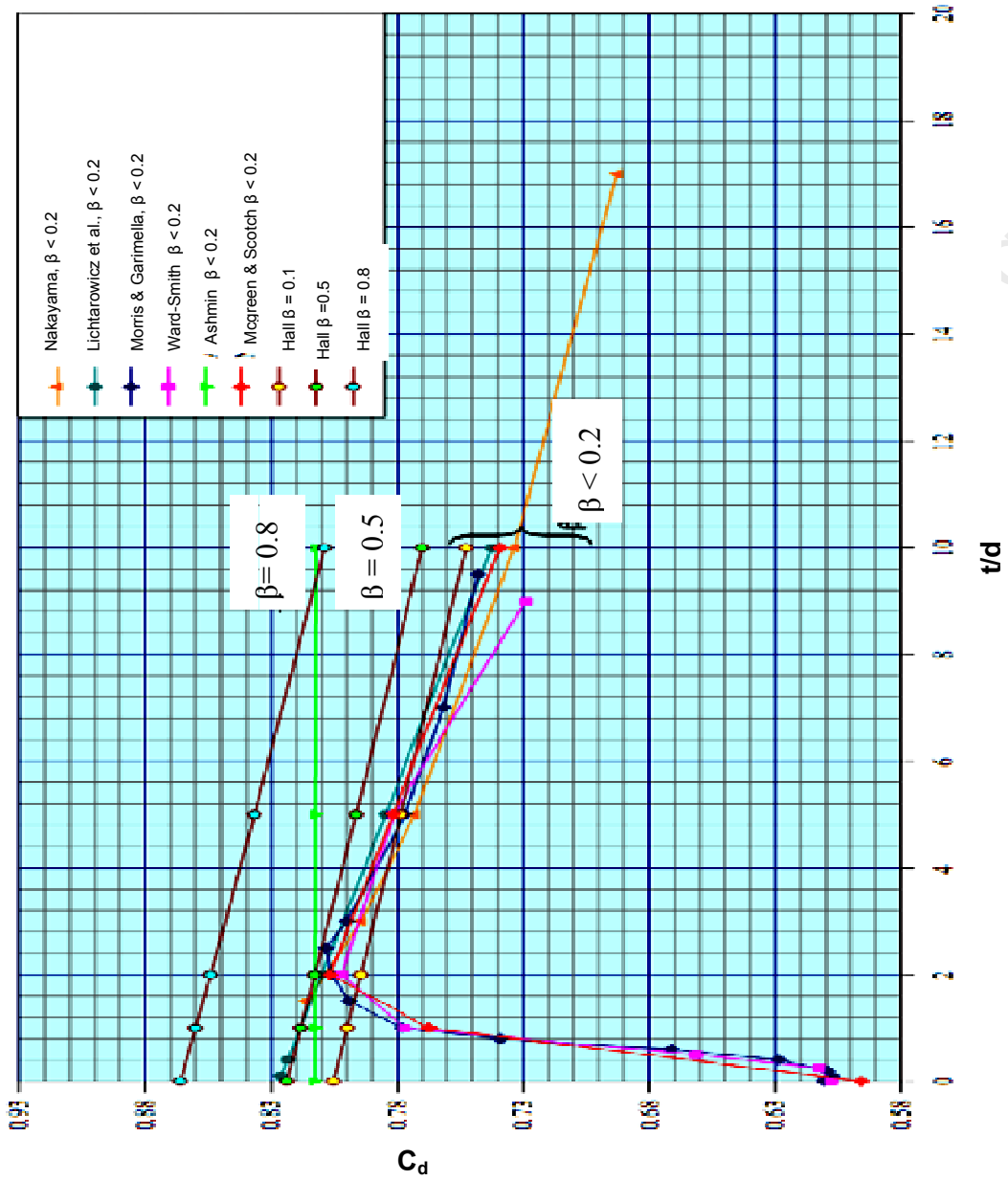

Figure 2.24 Available experimental discharge coefficient data against aspect ratio (ESDU, 2007)

2.9 Effects of non-standard orifice fittings

The prediction of discharge coefficient and the accuracy of the flow measurement are greatly affected by non-standard fittings and operating conditions. According to Bower (1995) a discharge coefficient error within ± 2% occurs because of non-standard installation. The most significant factors affecting the flow measurement accuracy depends on the following factors:

- Fluid properties;
- flow conditions;
- orifice fitting defects;
- orifice edge;
- recesses and protrusions and,
- pressure measurement.

2.9.1 Orifice fitting defects

A brief description of some common types of orifice fitting defects and non-standard fittings is presented in this section. The effect of non-standard fittings is also reviewed here.

2.9.1.1 Plate eccentricity

The parallel or longitudinal to the pressure tap axis eccentricity, e_{cl}, and perpendicular to the pressure tap axis eccentricity, e_{cn}, are allowed by the ISO 5167 (2002), ASME MFC-3M (2004) and ANSI/API 2530 (1995) standards:

$$e_{cl} \leq \frac{0.0025\,D}{0.1+2.3\beta^4} \qquad \text{Equation 2.84}$$

$$e_{cn} \leq \frac{0.005\,D}{0.1+2.3\beta^4} \qquad \text{Equation 2.85}$$

Where, e_{cl} and e_{cn} are the following,

$$e_{cl} = \frac{A - A'}{2} \qquad \text{Equation 2.86}$$

$$e_{cn} = \frac{B - B'}{2} \qquad \text{Equation 2.87}$$

The variables in Equation 2.86 and 2.87, A, A', B and B' are explained graphically in Figure 2.25 .

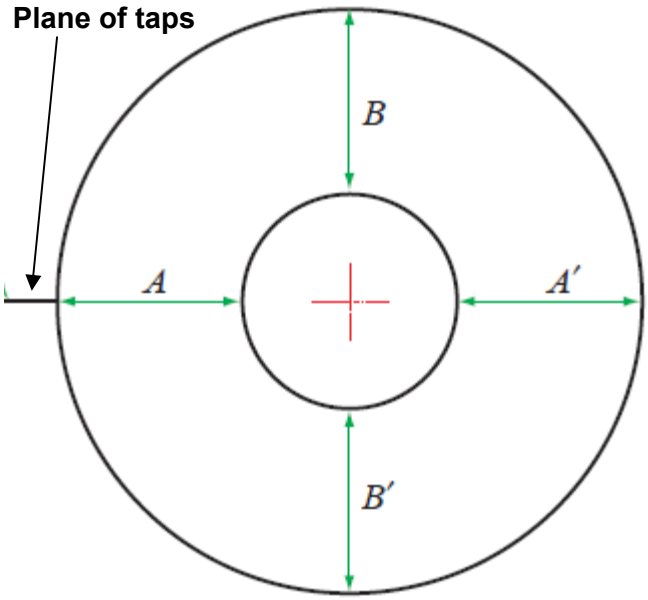

Figure 2.25 Eccentricity definition (ANSI/API, 1995)

The effect of eccentricity depends on β and the effect is smaller for larger β (Miller & Kneisel, 1969). According to Miller (1996) the maximum allowed eccentricity according to the standards can rise up to 1% if an additional uncertainty of 0.5% is acceptable for the discharge coefficient. The eccentricity toward the pressure tap causes the largest change on the discharge coefficient, the eccentricity normal to pressure tap causes the least influence on discharge coefficient. The effect of plate eccentricity on the discharge coefficient is considered not appreciable by Lakshmana Rao and sridharan (1972) and Ho and Leung (1985).

2.9.1.2 Seal gap, recess/protrusion

Kendrik (1997) states that no seal protrusion should be allowed. For seal gaps greater than 0.25 inches, the seal inner diameter must be 0.25% of the measured orifice bore. For seal gaps smaller than 0.25 inches, the seal is noted as recess and its inner diameter can be any amount larger than the orifice bore. The effect of protrusions at any location upstream or downstream of the orifice plate is significant and causes an increase in discharge coefficient which increases with the protrusion height and orifice bore diameter ratio. The effect of the protrusion is higher upstream of the orifice plate than downstream of orifice plate. The greatest effect is caused by protrusions adjacent

to the plate (Zedan & Teyssandier, 1985). ISO 5167 (2002) standard requires the upstream pipe steps to be less than 0.3% of pipe diameter.

2.9.1.3 Deposit of film coating

Deposits of fluids or scale cause a change in discharge coefficient over time and uncertainties outside those given in the standards. Morrow (1999) stated that a 1.6 mm layer of grease on an orifice plate can cause a 16% error. Compressor lubrication oil can form a thin liquid coating on an orifice meter surface, which, especially in the upstream section, can produce significant measurement errors.

2.10 Research studies based on orifices

This section serves as background to the orifice flow concept. Substantial work has been completed on the prediction of pressure losses in a piping system. A brief review of the work relevant to the investigation is discussed, with a short description and a summary of findings obtained.

Discharge coefficient data for sharp-edged circular orifice plates with β ratio varying from 0.2 to 0.8 were determined by Johansen (1930) for Reynolds number values in the range of $0 < Re \leq 5.7 \times 10^4$. The experimental results indicate that a variation in β ratio in turbulent flow does not vary the discharge coefficient in high range. Sahin and Akilli (1997) later confirmed the experimental results which compared favourably for the β ratio of 0.2 to 0.8 and having a constant thickness to diameter ratio of 0.06.

Kittredge and Rowley (1957) determined the loss coefficients experimentally in the laminar zone for common pipe fittings. They also concluded that an increasing friction coefficient with decreasing Reynolds number in laminar flow is by the disappearance of induced turbulence. They also reported losses for bends at low Reynolds numbers which are less than those caused by an equal length of straight pipe.

Hall (1963) published discharge coefficient data for long square-edged orifices with β and aspect ratio of 0.5 and 5 respectively. The author also published a correlation to

predict discharge coefficients for a β ratio range of 0.1 – 1. The published model is applicable only to the turbulent flow régime and for $Re_d \geq 10^4$.

Lakshmana Rao and Sridharan (1972) obtained pressure loss coefficients for five sharp square-edged long orifices with a constant β ratio of 0.2, varying the thickness to diameter ratio from 0.48 to 10.11. The author concluded that laminar friction loss increases with the increase in orifice thickness.

The critical Reynolds number at which flow downstream of an orifice or nozzle becomes turbulent or fully developed flow was determined by Lakshmana Rao et al., (1976) for 22 orifices and nozzles. The authors found two criteria to be uniformly applicable. The first criterion was based on the variation of the excess loss and a second was based on the variation of the pressure recovery length downstream of the orifice.

Durst et al., (1987) and Durst and Wang (1989) used 1-D LDV and numerical studies to investigate the flow through square-edged orifice plates in laminar and turbulent flows. They established that small recirculation upstream of the orifice plate and downstream recirculation with re-attachment length varied with Reynolds number. Also, secondary downstream recirculation bounded by main recirculation with extension and axial velocity overshoot in the orifice.

Reader-Harris et al., (1995) carried out experiments to establish the permissible steps in pipe work upstream of orifice plates. The authors found that if the first fitting is placed 10D upstream of the orifice plate, the existing requirements are unduly restrictive and that expansion steps of up to 2% of D and contraction steps up to 6 % of D can be permitted.

Different orifice geometries were studied by Zhang and Chai (1999) in order to minimize pressure drop. The authors concluded wall pressure distributions are strongly affected by the geometry of an orifice plate. Both sharp-edged and stream-lined orifice plates are able to meet energy dissipation requirements in a discharge conduit. A large pressure drop is however expected. An optimal orifice dissipater possesses a geometry which is neither sharp-edged nor streamlined.

Pressure losses in orifices for the flow of gas-non-Newtonian liquids were determined by Samanta et al., (1999) using sodium carboxymethyl cellulose (SCMC) and air. They derived a generalised correlation for predicting single and two-phase frictional pressure losses across orifices for non-Newtonian and gas-non-Newtonian liquid flows.

In 2001 Darin et al., found errors from transmitter inaccuracy and calibration irregularities varied with the measured pressure drop and ranged from 35% at a pressure difference in the order of 249 Pa to 1% at a pressure difference of the order of 24909 Pa. The authors recommended that for all β ratios a pressure difference less than 149 Pa should always be avoided. The dominant source of uncertainty shifted from measurement accuracy to turbulent flow fluctuations as the β ratios reduced, so the lower limit to produce errors within the standard uncertainty band, exhibited a local minimum.

Pressure drop characteristics of viscous fluid flow through orifices were studied by Bohra (2004). The author observed high viscous fluids flow could remain laminar, even at higher flow rates. He also found that the influence of aspect ratio decreased as higher Reynolds number was approached.

In 2004 Sahin and his co workers investigated the effects of the square-edged circular orifice plate thickness and Reynolds number on the flow characteristics using CFD analysis for both laminar and turbulent flows. The investigation was conducted by keeping the β ratio constant at 0.6 and varying the thickness to diameter ratio in the range of $0.08 \leq t/d \leq 1$ and for the Reynolds number range of $0 \leq Re \leq 2 \times 10^5$. The authors concluded that the discharge coefficient values were more sensitive to Reynolds number in the range of smallest values of thickness to diameter ratio. In turbulent flow the discharge coefficient values were higher for thicker orifice plates. The flow characteristics occurring in the forward face of the orifice plate did not show much variation for varying thickness of orifice plates.

A review published by ESDU (2007) identified the lack of pressure loss coefficient and discharge coefficient data in the open literature. It established experimental pressure loss and discharge coefficient for long square-edged orifices data for β ratio of 0.36, 0.4, 0.5 and 0.7 which had not been previously accomplished.

The effect of non-Newtonian fluid rheology on the performance of simplex atomisers, were investigated by Jog et al., (2008). The authors considered laminar flow of purely viscous shear thinning power law fluids. For the range of power law fluids studied, it was found that the discharge coefficient increased with the decrease of power law index. The variations in discharge coefficients for shear thinning fluid were slightly weaker. Since the flow and performance parameters varied with, the power law index, the discharge coefficient could be controlled by changing the fluids rheological properties.

2.11 Conclusions

The basic theory and literature regarding flow through orifices in terms of methods of calculating pressure loss coefficients, discharge coefficients, errors etc. has been reviewed. The literature shows various experimental and numerical methods used to study flow through long square-edged orifices. However, it was found that no correlation exists to predict loss coefficients in laminar flow for long square-edged orifices with larger β and aspect ratio. The review paper published by ESDU (2007) shows a lack of experimental loss coefficient data for β and aspect ratio of 0.36, 0.5 and 0.7 and 4, 5 and 5 respectively. Discharge coefficient data and correlations are insufficient for long square-edged orifices. No experimental discharge coefficient data in laminar flow was found in literature for β = 0.36, 0.5 and 0.7.

2.12 Research topics identified

From the literature review the following research topics were identified:

- Determination of experimental pressure loss coefficients for long square-edged orifices with β and aspect ratio of 0.36, 0.5 and 0.7 and 4, 5 and 5 respectively;
- determination of experimental discharge coefficients in laminar flow especially for β and aspect ratio of 0.36, 0.5 and 0.7 and 4, 5 and 5 respectively and,
- development of a correlation to predict pressure loss coefficients and discharge coefficients in laminar to turbulent flow for long square-edged orifice plates.

This work will address all these topics, except for the development of a correlation for predicting discharge coefficients.

CHAPTER 3

3.1 Introduction

In this section the methods of investigation and apparatus used to obtain loss and discharge coefficient data are described. A detailed description of the orifice test rig is also provided in this chapter. Different error analysis equations are also presented. The objective of this experimental work was to conduct:

- Accurate in-line rheological characterisation of all the slurries, using tube viscometry (three pipe diameters) and,
- accurate pressure drop measurements, to determine loss and discharge coefficient data.

An important aspect of the experiments was that the identical slurry was used to test all orifices of different β ratios and thicknesses.

3.2 Description of the orifice test rig

The experimental rig consisted of five lines of PVC pipes with diameters ranging from 46 mm to 100 mm internal diameter (ID). Each line was 25 m long, to allow a fully developed flow before and after each test orifices. Test fluids were mixed in a 1.7 m^3 mixing tank. The tank was rubber-lined to avoid chemical reactions of fluid with metal. The fluids were circulated in a continuous loop, as follows:

- Fluids were pumped out with a positive displacement pump from the mixing tank.
- A heat exchanger was used to maintain the slurry temperature. Fluids were pumped through a heat exchanger before being pumped to the test sections. The heat exchanger was followed by two valves coupled in parallel that directed the flow either to the top part of the rig (which contained smaller pipes 50, 63 and 2 x 46 mm) or the lower part (which contained a larger pipe, 100 mm ID).
- Each of the two routes was fitted with a flow meter. After the flow meters the fluids could enter any of the five test sections.
- An on/off valve was situated at each end of every test pipe for isolation so that only one line was tested at a time. A similar setup was created at the end of each test section.

- After a fluid passed through a test section it was collected via a common pipe and directed to a mixing tank. The two flow meters (50 mm and 65 mm bore diameter, maximum flow rate of 5 and 11 l/s respectively) were installed in the common pipe to ensure accurate flow rate measurements over a wide range. At the outlet it was possible to divert the fluid through a weigh tank used for calibration purposes.

A schematic of the test rig is given in Figure 3.1:

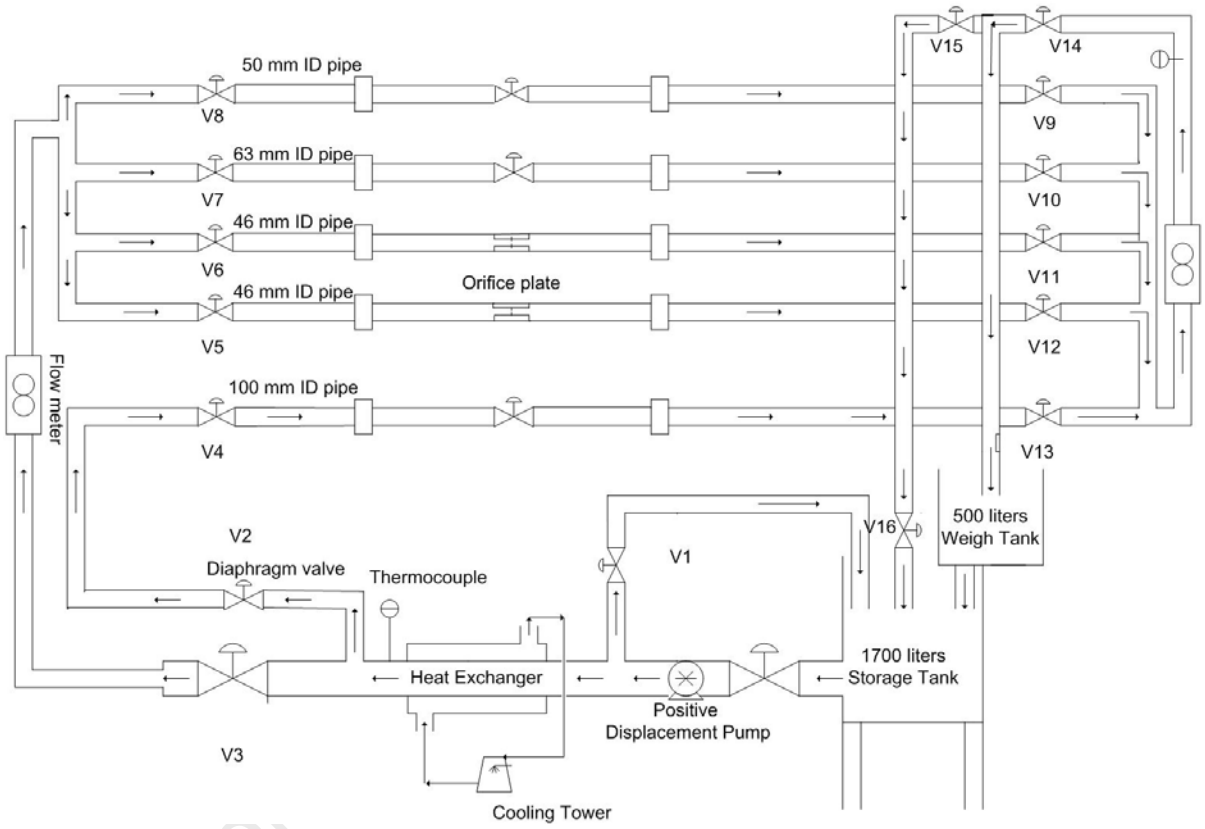

Figure 3.1 Schematic diagram of the experimental setup

3.3 Instrumentation

This section presents all the instruments used to attain pressure drop data.

3.3.1 Pressure transducers

A point pressure transducer (PPT) and a differential pressure (DPT) transducer were used to measure the static and differential pressure in the test sections respectively.

Pressure gradients were measured with a set of 11 point pressure transducers of the type PHPWO1V1-AKAYY-OY [GP] version 25.0 (Fuji Electric). The instruments had a maximum range of 130 kPa to 500 kPa with a precision of 0.25 %. The output of these instruments was a DC current ranging from 4 to 20 mA, proportional to the pressure applied. The range and span of these instruments were adjusted by a handheld communicator (HHC).

Two DP transducers of the type IKKW35VI-AKCYYAA [DP], version 25.0 (Fuji Electric), with a maximum range of 6 kPa and 130 kPa respectively were used to measure differential pressures. The cells had the same characteristics as the PPT's, i.e. a precision of 0.25 %, and could be adjusted with a handheld communicator.

All pressure tappings were connected to 3 mm Nylon tube pressure lines filled with water. The pressure from the test point was transmitted to the pressure transducers by opening a valve connecting the tapping to the pressure line. The valves, as well as the pressure tappings, were numbered. Solids pods were installed between the pressure tappings and the pressure line to collect any solid particles within the test fluid, to prevent them from entering the pressure lines and transducers. Each pod was fitted with a valve on top for flushing away air bubbles and at the bottom for flushing away any solid particles or viscous fluids to a collecting gutter. A schematic diagram of the pod is presented in Figure 3.2.

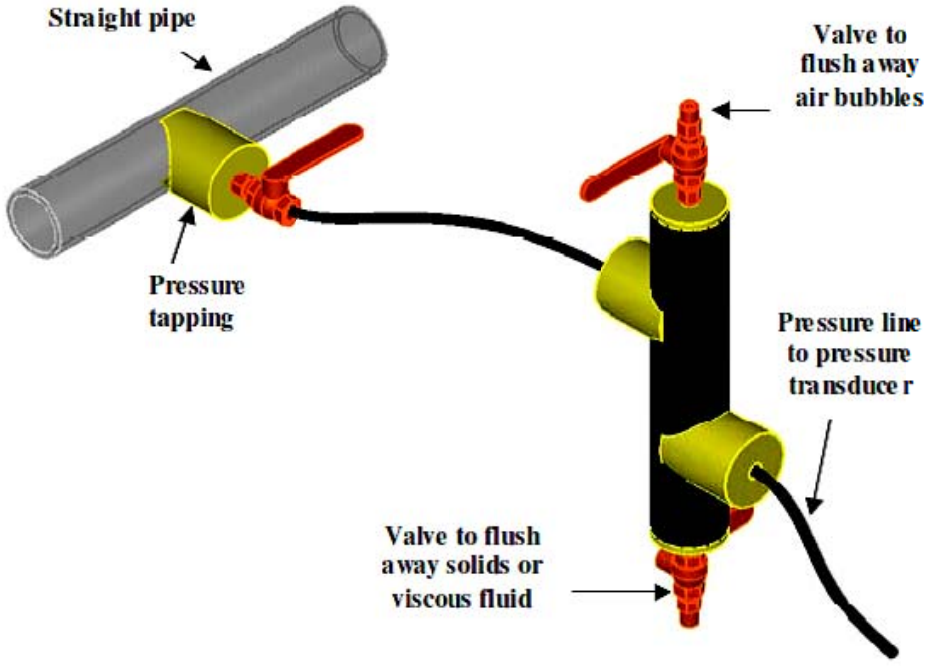

Figure 3.2 Pressure tapping, solids pod and connection to pressure transducer (Pienaar, 2004)

Table 3.1 presents the axial distances of the pressure tappings from the orifice upstream and downstream faces used in the study.

For each pipe the non-dimensionalized axial distances and the distances from the first point were recorded as illustrated in Table 3.1. The negative points for the non-dimensionalized axial distance refer to the points upstream the orifice plate.

Table 3.1 Different tapping locations

		Upstream						Downstream				
Beta ratio	**Tapping No.→**	**1**	**2**	**3**	**4**	**5**	**6**	**7**	**8**	**9**	**10**	**11**
0.36	**axial distances**	-6.99	-4.66	-3.77	-2.39	-0.10	-0.06	0.06	2.38	4.68	6.98	9.28
	Distances [m]	0.00	-2.33	-3.22	-4.60	-6.89	-6.93	7.05	9.37	11.67	13.97	16.27
0.5	**axial distances**	-6.99	-4.69	-3.77	-2.40	-0.11	-0.09	0.08	2.39	4.69	6.99	9.29
	Distances [m]	0.00	-2.30	-3.22	-4.60	-6.89	-6.91	7.07	9.38	11.68	13.98	16.28
0.7	**axial distances**	-7.03	-4.73	-3.81	-2.44	-0.14	-0.11	0.11	2.33	4.63	6.93	9.24
	Distances [m]	0.00	-2.30	-3.22	-4.60	-6.89	-6.93	7.14	9.36	11.66	13.96	16.27

3.3.2 Handheld communicator (HHC)

A Fuji electric handheld communicator, type FXY 10AY A3, was used. This portable instrument was connected to the PPT or DP transducer to change parameters such as: Data display, range, span, time constant, units, calibration, etc. It was used mainly to change the ranges and to calibrate the transducers.

3.3.3 Data acquisition unit (DAU)

A Hewlett Packard (HP) data acquisition unit (DAU) (type HP 34970A) was connected to a computer. The data acquisition unit (DAU) received analogue signals through various channels from different parts of the rig and converted the analogue signals to digital signals compatible with the central PC. The central PC used was a Dell Optiplex 745 with Core 2 Duo processor. Test programmes were written in Visual Basic 6.

3.3.4 Flow meters

Two magnetic flow meters were installed vertically on the test rig:

- A Krohne IFC 010D of 50 mm internal diameter with a maximum flow rate output of 5 l/s and,
- a Krohne Optiflux 4000 of 65 mm internal diameter with a maximum flow rate output of 11 l/s.

3.3.5 Load cell and weigh tank

A load cell and weigh tank, (bucket and stop watch method), was used to obtain fluid flow rates for comparison purposes with the electromagnetic flow meters. The output voltage of the load cell varied linearly with the applied force and was proportional to the input voltage. The resistors were connected to a power supply connected to the data acquisition unit (DAU). The input voltage divided by the output voltage gave a non-dimensional load cell reading independent of input voltage. An accurate calibration of the load cell was essential and that procedure is given in section 3.4.1.1.

3.3.6 Pump

A progressive cavity positive displacement pump (B9602-C1 EN8N1T), driven by a 15 kW electric motor, was used to circulate the fluid in the test loop. The pump was connected to a Yaskawa VSD, (variable speed drive) of type (V1000) to obtain the desirable flow rates. A maximum flow rate of $\approx$ 7 l/s was used for the test runs to prevent cavitation. Because of its destructive effects, the phenomenon of cavitation has been something designers strive to eliminate (Moseley et al., 1975).

3.3.7 Heat exchanger

A double pipe heat exchanger was installed at the inlet of the rig to keep the test fluids at constant temperature.

3.3.8 Mixer

A mixer driven by a 3 kW electric motor was installed in the mixing tank. The mixer was used during the test to ensure the fluid particles remained suspended.

3.3.9 Long orifices

Three differently sized sharp square-edged orifices were machined from Perspex in the Mechanical Engineering workshop of the Cape Peninsula University of Technology. The orifices were machined using a high speed drill. They were drilled out from the orifice exit face to prevent the formation of burrs. It was shown by Ohrn et al., (1991) that variations in the nature of a sharp-edged entry might give rise to considerable variations in the discharge coefficient. The orifice dimensions are presented in Table 3.2 and a schematic diagram presented in Figure 3.3. For illustration purposes, a photograph is also presented in Figure 3.4.

Table 3.2 Different orifice dimensions

Orifice bore diameter, d, (mm)	β ratio	Orifice bore thickness, t, (mm)	t/d ratio
16.56	0.36	66.21	4.00
23.00	0.50	115.00	5.00
32.00	0.70	161.00	5.00

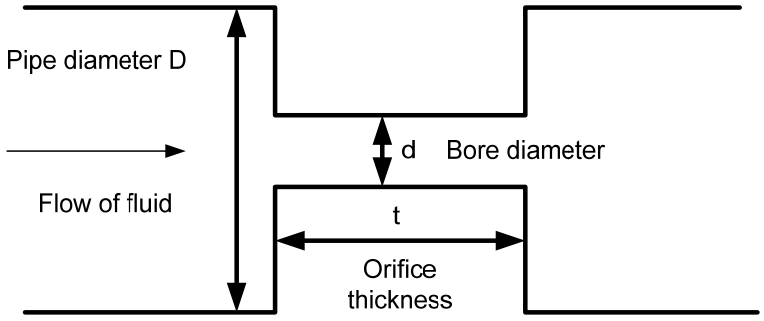

Figure 3.3 Schematic of a long square-edged orifice

Figure 3.4 Photograph of a long (tube) square-edged orifice

3.4 Experimental procedures

In this section the procedure used to collect pressure drop data is presented. It consists of the calibration of different instruments, slurry density tests, pipe internal diameter test, conducting tests to measure the viscous properties of fluids and also performing tests to measure different orifice pressure drop data.

3.4.1 Calibration procedures

The aim of the calibration was twofold: firstly, to ensure measuring instrument readings were valid (normally accomplished by double checking the measurement against other devices) and secondly, to ensure readings appearing on the PC via the DAU were as close as possible to actual readings.

3.4.1.1 Load cell

Procedure followed for the load cell calibration was:

1. The calibration program was loaded on the computer;
2. channel 118 on the DAU was selected, dedicated to capture the voltage induced on the load cell;

3. the water flow was diverted into the weigh tank and filled up to a prescribed level;
4. the water flow was redirected to the mixing tank;
5. voltage indicated on the DAU was recorded; a bucket was used to collect all water from the weigh tank and weighed on the portable scale;
6. steps 4 to 5 were repeated for different water levels and,
7. plots were made of weight versus voltage to determine the slope and the intercept of the linear relationship.

To begin the calibration of the load cell, the weigh tank, was emptied. Nothing was permitted to disturb the tank. The linear relationship of the weight versus the voltage for load cell calibration is provided in Figure 3.5.

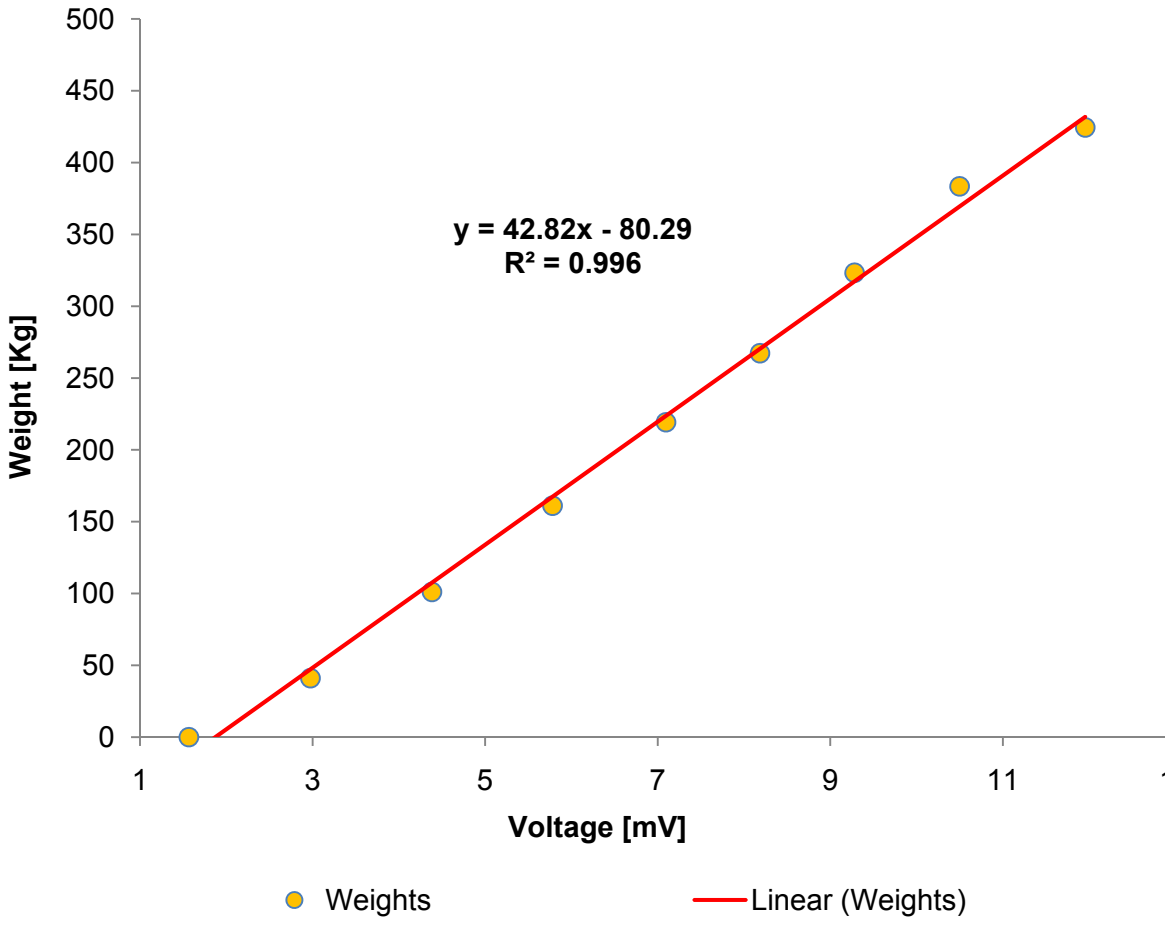

Figure 3.5 Calibration constants for load cell

3.4.1.2 Flow meter

The following steps were followed in calibrating the flow meter:

1. The flow meter calibration programme was loaded on the computer and channel 118 on the DAU was selected;
2. the time interval at which the weight of the tank should be recorded by the computer program was chosen;
3. water was pumped through the Krohne flow meter and into the weigh tank;
4. the valve at the bottom of the weigh tank was closed to accumulate water;
5. the computer programme was begun and halted when the tank is almost full;
6. the voltage reading on the DAU was recorded;
7. the weigh tank was emptied by opening the valve at the bottom of the tank;
8. the speed of the pump was varied to change the flow rate of water through the rig;
9. steps 4 to 8 were repeated to record another set of data.
10. Similar procedure was followed to calibrate another flow meter.

The mass flow rate through the flow meters were determined as the ratio of the recorded mass of the weigh tank to the time it took to fill it, also known as the 'bucket and stopwatch' method. It was converted to the volumetric flow rate by dividing the ratio with the density of water at its recorded temperature.

Figure 3.6 indicates good agreement for water flow rate between the 'bucket and stopwatch' method and the electromagnetic flow meter.

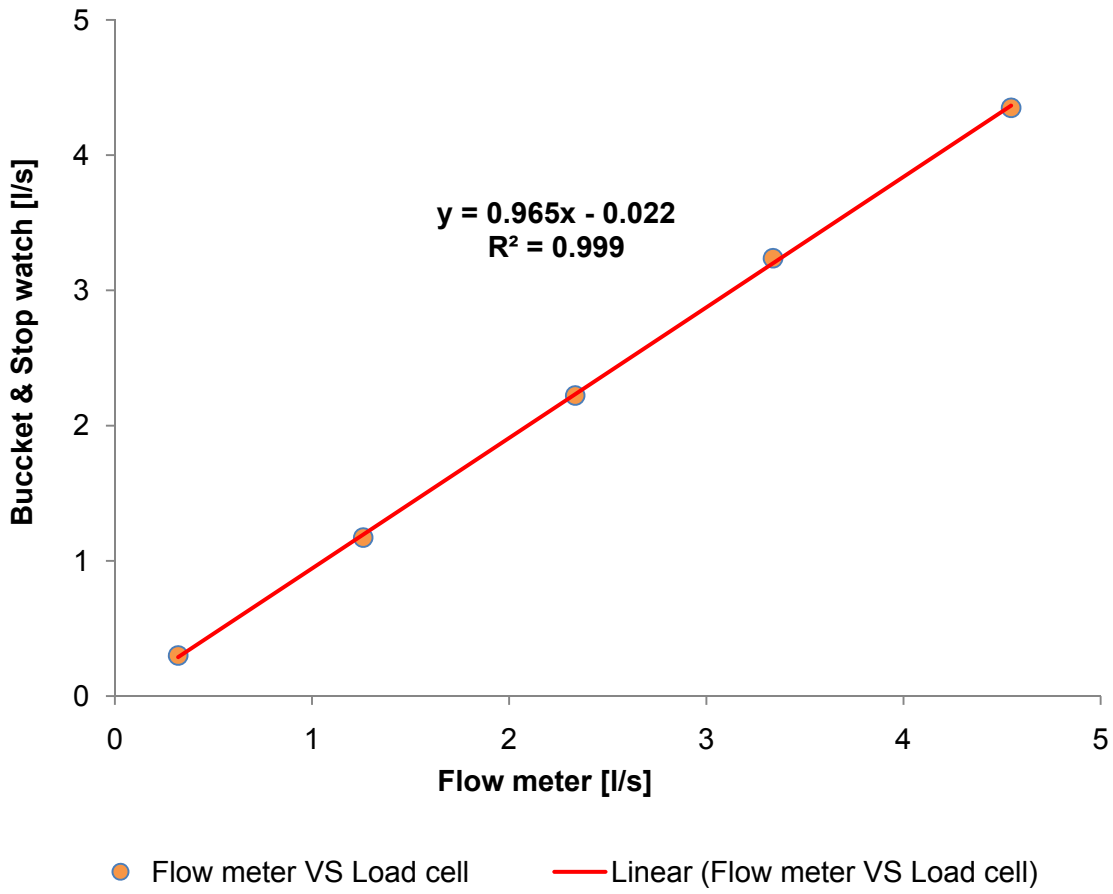

Figure 3.6 Flow rate comparison between two different methods

The linear relationship of the flow rate versus the voltage for Krohne flow meter calibration is given in Figure 3.7.

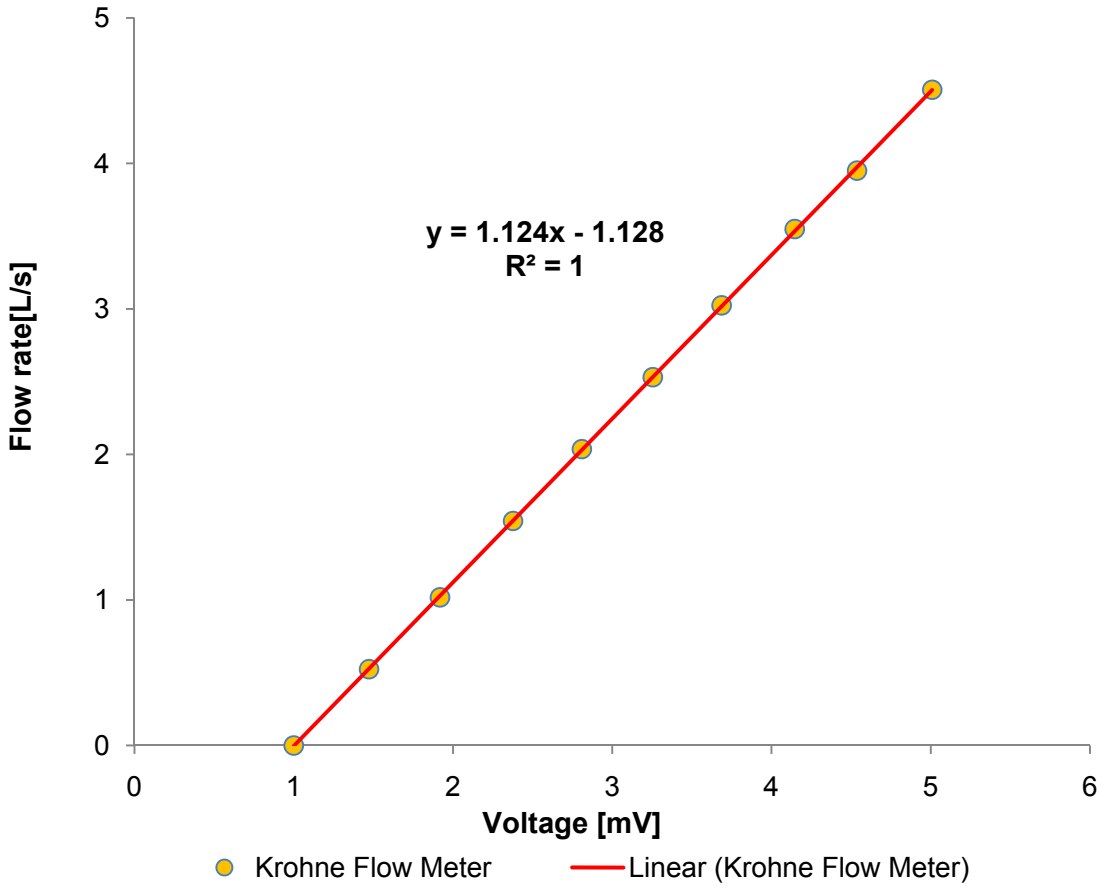

Figure 3.7 Krohne flow meter calibration line

3.4.1.3 Pressure transducer (PT)

The point pressure and differential pressure transducers were calibrated using a handheld communicator. A known pressure was applied directly to the transducers using a hydraulic pump connected to a digital manometer.

The calibration procedure was as follows:

1. Channel 101 was selected on the DAU after opening the calibration program;
2. pressure transducer caps were opened and set to zero;
3. the pipe valves leading to the transducers were opened and exposed to the atmosphere to release any pressure induced by the system;
4. the handheld communicator was connected to the transducers and activated;

5. the handheld communicator was set to a desired pressure range, either 0 - 130 kPa or 0 - 500 kPa, and was also set on data recording mode;
6. pressure recorded by the handheld communicator and the voltage recorded by the DAU were read - this was considered as the “zero mark”;
7. pressure was applied to the transducers and both the pressure and the voltage reading recorded on the handheld communicator and the DAU, respectively;
8. pressure on the transducers was continuously increased, and pressure and voltage readings recorded simultaneously to acquire at least six (6) different readings and,
9. pressure readings against the voltage readings were plotted to determine the linear relationship between them. The slope and the intercept of this linear relationship were used to relate the pressure applied by the test fluid in the rig to the voltage recorded by the DAU.

The linear relationship of the pressure versus the voltage for point pressure transducer calibration is given in Figure 3.8:

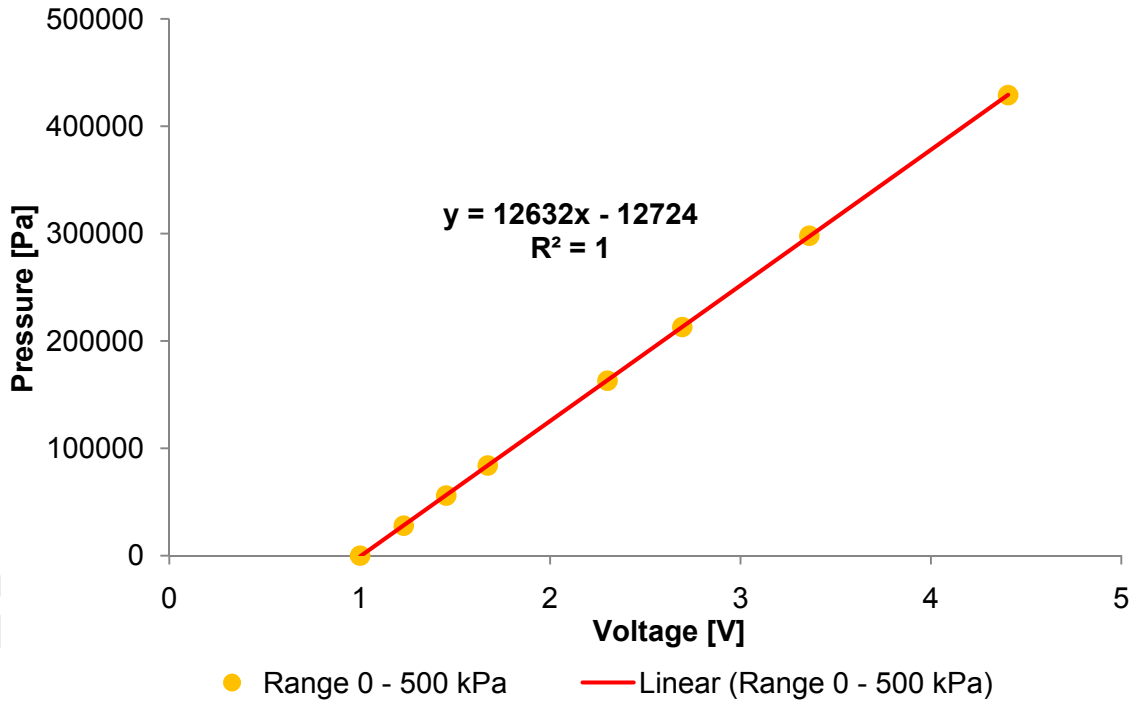

Figure 3.8 Calibration curve of a 500 kPa point pressure transducer

The calibration of the DP cell was conducted in a similar manner to the procedure used to calibrate the point pressure transducers. The only difference was the channel used on the DAU to record the voltage produced by the pressure in the system. Channel 115 and 116 of the DAU were used to calibrate the DP cells for a pressure drop range of 6 kPa and 130 kPa respectively. The linear relationship of the pressure versus the voltage for the 130 kPa differential pressure transducers are given in Figures 3.9 and 3.10.

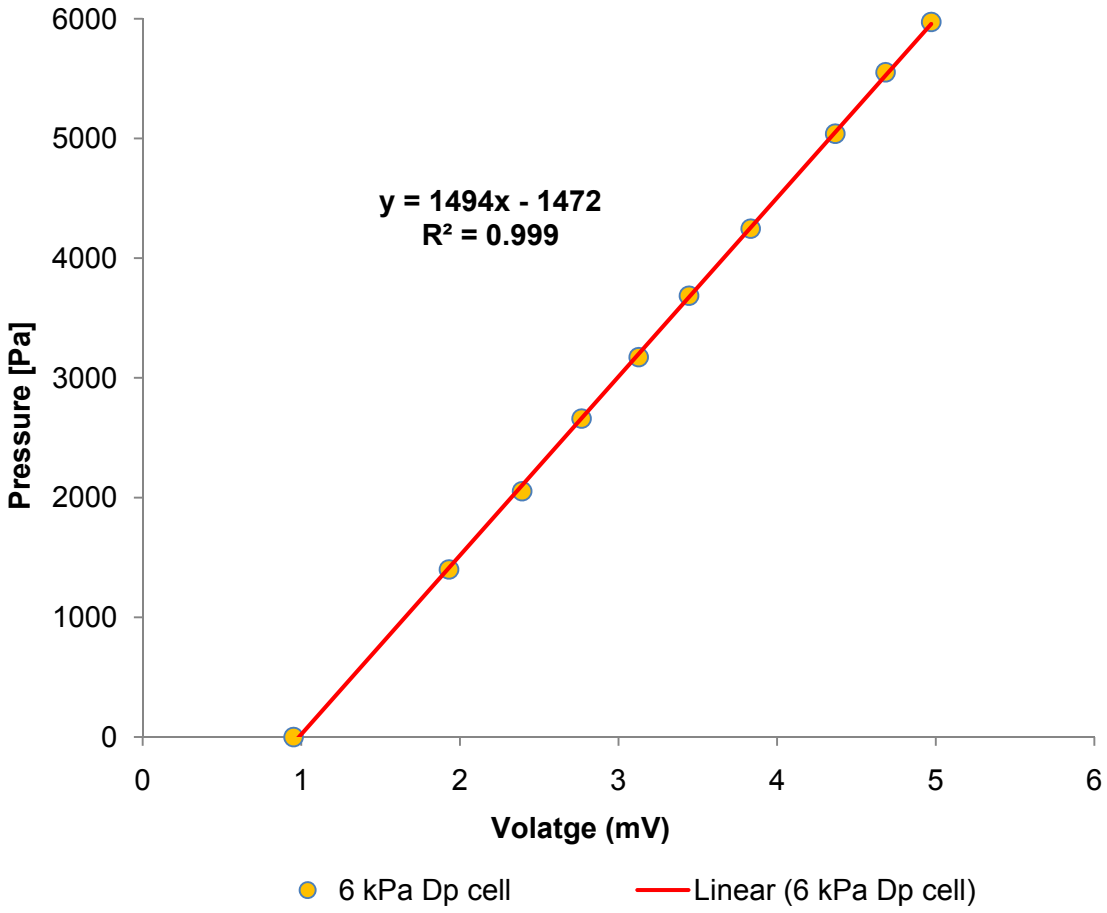

Figure 3.9 Calibration curve for 6kPa DP cell

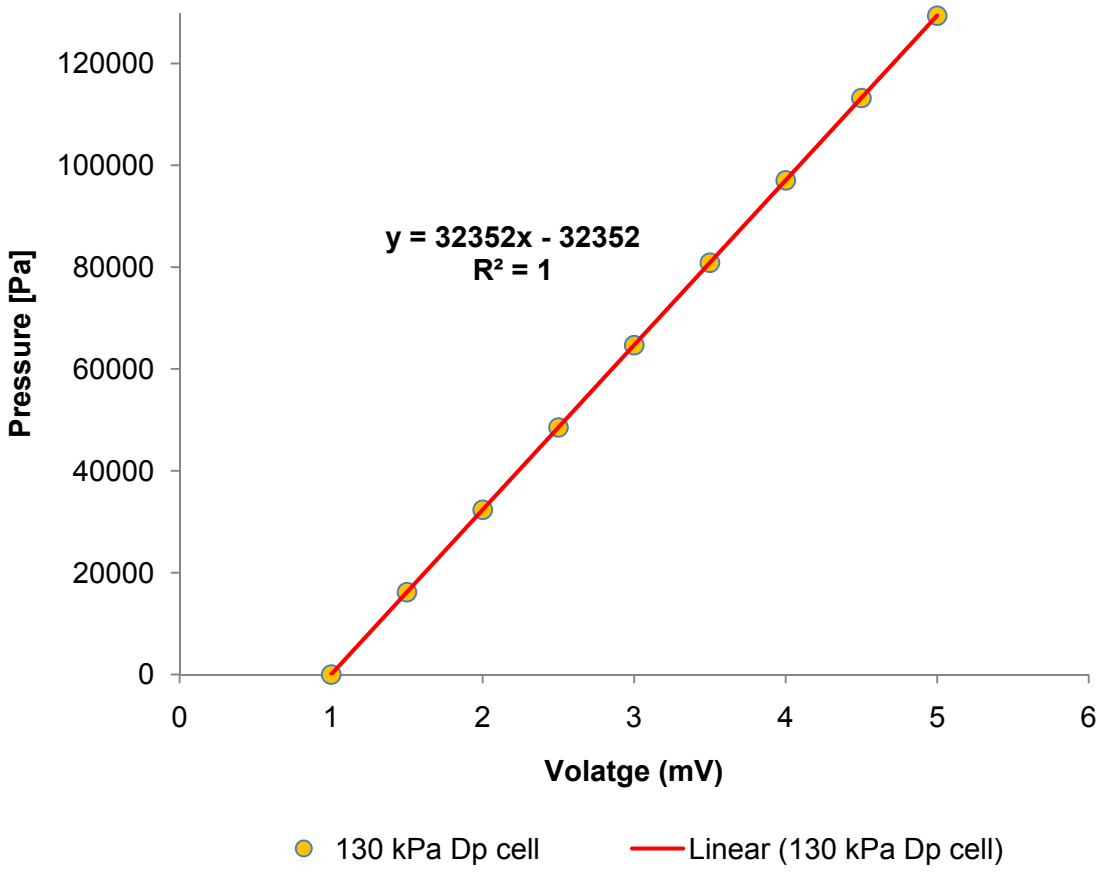

Figure 3.10 Calibration curve for 130 kPa DP cell

3.4.2 Fluid relative density test

The slurry density (ρ) and the relative density (RD) were determined carefully for each fluid tested. Procedures followed were:

1. Three clean, dry 250 ml volumetric flasks were weighed (M_1);
2. a slurry sample was taken from a tapping in the pipe wall of any of the 6 pipes and was weighed (M_2);
3. the volumetric flasks were filled to the 250 ml level with clear water and again weighed (M_3);
4. the volumetric flasks were emptied, filled with clear water then re-weighed again (M_4) and,

5. the relative density ρ_m defined as $\rho_m = \rho / \rho_w$.

$$RD = \frac{\text{Mass of fluid}}{\text{Mass of equal volume of water}} = \frac{M_2 - M_1}{(M_4 - M_1)\ \ (M_3 - M_2)} \quad \text{Equation 3.1}$$

3.4.3 Internal pipe diameter test

The internal pipe diameter (D) was determined by measuring the mass of water (M_w), required to fill a known length of pipe (L). The internal diameter was calculated using Equation 3.2:

$$D = \sqrt{\frac{4 M_w}{\rho_w \pi L}} \quad \text{Equation 3.2}$$

3.4.4 Clear water test

Water tests were conducted in the 46 mm ID pipe of the test rig, after the calibration of the flow meters and pressure transducers, to ensure the accuracy, credibility and precision of the experimental apparatus.

The pipe roughness was determined by measuring the pressure drop across a known length of pipe and by comparing it with the Colebrook and White Equation, Equation 2.19 (Kirkup, 2002). Comparisons of the experimentally obtained shear stresses (τ_o) with that of the calculated shear stresses using the friction factor obtained from Colebrook and White are shown in Figure 3.11. The value of k was found to be 10 μm, which is acceptable for smooth wall pipes. Table 3.3 presents typical design hydraulic roughness values of different materials.

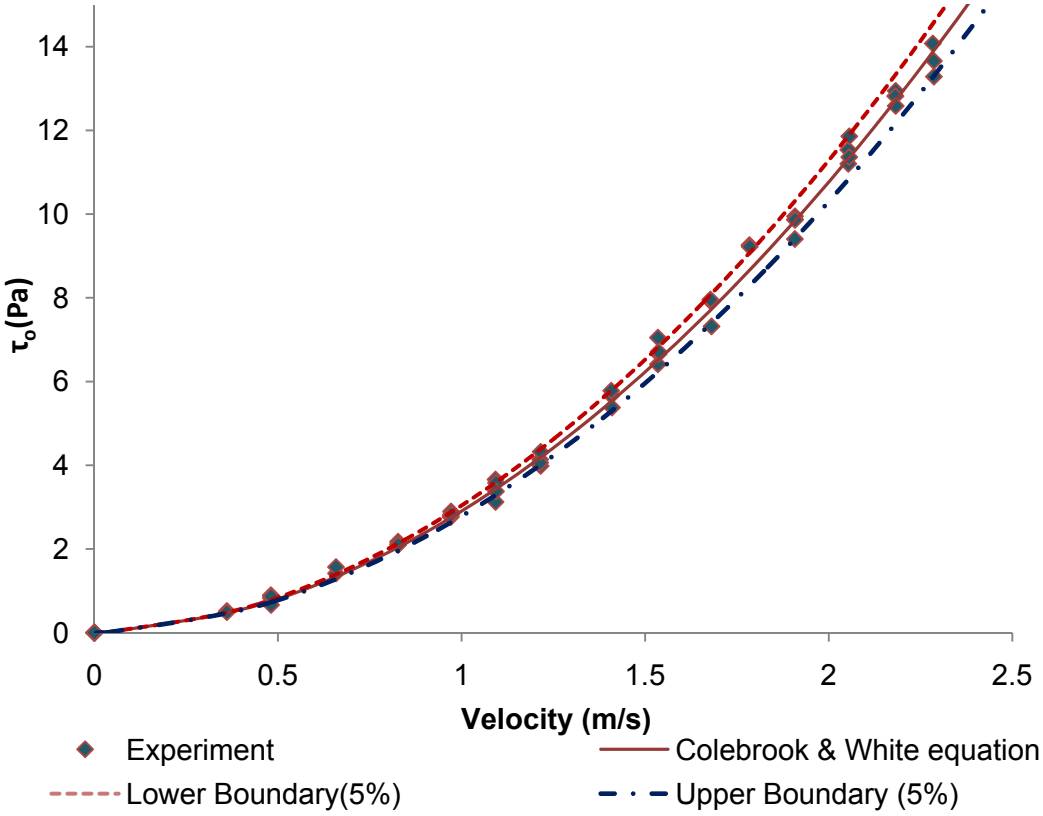

Figure 3.11 Clear water test comparison with Colebrook & White

Table 3.3 Hydraulic pipe roughness values (Paterson & Cooke, 2010)

Pipe Material and Condition	**Typical Design Hydraulic Roughness (μm)**
Steel (new)	50 (seamless) to 75 (welded)
Steel (corroded)	200 to 3000
Polyethylene (flanged or welded with beads removed)	20 (Water) to 50 (slurry)
Rubber lined flanged pipes	200
Rubber hose	200 (smooth bore) to 2000 (internal ribs)
Polyurethane lined pipe	20
Cement mortar lined	100 to 300
Concrete	300 to 3000
Fibre cement	75

3.4.5 Straight pipe test

Three different pipe diameters (46, 25 and 63 mm inner diameter) were used to perform the rheological characterization of the test fluids. An electromagnetic flow meter was used to measure the flow rate of fluid flowing in the pipes. The differential pressure drop was measured across a known length of the pipe. The operator increased or decreased the flow rates smoothly, after which the pressure and flow rate readings were simultaneously taken. One reading yielded one point on the graph of shear stress versus pseudo-shear rate. The graphs obtained needed to be co-linear in the laminar region as shown in Figure 3.12 to ensure nonexistence of wall slip. The rheological constants were then calculated using the appropriate rheological model.

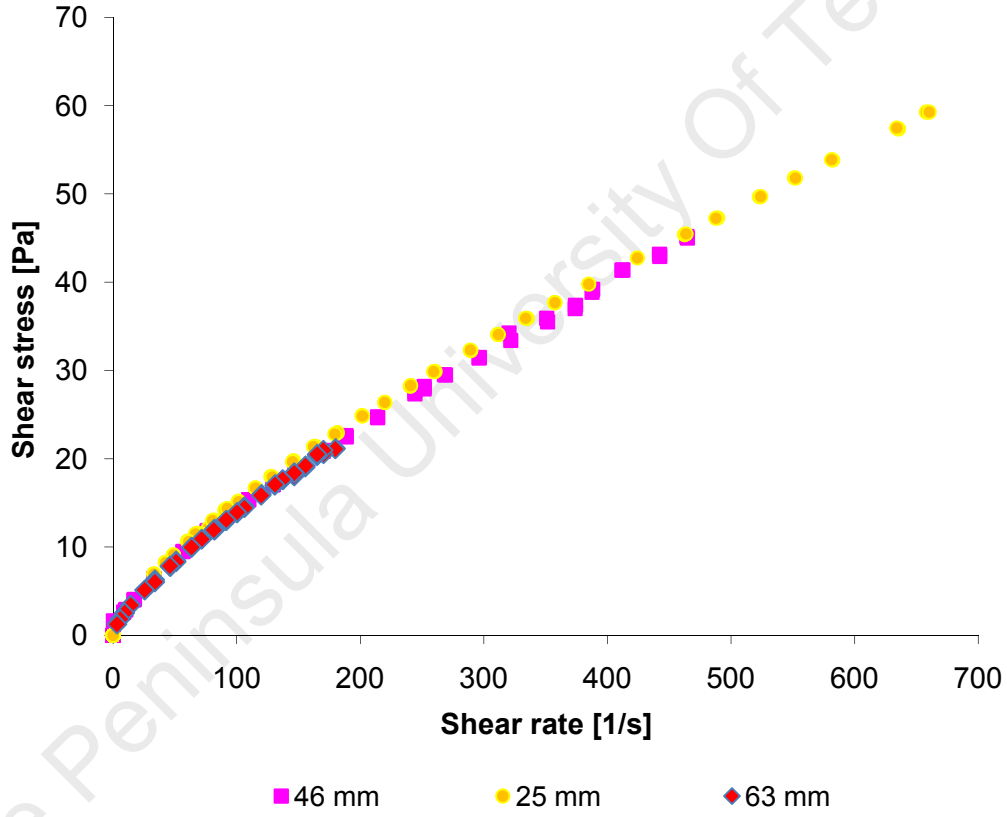

Figure 3.12 A typical pseudo-shear diagram obtained from straight pipe test

3.4.6 Pressure grade line test

The measurement of the pressure grade line was tedious. Care had to be taken to ensure the correct operating conditions to obtain optimum pressure drop results. The general orifice test procedure was:

1. Valve V1 was open fully (Figure 3.1) to ensure no build up of pressure in the rig if the wrong valves or no valves were open;
2. the positive displacement pump was switched on and was set at the desired flow rate;
3. all the valves were open to circulate the test fluid in the rig;
4. valve V1 was closed and the rig was run for an hour to thoroughly mix the test fluid;
5. all the valves were closed, except valve V5, V12 and V14;
6. the pressure pods and the line board were flushed and filled with tap water to ensure there were no air bubbles in the nylon tubes;
7. axial distances between the selected pressure tappings were recorded in the appropriate column of the computer programme;
8. the rheological characteristics obtained from the straight pipe test were used to fill the necessary column of the computer programme;
9. valves of the tappings leading to the pressure pods were open;
10. the HHC was used to select the applicable pressure range to be used during the test;
11. the computer programme was set to the determined pressure range and the chosen pipe diameter;
12. appropriate valves on the pressure line board were opened and test begun;
13. a time interval of 5 sec was allowed before the next valve was opened to record the pressure reading. It was done to stabilize the pressure (Pienaar, 2004) and,
14. step 12 was repeated until the last pressure reading was recorded.

This test run yielded one point on the graph of K versus Reynolds numbers. The flow rate was changed and the same procedure repeated to obtain another experimental point. Figure 3.13 shows a typical pressure grade line.

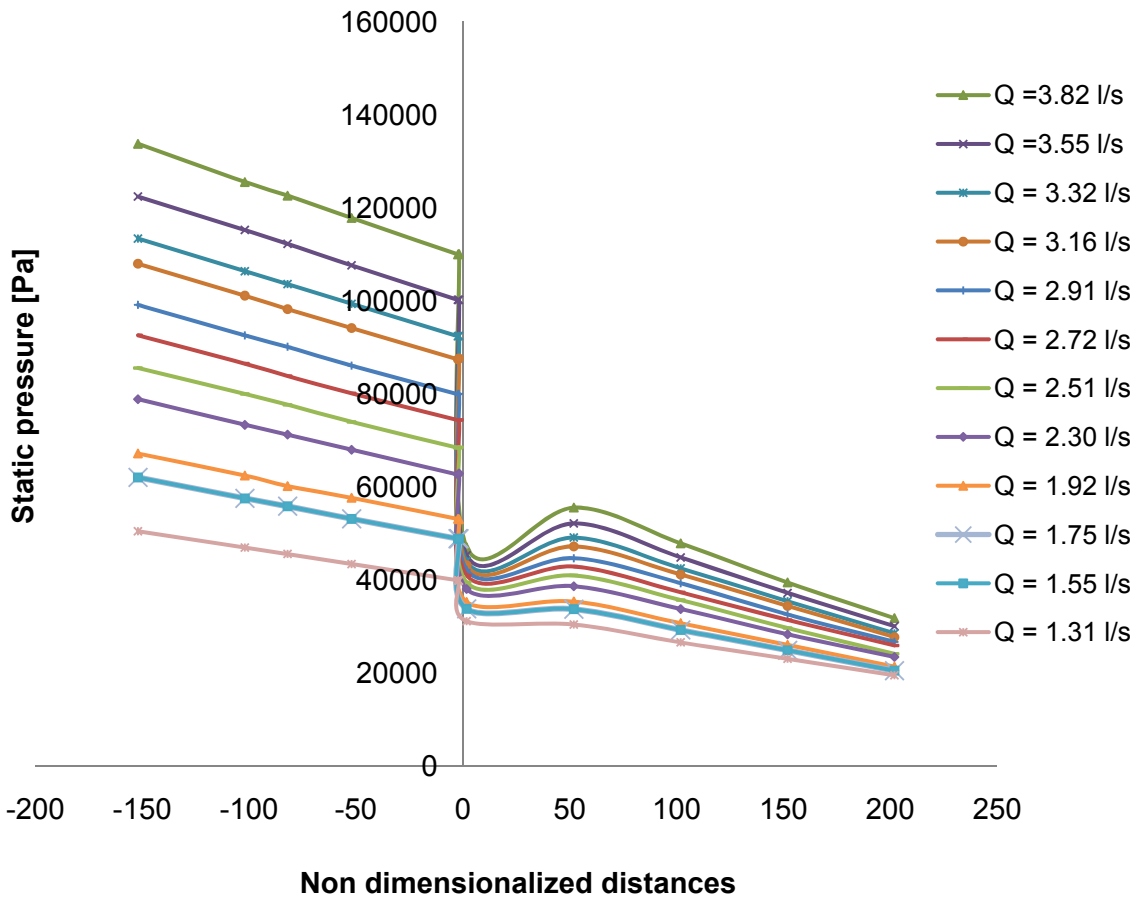

Figure 3.13 Typical Pressure grade line graph

3.4.7 Material tested

A Newtonian fluid (water) was used for the calibration of the orifice test rig and non-Newtonian fluids (CMC and kaolin at different concentrations) were tested to derive and to provide loss coefficient data.

3.4.7.1 Water

The test water had the following properties:

- pH of 9;
- total alkalinity 35 mg/l and,
- $CaCo_3$ and an ionic strength of less than 0.01 molar scale.

3.4.7.2 Carboxymethyl cellulose (CMC)

CMC is used in drilling mud, in detergents as a soil-suspending agent, in resin emulsion paints, adhesives, printing inks, as a protective colloid in general and as a stabiliser in foods. The flow properties of the CMC solutions proved to be constant throughout the test work. The concentrations tested were 4, 5, 7 and 8% by mass. At a high concentration, dissolution of the CMC in water deteriorated and required long periods of mixing time to achieve homogeneous solutions.

The CMC was obtained in granular form, which easily dissolved in water at low concentrations. Municipal tap water was used for this research work. Solutions of CMC are stable between a pH of 2 and 10. Below pH 2, precipitation of the solids occurs. The pH of the solutions tested for this study was pH 9.0 at 20 ^{0}C.

3.4.7.3 Kaolin

Kaolin clay was mixed with tap water in preparation of the slurry to be tested. A mixer, in the mixing tank was used to mix the solution thoroughly. The kaolin slurry was mixed in volumetric concentrations of 8, 14 and 20%. In terms of mass concentrations the concentrations of the suspension were 21%, 32% and 39% respectively. Figure 3.14 was used to convert the volumetric concentration to mass concentration.

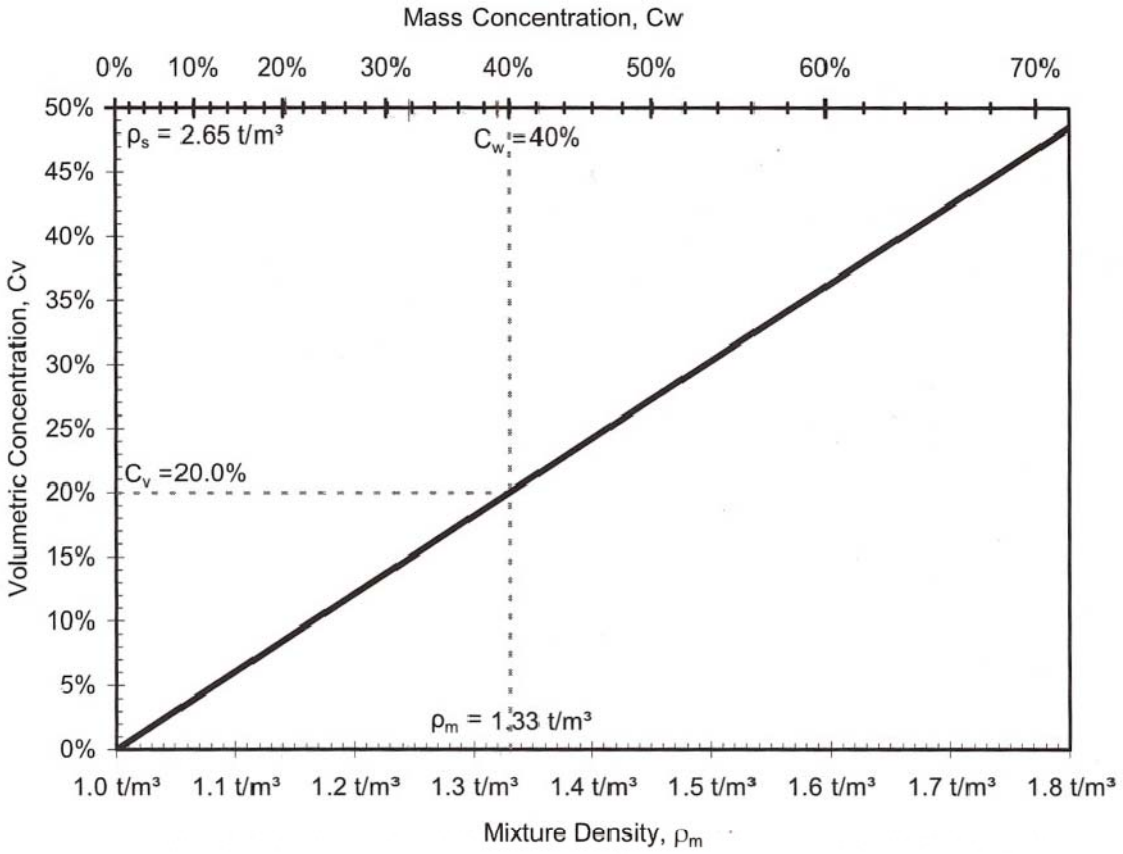

Figure 3.14 Concentration conversion table (Paterson & Cooke, 2010)

3.5 Experimental errors

It is not always possible to achieve absolute accuracy and precision unless the data are discrete numbers. According to Benzinger and Akshay, (1999) it is always important to be able to determine the margins of error which may be found in a set of data and to know how they are affected in various arithmetic processes such as addition, multiplication etc. Normally three types of errors are found:

- **Gross error** - Gross errors are due to blunders, equipment failure and power failure. A gross error is immediate cause for rejection of a measurement (Benzinger & Aksay, 1999).
- **Systematic error** - Systematic errors result in a constant bias in an experimental measurement. Systematic errors are those that are due to known conditions.
- **Random error** - Random errors are those that are due to chance variation.

3.6 Evaluation of errors

The absolute error is the difference between the true value of any number or quantity and the value obtained or used for that number or quantity in a given circumstance. If the true value of a number or quantity is X, the value obtained or used for that number or quantity is A, and the absolute error is ΔA then:

$$X = A \pm \Delta A \qquad \text{Equation 3.3}$$

This means that X is comprised between A – ΔA and A + ΔA. ΔA is called the maximum error or absolute error. If X is a quantity, ΔA is expressed in the same unit. ΔA is here the smallest division of the instrument, and the smallest value detected by the instrument (Barry, 1991). ΔA is calculated from the standard deviation of a set repeated measurement as well. The absolute error for ΔA at a 99,9% confidence interval is given by the equation:

$$\Delta A = 3.29\,\sigma \qquad \text{Equation 3.4}$$

where σ is the standard deviation

If a 95% confidence level is considered, then the absolute error may be approximated by:

$$\Delta A = 2\,\sigma \qquad \text{Equation 3.5}$$

The relative or percentage error of a number or quantity is calculated by:

$$\delta A = \frac{\Delta A}{A} \qquad \text{Equation 3.6}$$

3.7 Combined errors

When a variable is a result of a computation of other variables with their subsequent errors, the resulting error is the combination of the independent variables errors. Quantities such as inner pipe diameter, shear stress and shear rate are dependent on more than one measurement. Errors are unavoidable when analogue signals from instruments such as a flow meter, a pressure transducer etc are converted into a digital signal by the DAU. Haldenwang (2003) and Slatter (1999) refer to Brinkworth (1968) for a procedure that quantifies the combined error using a root mean square approach. The highest expected error ΔX, if X is a function of N quantities, is:

$$\left(\frac{\Delta X}{X}\right)^2 = \Sigma\left(\frac{\partial X}{\partial N}\right)^2\left(\frac{N}{X}\right)^2\left(\frac{\Delta N}{N}\right)^2 \qquad \text{Equation 3.7}$$

3.7.1 Axial distance

The axial distances were measured in mm using a measuring tape. The absolute error on measurements was 0.001 m.

3.7.2 Weight

The mass of all samples was measured using the weighing scale graduated in grams. The absolute error on measurements was 0.001 kg.

3.7.3 Flow rate

The flow meters used were accurate to 0.001 l/s, which can be assumed as the absolute error.

3.7.4 Pressure

The pressure transducers used were accurate at 0.25%. Care was taken in calibration to obtain a correlation coefficient of 0.999. Such calibration could rise to an average error of 0.35% (Baudouin, 2003).

3.7.5 Pipe diameter

The pipe diameter was calculated accurately using Equation 3.2. The highest expected error in calculating the pipe diameter was obtained by applying Equation 3.2 and 3.7, and that yielded:

$$\left(\frac{\Delta D}{D}\right) = \pm\frac{1}{2}\sqrt{\left(\frac{\Delta M_{H2o}}{M_{H2o}}\right)^2} + \sqrt{\left(\frac{\Delta L}{L}\right)^2} \qquad \text{Equation 3.8}$$

Summary of combined errors for a pipe diameter is presented in Table 3.4

Table 3.4 Expected Highest errors for 46 mm ID diameter pipe

Pipe diameter(mm)	Expected error (ΔD/D) %
46	0.33

3.7.6 Velocity

Velocity in a pipe can be established accurately by using Equation 2.13. The highest expected error for the velocity estimation can be found by using the following equation:

$$\frac{\Delta V}{V} = \pm\sqrt{\left(\frac{\Delta Q}{Q}\right)^2 + 4\left(\frac{\Delta D}{D}\right)^2} \qquad \text{Equation 3.9}$$

3.7.7 Pseudo shear rate

The highest expected error for pseudo shear rate was found by using the following equation:

$$\frac{\Delta\dot{\gamma}_0}{\dot{\gamma}_0} = \pm\sqrt{\left(\frac{\Delta Q}{Q}\right)^2 + 5\left(\frac{\Delta D}{D}\right)^2} \qquad \text{Equation 3.10}$$

3.7.8 Wall shear stress errors

The highest expected errors for wall shear stress are calculated as follows:

$$\frac{\Delta\tau_0}{\tau_0} = \pm\sqrt{\left(\frac{\Delta(\Delta P)}{P}\right)^2 + \left(\frac{\Delta D}{D}\right)^2 + \left(\frac{\Delta L}{L}\right)^2} \qquad \text{Equation 3.11}$$

3.7.9 Pressure loss coefficient

Pressure loss due to the orifice is related to Equation 2.54. Using Equation 3.7 for highest expected error analysis yields the following equation:

$$\left(\frac{\Delta K_{or}}{K_{or}}\right)^2 = \left(\frac{\Delta\left(\Delta P_{or}\right)}{\Delta P_{or}}\right)^2 + \left(\frac{\Delta\rho}{\rho}\right)^2 + 4\left(\frac{\Delta Q}{Q}\right)^2 + 16\left(\frac{\Delta D}{D}\right)^2 \qquad \text{Equation 3.12}$$

3.7.10 Discharge coefficient

The highest expected error in calculating discharge coefficients was found by means of the following equation:

$$\left(\frac{\Delta C_d}{C_d}\right)^2 = \left(\frac{\Delta Q}{Q}\right)^2 + 0.25\left(\frac{\Delta(\Delta P)}{\Delta P}\right)^2 + \left(\frac{\Delta A_2}{A_2}\right)^2 + 0.25\left(\frac{\Delta \rho}{\rho}\right)^2 + \left(\frac{4\beta^6 \Delta\beta^2}{\left(1-\beta^4\right)^2}\right) \quad \text{Equation 3.13}$$

A sample of 25 readings at constant flow rates were collected to evaluate the accuracy and precision of the rig in capturing data relevant to orifice coefficient determination.

Table 3.5 presents typical highest expected error in calculating both orifice pressure loss and discharge coefficient data for 0.36, 0.5 & 0.7 diameter ratios.

Table 3.5 Highest expected error in calculating K_{or} and C_d

β	$\left(\frac{\Delta K_{or}}{K_{or}}\right)_{Calc}$ %	$\left(\frac{\Delta K_{or}}{K_{or}}\right)_{Exp}$ %	$\left(\frac{\Delta C_d}{C_d}\right)_{Calc}$ %	$\left(\frac{\Delta C_d}{C_d}\right)_{Exp}$ %
0.36	5.23	4.45	1.72	0.97
0.5	16.9	1.65	9.60	0.36
0.7	49.0	49.1	24.5	1.39

It can be seen from Table 3.5 that the experimental error was always less than or equal to the highest expected error. This kind of agreement shows the credibility of the experimental work.

3.8 Conclusion

A summary of the conclusions are presented below:

a) The test rig and experimental equipment used were described and proved to be reliable to measure pressure loss and discharge coefficient data for different orifices.
b) Detailed dimensions of the long orifices used were presented.

c) The basic operation used to collect experimental pressure loss and discharge coefficient data were presented. The results are presented in Chapter 4 with the presentation of K_{or} and C_d against Re_{MR}.
d) The materials tested, as well as their practical purposes, were outlined.
e) Water was tested in the 46 mm ID straight pipe to establish credibility, accuracy and precision of test equipment. Straight pipe results correlated well with the Colebrook-White equation. Rheological characterizations of the non-Newtonian fluids are presented in Chapter 4.
f) Experimental errors have been quantified and found to be within acceptable limits.

CHAPTER 4

4.1 Introduction

The analysis of the experimental results is explained in detail in this chapter. The objective of this work was to determine pressure loss and discharge coefficient data in long square-edged orifices. The work in this chapter is divided into three parts:

1. Presentation of straight pipe results
    a. Friction factors, for water, obtained in straight pipes.
    b. Rheological characterisation of non-Newtonian fluid used, applying tube viscometry. It consisted of using the data points in laminar flow from the test data of (τ_0, 8V/D) to obtain the rheological constants τ_y, K and n (Slatter, 1994).
2. Presentation of plots of K_{or} for different t/d and β ratios against Re_{MR}.
3. Presentation of plots of C_d for different t/d and β ratios against Re_{MR}.

4.2 Straight pipe results

The results obtained in the straight pipe section are presented in this section of the thesis for both water and non-Newtonian fluids. The straight pipe results are important for establishing credibility of the test rig, as well as for the rheological characterization of non-Newtonian fluids.

4.2.1 Water

Water tests were conducted to ensure credibility and accuracy of the test rig. A plot of the Blasius friction factor against Reynolds number (Re) for water for the 46 mm ID pipe is presented in Figure 4.1.

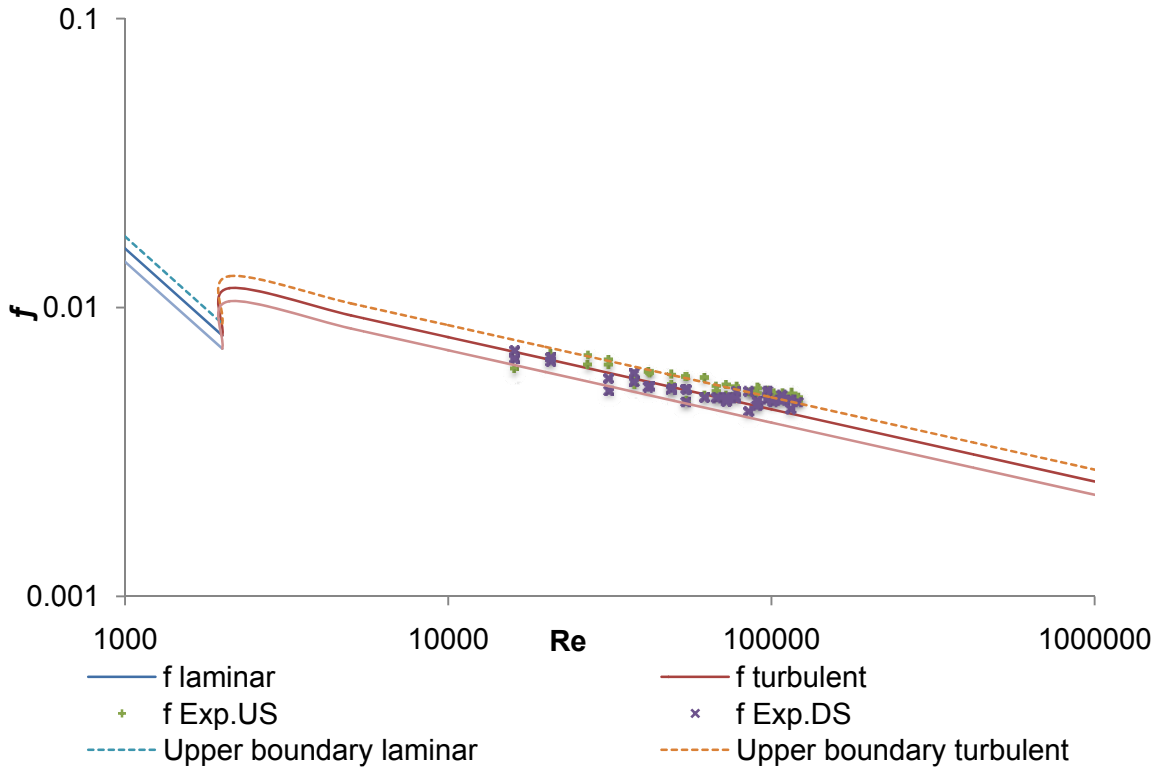

Figure 4.1 Friction factor for 46 mm ID pipe

It can be seen from Figure 4.1 that about 85% of the data are within ± 10% of the theoretical prediction for the 46 mm ID pipe. This kind of agreement indicated the validity and degree of accuracy of the experimental technique and equipment used in this experimental study.

4.2.2 Non-Newtonian fluids

The non-Newtonian fluids selected were kaolin suspensions and CMC solutions which typically displayed yield pseudo plastic and pseudo plastic behaviour (Fester et al., 2007). But, the kaolin suspension used for this work did not represent any yield pseudoplastic behaviour; rather they exhibited power law behaviour. Rheological constants obtained for the non-Newtonian fluids are presented for kaolin of 8%, 14% and 20% concentration by volume (C_v) or 21%, 32% and 39% by mass (C_m) as well as CMC 4%, 5%, 7% and 8% concentration by mass.

The objective of this section is to explain how the different rheological constants were obtained for both polymeric solutions and the kaolin suspensions.

4.2.2.1 Fitting of pseudo plastic model for CMC

The power law model was used to model flow behaviour of CMC and fitted to the laminar shear stress and shear rate data from three different straight pipes to determine K' and n'. A power law trend curve was fitted to the wall shear stress (τ_0) and pseudo shear rate (8V/D) data to obtain the constant n' (apparent flow behaviour index) and K' (apparent fluid consistency index). A typical example of the pseudo plastic model fit is given in Figure 4.2 for a 4% CMC solution. Table 4.1 gives the rheological constants obtained for CMC 4%, 5%, 7% and 8%.

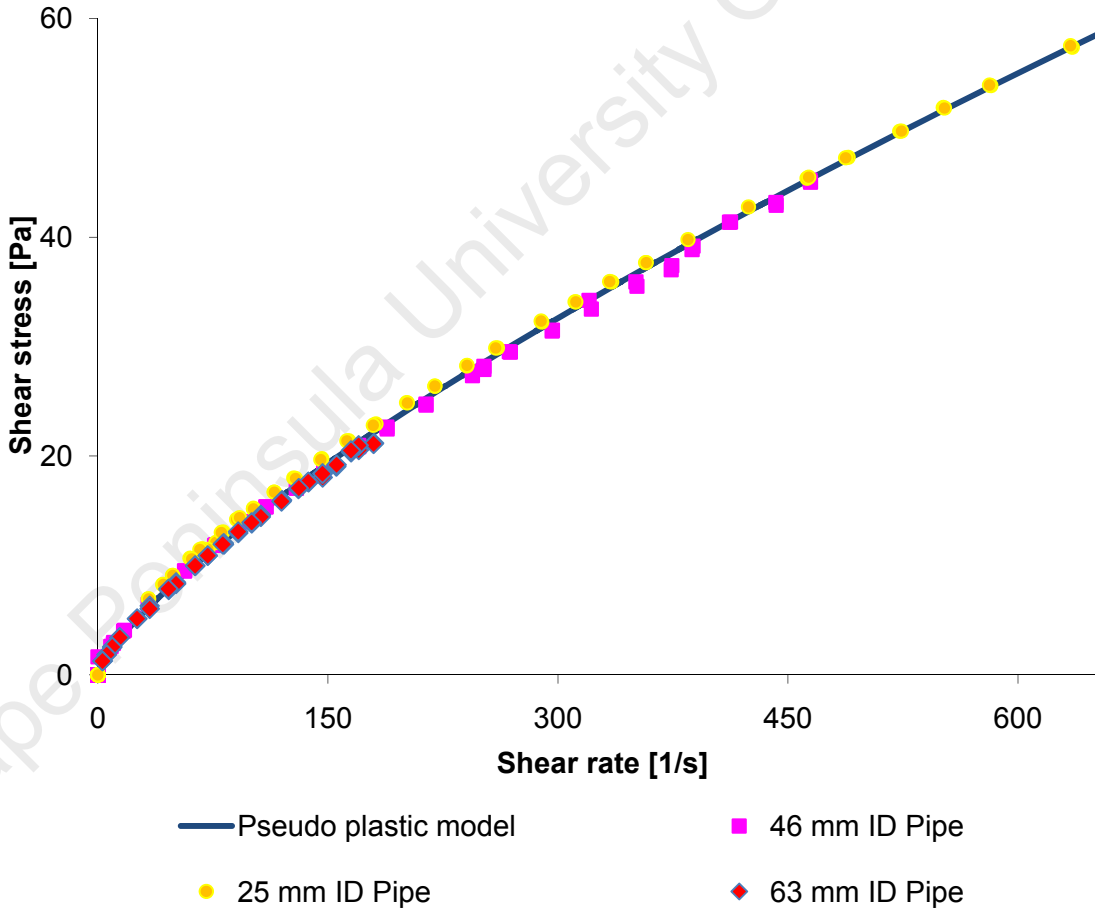

Figure 4.2 Pseudo shear diagram of CMC 4%

A flow curve of all the concentration of CMC tested is presented in Figure 4.3.

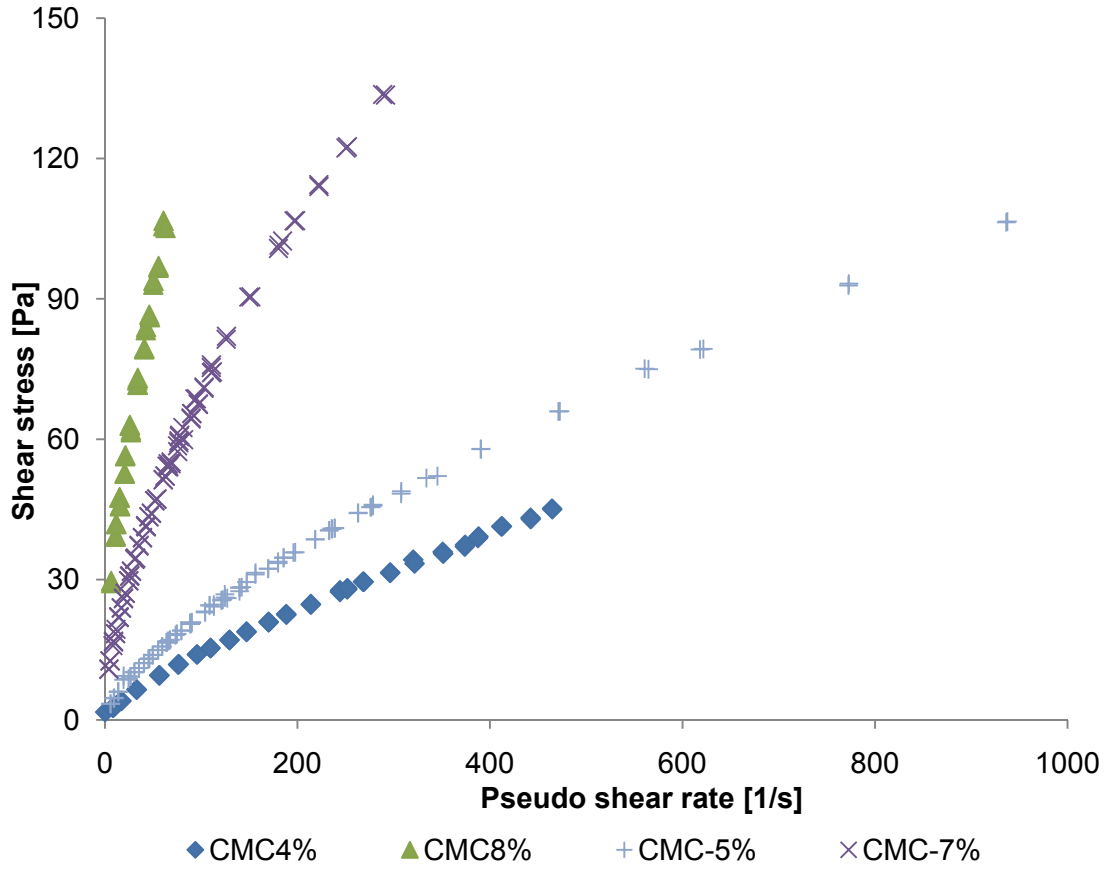

Figure 4.3 Flow curves of different CMC concentrations

Table 4.1 Rheological parameters for CMC

RD	C_m (%)	K'(Pa.s$^{n'}$)	n'
1023.2	4	0.436	0.75
1028.1	5	1.38	0.64
1041.4	7	3.84	0.61
1043.0	8	8.30	0.60

4.2.2.2 Rheological characterisation of kaolin suspensions

Both yield pseudo plastic (Herschel–Bulkley) and power law (Ostwald de-Waele) model was used initially to determine the kaolin flow behaviour. The yield pseudo plastic model produced an average root mean square error of 0.07 with a small yield stress values ($0.1 \le \tau_y \le 1$), which was insignificant for practical purposes in the context of this work. The power law model produced an average root mean square error of 0.03 (R^2 = 0.98). Thus, the power-law, was selected to depict the rheological behaviour of the kaolin suspension. A similar approach was followed by Polizelli et al., (2003) and an identical conclusion was reached. A typical example of the power law model fit is given in Figure 4.4 for a 14 % volumetric concentration of kaolin suspension.

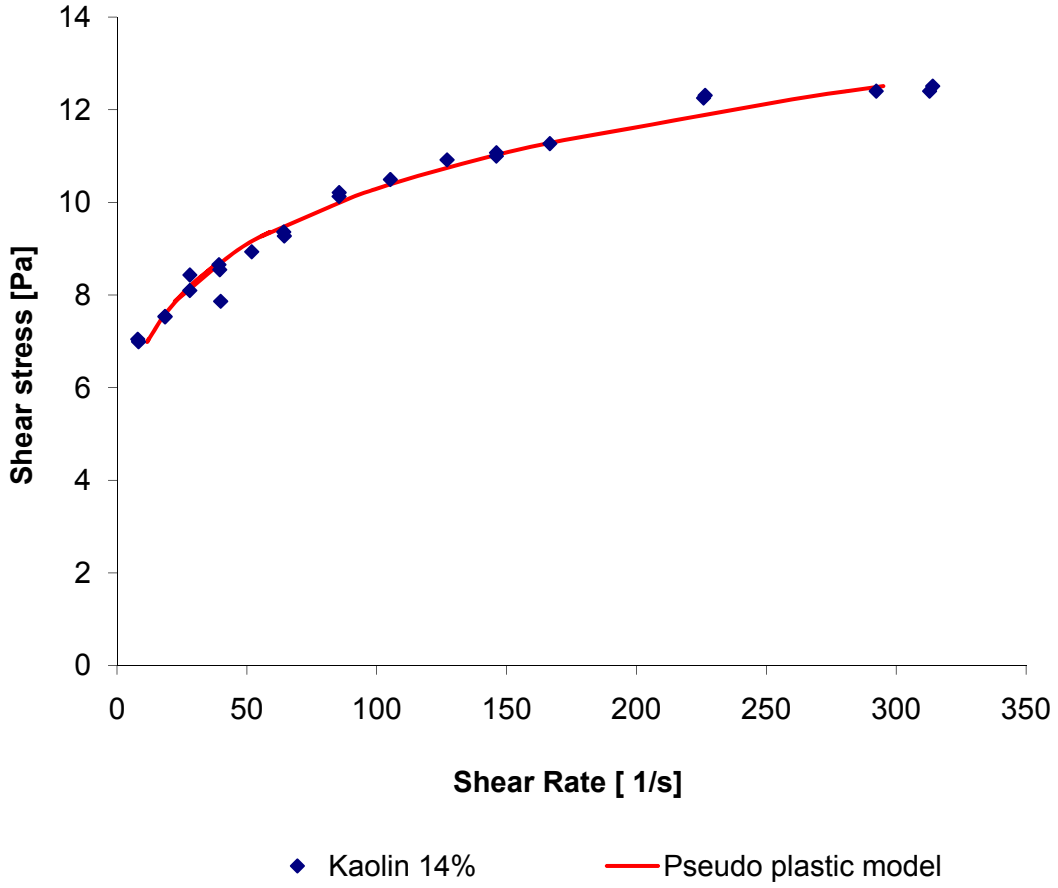

Figure 4.4 Pseudo shear diagram of 14 % kaolin

A flow curve of different kaolin suspension concentrations is presented in Figure 4.5. Table 4.2 gives the rheological constants used in this work for kaolin 8%, 14% and 20% volumetric concentration.

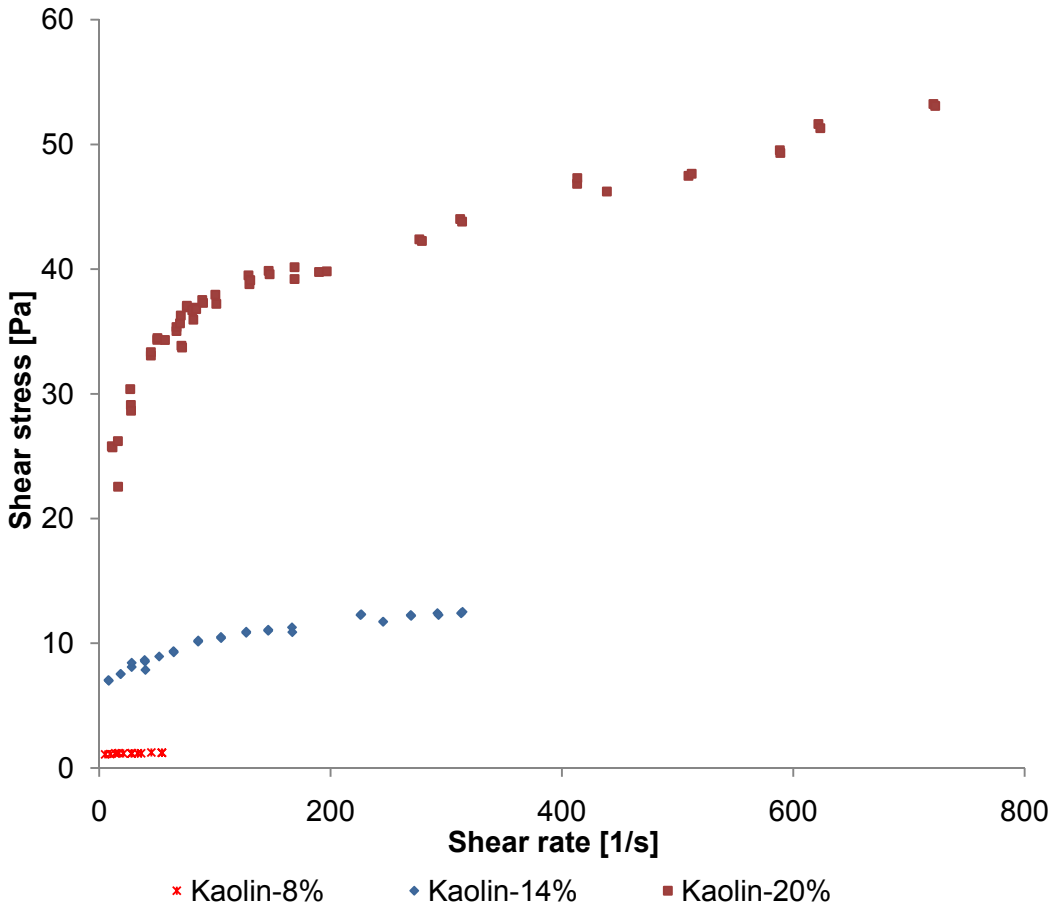

Figure 4.5 Pseudo shear diagram of different kaolin suspension concentrations

The rheological parameters for all kaolin suspensions are given in Table 4.2.

Table 4.2 Rheological characteristics of different kaolin concentration used

RD	%Concentration(V)	%Concentration(m)	K'(Pa.s^n)	n'
1140	8	21	0.06	0.50
1242	14	32	3.91	0.18
1324	20	39	16.0	0.15

A combined flow curve for both CMC and kaolin suspension is presented in Figure 4.6.

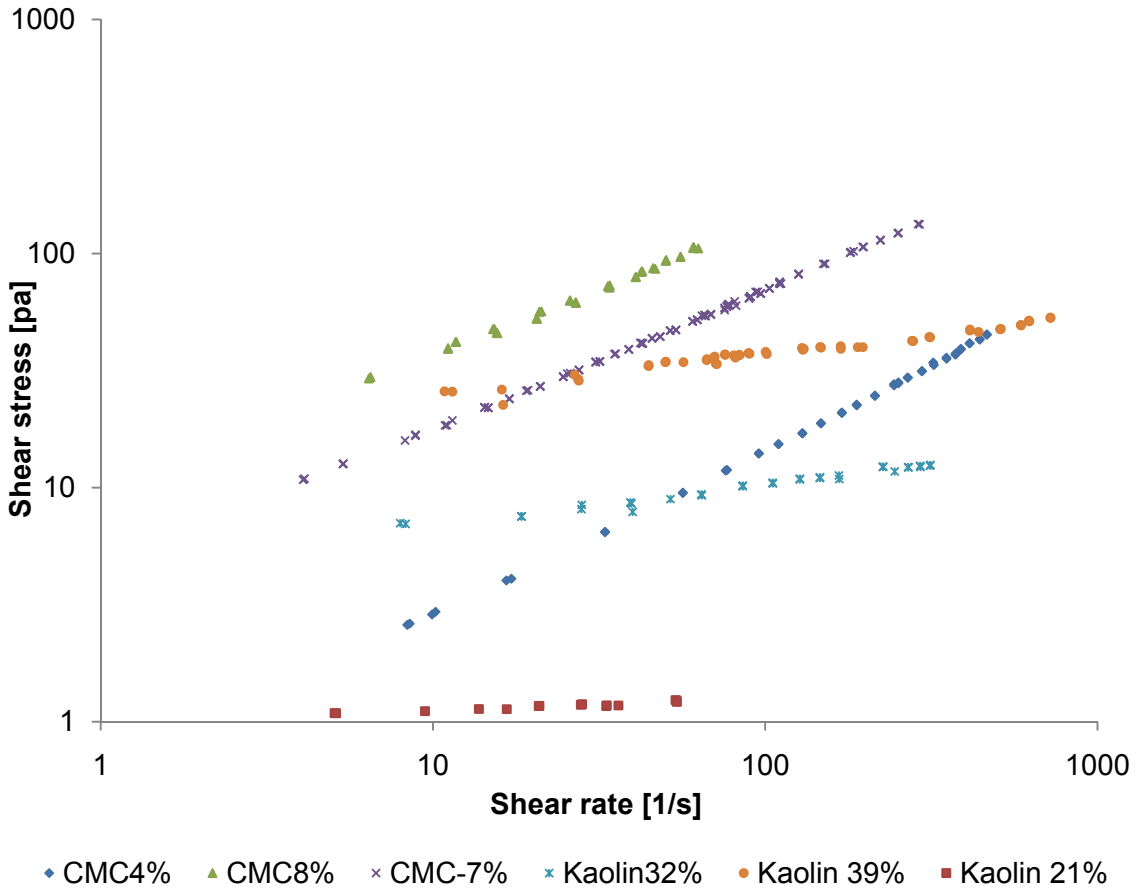

Figure 4.6 Flow curve comparison for both CMC and kaolin at different concentrations

Table 4.3 presents a table with all the rheological parameters obtained for both CMC and kaolin at different concentration.

Table 4.3 Different rheological parameters used for CMC and Kaolin

% Mass Concentration	RD (Kg/m^3)	Fluid Type	K'	n'
4	1023.2	CMC Solution	0.436	0.75
5	1028.11	CMC Solution	1.38	0.64
7	1041.4	CMC Solution	3.84	0.61
8	1043	CMC Solution	8.30	0.60
21	1140	Kaolin Suspension	0.06	0.50
32	1242	Kaolin Suspension	3.91	0.18
39	1324	Kaolin Suspension	16.0	0.15

4.2.2.3 Friction factor evaluation

To evaluate the accuracy of the rheological parameters friction factors were calculated using Re_{MR} which accommodated the rheological parameters and they were compared against the theoretical friction factors. This was repeated for all CMC and kaolin concentrations. Figure 4.7 presents the comparison. It can be seen from Figure 4.7 that the experimental friction factors agreed well with the theoretical friction factors for both laminar and turbulent flow. This type of agreement indicated the validity and degree of accuracy of the experimental technique and equipment used for this experimental study.

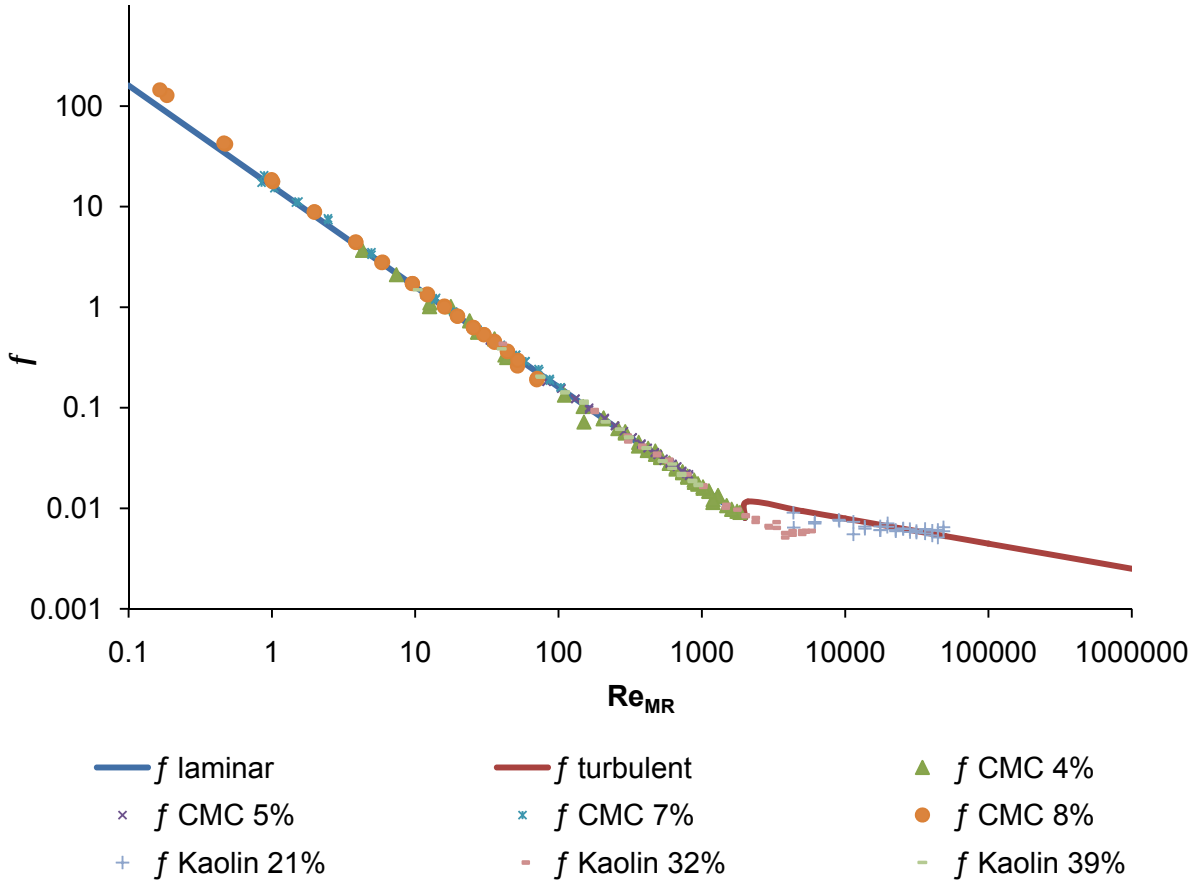

Figure 4.7 Comparison of friction factor for different fluids

4.3 Graphical presentation of pressure loss coefficient K_{or} against Re_{MR}

It is customary in the field of fluid mechanics to present pressure loss coefficient data against Reynolds number on a logarithmic scale graph for the purpose of analysing results (Edwards et al., 1985; Turian et al., 1997; Pienaar, 1998; Kazadi, 2005; Mbiya, 2008). Re_{MR} was used in this work to make such representations.

4.3.1 Pressure loss coefficient for orifice β = 0.5, t/d = 5, orifice

Figure 4.8 shows the pressure loss coefficient of a square-edged long orifice with dimension of β = 0.5 and t/d = 5 in from laminar to turbulent flow régimes. Turbulent flow occurs earlier at a Reynolds number of around 1000. Different fluids have been tested to fill the range of Reynolds numbers. However, not all fluids could be tested in turbulent flow because of the pump capacity. The transition régime is found to be in the range of Reynolds numbers 100 - 1000 (approx) depending on the fluids. It can also be seen

transition from laminar to turbulent flow was not smooth. This can be explained as the interaction between the secondary flow and the core region that tended to delay the onset of turbulence to well below the Reynolds number at which straight pipe flow could become turbulent. The K_{or} value was constant in turbulent flow and found to be 17.70. But for laminar flow the loss coefficient increased with decreasing Reynolds number. In this region the viscous forces dominated the inertia forces. The loss coefficient in laminar flow can be correlated by using the following equation:

$$K_{or} = \frac{C_{or}}{Re_{MR}} \qquad \text{Equation 4. 1}$$

The laminar flow orifice loss coefficient constant, C_{or}, for 0.5 diameter ratio orifice was found to be 1500.

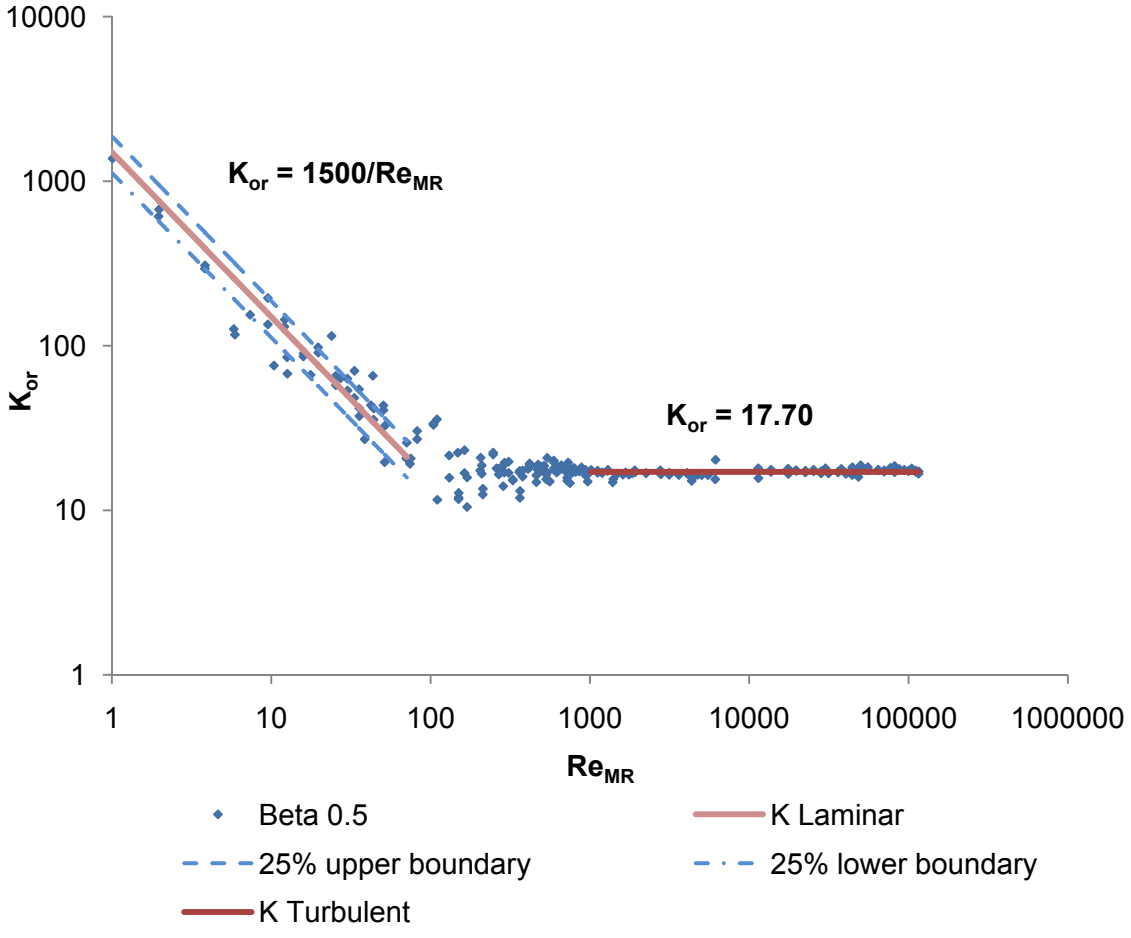

Figure 4.8 Pressure loss coefficient data for orifice β = 0.5, t/d = 5

Figure 4.8 presents a plot of loss coefficient data. It can be seen from the graph that about 85% of data falls within ± 25% range, comparing to Equation 4.1.

4.3.2 Pressure loss coefficient for β = 0.7, t/d = 5, orifice

Figure 4.9 presents the pressure loss coefficient of a square-edged long orifice with a dimension of β = 0.7 and t/d = 5 from laminar to turbulent régime. The turbulent flow occurs earlier at a Reynolds number of around 1000. Transition régime is found to be in the range of a Reynolds number of about 100 - 1000 depending on fluids used. The K_{or} value in turbulent régime was found to be 2.33. The loss coefficient in laminar flow can be correlated by using the following Equation 4.1. C_{or}, was found to be 800.

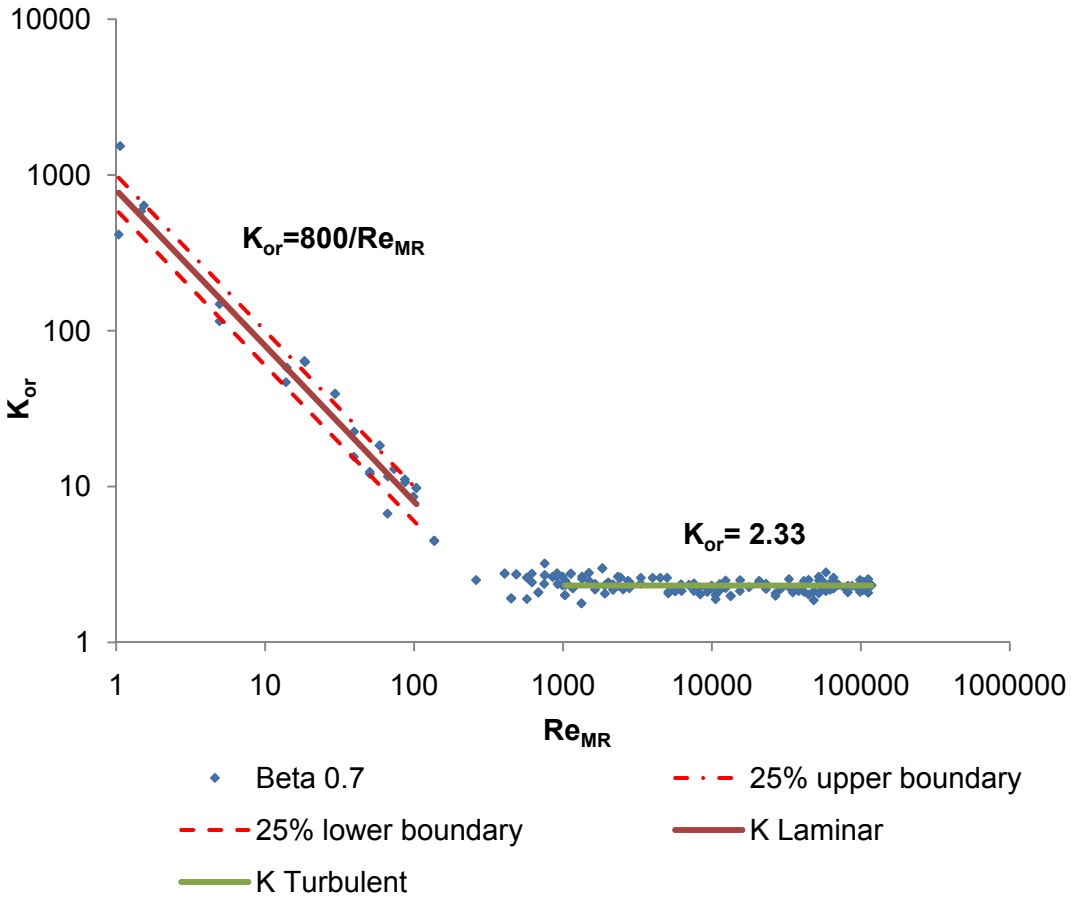

Figure 4.9 Pressure loss coefficient data for β = 0.7, t/d = 5

Figure 4.9 presents a plot of Equation 4.1 against the laminar flow loss coefficient data. It can be seen from the graph that ± 75% of data falls within ± 25% range. The data is more scattered because of a higher β ratio. According to Husain and Teyssandier (1984) pressure fluctuation increases with β. As the beta ratio decreases the dominant source of uncertainty shifts from measurement accuracy to turbulent flow fluctuations (Darin et al., 2001).

4.3.3 Pressure loss coefficient for β = 0.36, t/d = 4, orifice

The pressure loss coefficient K_{or} for 0.36 diameter ratio orifice is presented in Figure 4.10. The laminar flow region can be described by Equation 4.1 as shown in Figure 4.10. It can be seen from Figure 4.10 that the transition from turbulent to laminar is smoother comparing to 0.5 and 0.7 diameter ratio orifices. The turbulent régime also occurs earlier at around a Reynolds number of 400. An average K_{or} value of 76 was obtained in turbulent régime. The laminar flow loss coefficient was found to be 3300 for 0.36 diameter ratio orifice. It can be seen that almost 88% of the data fell within ± 25% range.

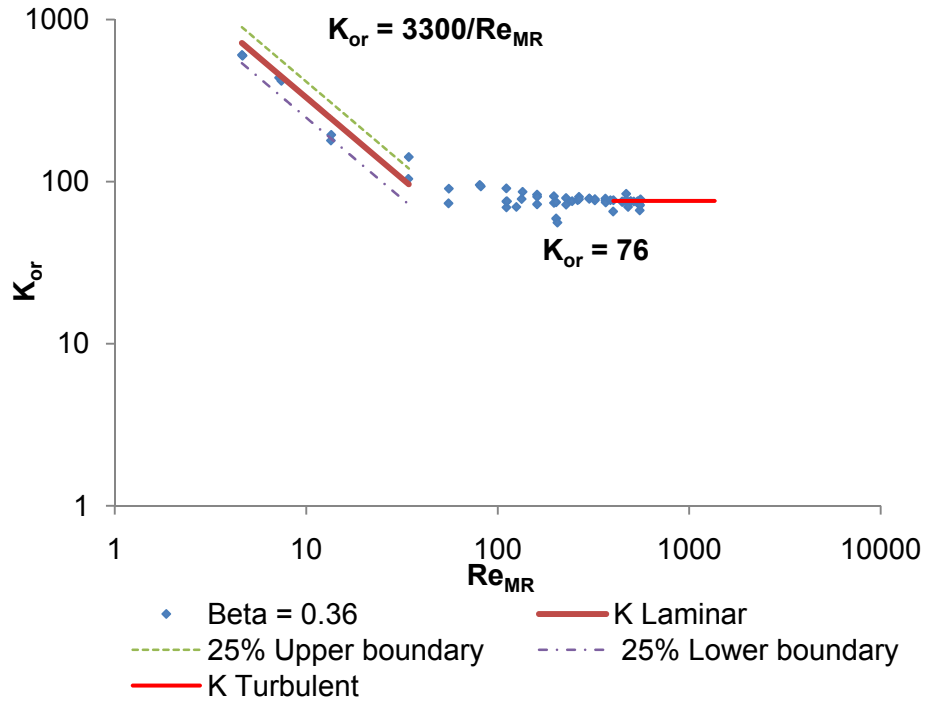

Figure 4.10 Pressure loss coefficient data for orifice β = 0.36, t/d = 4

Table 4.4 presents loss coefficients for β = 0.5, 0.7 and 0.36 orifices. It can be seen that the K_{or} increased with the decrease in β ratio. Figure 4.11 presents the loss coefficients for all the different β ratios tested for comparison purposes. It is noticeable from Figures 4.8, 4.9 and 4.10 that the laminar flow loss coefficient was inconsistent, but rather increasing with a decrease in β ratio.

Table 4.4 Turbulent flow pressure loss coefficients for all β ratios tested

β	**K_{or}**	**Std Dev**
0.36	76.0	± 1.90
0.50	17.7	± 0.47
0.70	2.33	± 0.15

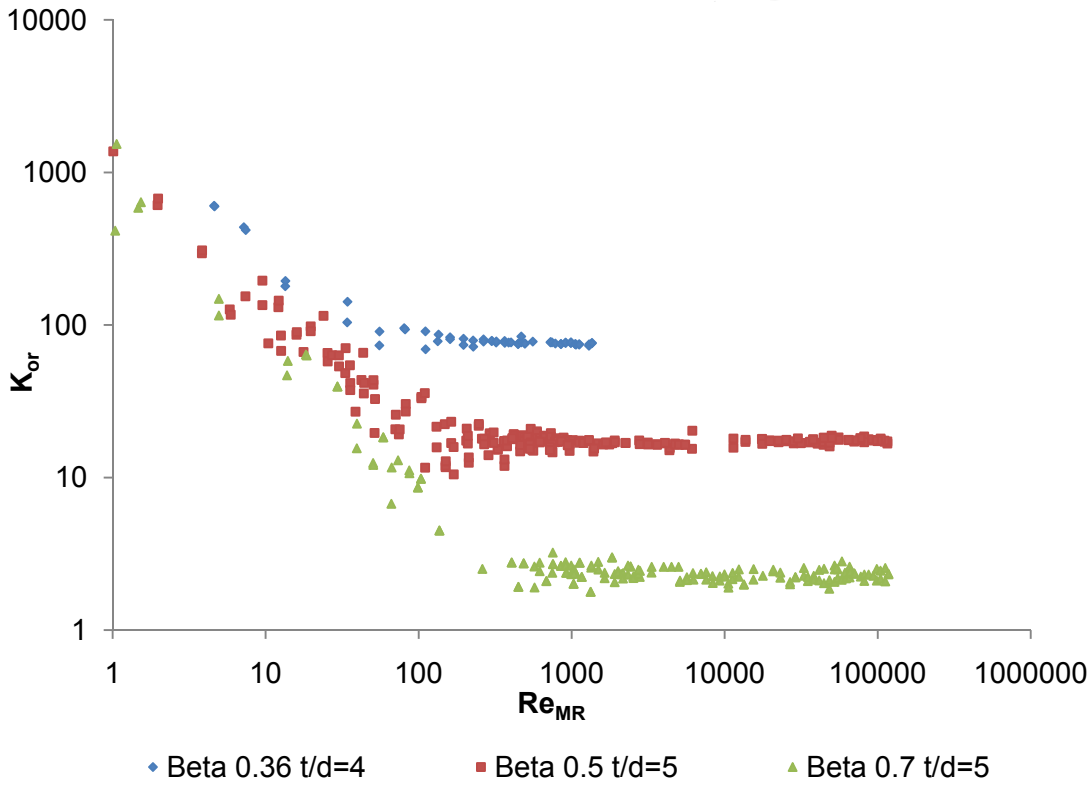

Figure 4.11 Comparison of pressure loss coefficients for β ratio of 0.5 , 0.7 and 0.36 orifice

4.4 Graphical presentation of discharge coefficient C_d against Re_{MR}

The discharge coefficient C_d was plotted against the pipe Reynolds number, similarly to the pressure loss coefficients and is given in Figures 4.12, 4.13 and 4.14 for β ratios of 0.5, 0.7 and 0.36 respectively. Both standard methods, namely the Flange and D & D/2 tapping methods, were evaluated for determining the discharge coefficient. Figure 2.18 and Table 2.4 in Chapter 2 were used for obtaining tapping specification. A comparison of the Flange and D & D/2 tapping methods presented in Figure 4.12 indicated no discrepancies in results and therefore all the data is presented for the Flange tapping method only. Figure 4.15 presents the effect of diameter ratio on C_d.

4.4.1 Discharge coefficients for β = 0.5, 0.7 and 0.36 orifices

Figure 4.12 presents the discharge coefficients for the orifice β = 0.5 for both tapping methods against Reynolds number. No discrepancies were found between the C_d data obtained using two different tapping methods. It can be seen from Figures 4.12, 4.13 and 4.14 that in laminar flow trends for discharge coefficient, C_d, increased with Reynolds number until it reached a peak. In the transition region, which is in this case in the Reynolds number range of about 2000 - 10000, C_d decreased with the Re_{MR}. In the turbulent flow régime above Re_{MR} > 10000, C_d is nearly constant for β = 0.5 and 0.7. An average C_d value of 0.79 and 0.83 was determined for β = 0.5 and 0.7 respectively in the turbulent régime for Re_{MR} > 10000. For β = 0.36 the Reynolds number ranged only up to 1000. So, a constant C_d value could not be provided. But a plot of C_d values against Reynolds number has been provided in Figure 4.14.

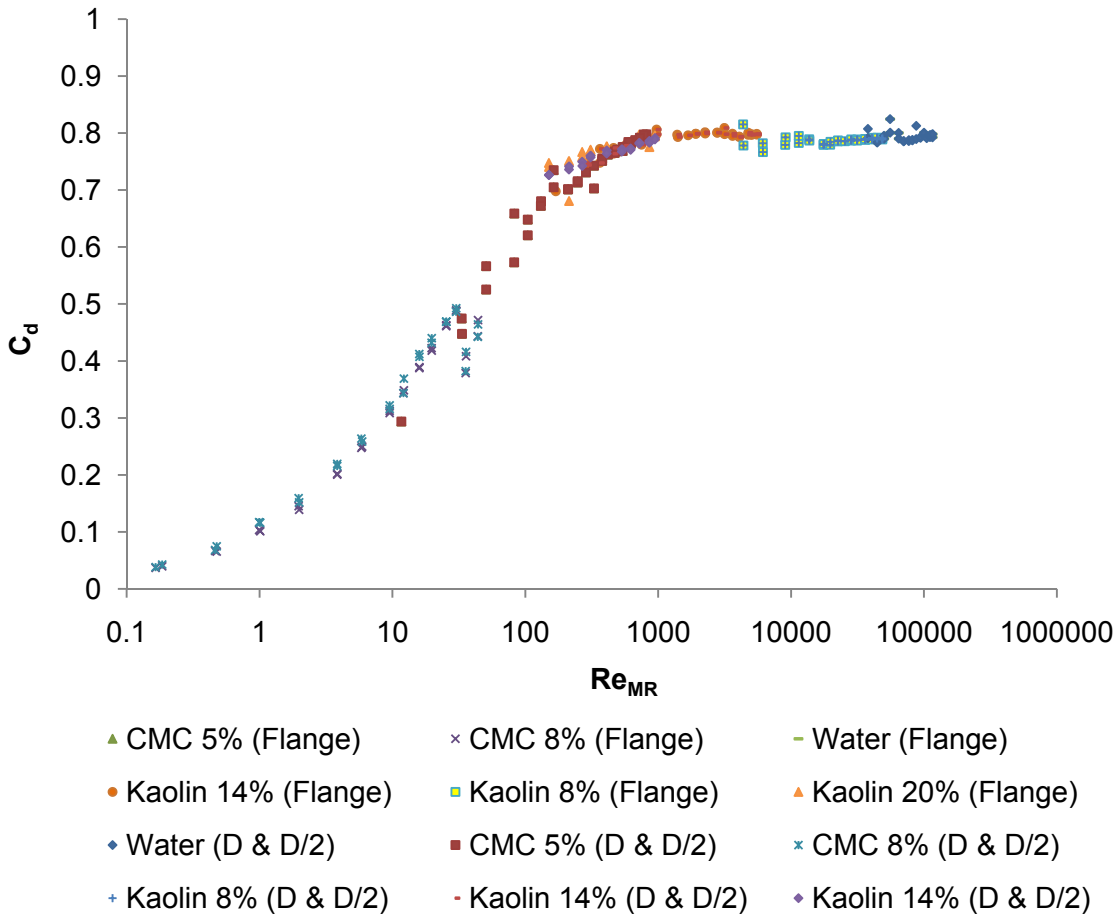

Figure 4.12 Discharge coefficient values obtained using Flange and D & D/2 tapping method for β = 0.5, t/d=5 square-edged long orifice

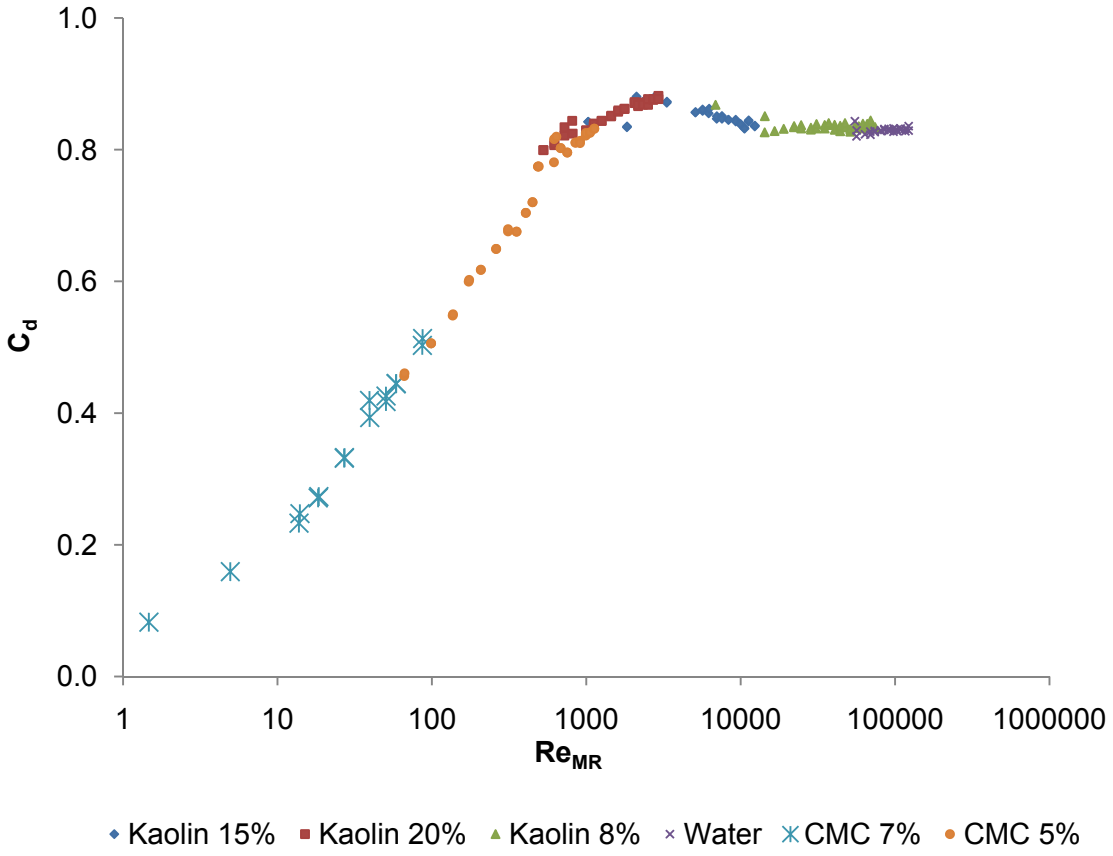

Figure 4.13 Discharge coefficient values obtained using Flange tapping method for β = 0.7, t/d = 5 square-edged long orifice

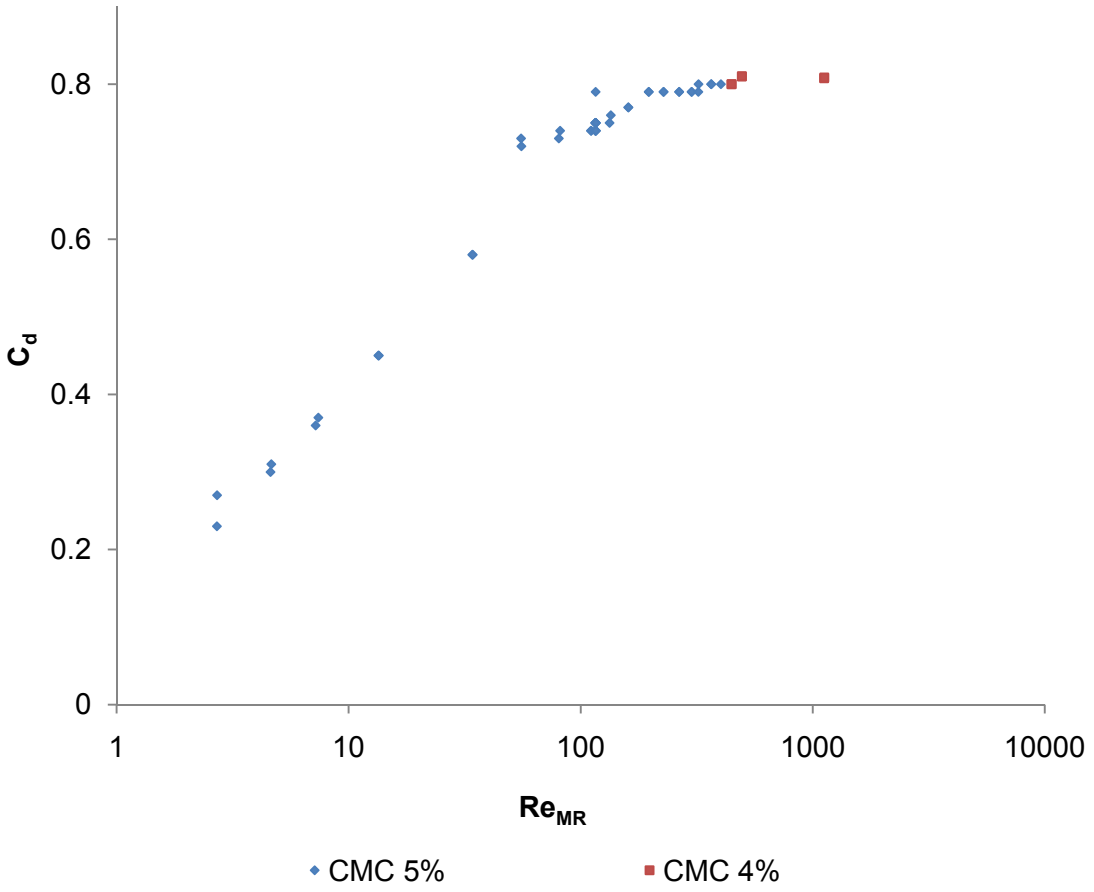

Figure 4.14 Discharge coefficient for beta = 0.36 and t/d = 4 orifice

Discharge coefficient data obtained using the Flange tapping method for all three different β ratios are presented in Figure 4.15 to evaluate the effect of β ratios on the discharge coefficient. In laminar flow, the effect of the diameter ratio was to shift the curves towards higher Reynolds numbers, *i.e*. for a given value of Re_{MR}, C_d values were lower for greater values of β. The peak value increased with the diameter ratio and shifted toward a higher Reynolds for greater values of β (ESDU, 2007). Table 4.5 presents different discharge coefficients with their standard deviations.

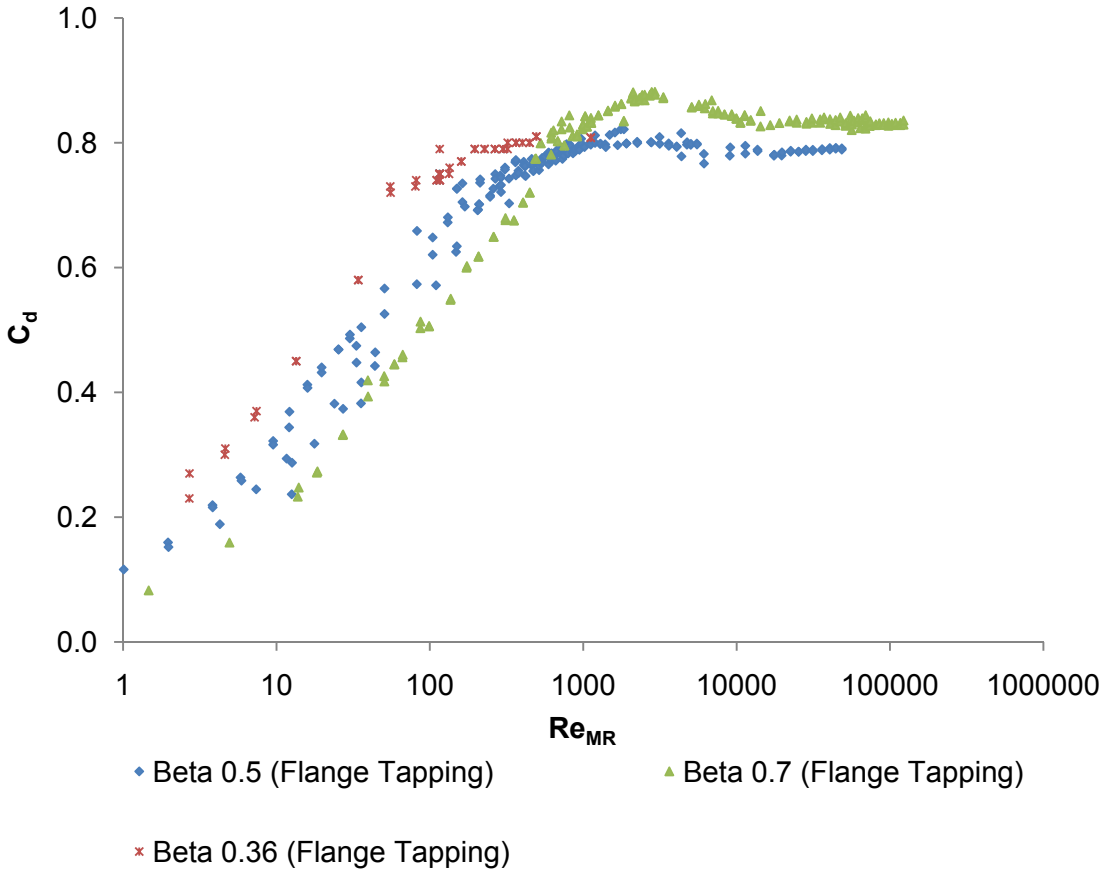

Figure 4.15 Discharge coefficient comparison for different diameter ratio orifices

Table 4.5 C_d values for different β ratios

β	**C_d**	**Std Dev**
0.5	0.79	± 0.0082
0.7	0.83	± 0.0044

4.5 Conclusions

In conclusion this chapter has outlined results obtained from an orifice test rig. Theoretical and experimental friction factors were compared to ascertain the accuracy and credibility of equipment used.

The rheological characteristics of the different fluids were measured using tube viscometry. The pseudo plastic model was found to best describe the flow behaviour of both polymeric solutions and the kaolin suspensions. The theoretical and experimental friction factors against Reynolds number were compared to evaluate the accuracy of the rheological parameters.

Pressure loss coefficient data for different β ratios was presented from laminar to turbulent flow régime. It was found that the pressure loss coefficient depended mainly on the β ratios for both laminar and turbulent flow régime. Different laminar flow orifice loss coefficients constants, C_{or}, for different β ratios were presented in Chapter 4 as well as constant turbulent flow constants, K_{or}.

The discharge coefficient data, C_d, presented in this chapter was found to be dependent on β ratio resembling the pressure loss coefficient. Discharge coefficient values were found to be nearly constant for higher Reynolds numbers. An average C_d value was also provided for the range of Reynolds number ranging between 10000 to120000. The two different tapping methods were also evaluated and were found to be mutually acceptable.

Comparisons between the experimental data and data available in the literature are presented in Chapter 5.

CHAPTER 5

5.1 Introduction

A comparison between experimental pressure loss and discharge coefficient data obtained in this work with that available in open literature is presented in this chapter. The experimental work is compared with Hall (1963), Ward-Smith (1971), Lakshmana Rao and Sridharan (1972), Idel'chik et al., (1994) and ESDU (2007). No correlation was found to predict pressure loss coefficient for β = 0.36, 0.5 and 0.7 from laminar to turbulent flow. A new empirical correlation was, therefore, developed for the prediction off pressure loss coefficients for long square-edged orifices. This new correlation offers advantages over those found in the literature. The proposed correlation covers a wide range of Reynolds numbers ($20 \leq Re_{MR} \leq 10^5$) and accommodates both Newtonian and non-Newtonian fluids, unlike other correlations which accounts only for Newtonian fluid and mostly in the range of Re $>10^4$. The goal of this work was to report pressure loss and discharge coefficient data to the open literature; hence Chapter 5 will essentially focus on the following areas:

- Comparison of the experimental data with the open literature and,
- new correlation for determining pressure loss coefficient for long square-edged orifice plates.

5.2 Pressure loss coefficients comparison

Pressure loss coefficients for orifices with β ratios of 0.36, 0.5 and 0.7 and aspect ratios of 4, 5 and 5 respectively are compared with Ward-Smith (1971) and Idel'chik et al., (1994) models. A summary of different authors' work is presented in Table 5.1. Bohra (2004) published correlations [Equation 2.76 and 2.77] to predict loss coefficients in the range of laminar-transitional flow, but they are applicable only for small β ratios i.e β = 0.022, 0.044 and 0.137. Hasegawa et al., (1997) [Equation 2.75] published correlation which is valid for β = 0.1 in laminar flow only. Hence, because of a lack of experimental data and correlations, the experimental loss coefficients in laminar and transitional flow could not be verified for the three different orifices studied.

Table 5.1 Summary of Data for comparison with the experimental work

Author	Equation / Experimental data	Re	Technique
Hall (1963)	$C_d = 1 - 0.184\left(\left(\frac{t}{d}\right) - 1 + k(\beta(Re_d^{0.25}\right)^{0.8} Re_d^{-0.2}$	Turbulent flow	Correlation
Ward – Smith (1971)	$K_{or} = \left[\frac{1}{0.608\beta^2\left(1-\beta^{5.2}\right)\left(1+\left(\frac{t}{d}\right)^{3.5}\right)+\beta^{7.2}} - 1\right]^2$	> 10^4	Correlation
Lakshmana Rao& Sridharan (1972)	Plot of K_{or} Vs Re for different β ratios i.e β = 0.2 for long orifice	10^1 – 2 x10^3	Experimental
Idel'chik et al., (1994)	$K_{or} = \left[\left(0.5 + \tau\sqrt{1-\beta^2}\right)\left(1-\beta^2\right)^2 + 0.02\frac{t}{d}\right]\left(\frac{1}{\beta^2}\right)^2$	>10^5	Correlation

5.2.1 Comparison between literature and new data for β = 0.36 and t/d = 4

A comparison of the experimental data for the orifice with β = 0.36 and t/d = 4 with Ward-Smith (1971) [Equation- 2.72] is presented in Figure 5.1. Experimental data was compared with the Equation 2.74 (Idel'chik et al., 1994) and presented in Figure 5.2. Data was generated up to Reynolds number of 1000. Figure 5.1 shows that after a Reynolds number of about 400, the data tended towards a constant K_{or} value. Although the model published by Ward-Smith has an applicability range of Re > 10^4 but it can be seen from Figure 5.1, 5.3 and 5.5 that the constant values obtained are within 10% of that predicted by Ward-Smith at Re >10^4. Figure 5.1 indicates the experimental data is within a 10% error margin compared to Ward-Smith. Experimental loss coefficient and loss coefficients predicted by Idel'chik et al., (1994) are also found to be within 10% error margin using a value of τ = 1.14. It can also be seen from Figure 5.2, 5.4 and 5.6 that the constant value obtained are within 10% of that predicted by Idel'chik et al., (1994). Table 5.2 presents the relative percentage error of the data compared to the two published models.

Table 5. 2 Comparison of K_{or} with literature for β = 0.5 and t/d = 5

Experimental	Idel'chik et al., (1994)	Ward-Smith (1971)	%error (Ward-Smith)	%error (Idel'chik et al.,)
76	76.18	76.18	± 0.23	± 0.23

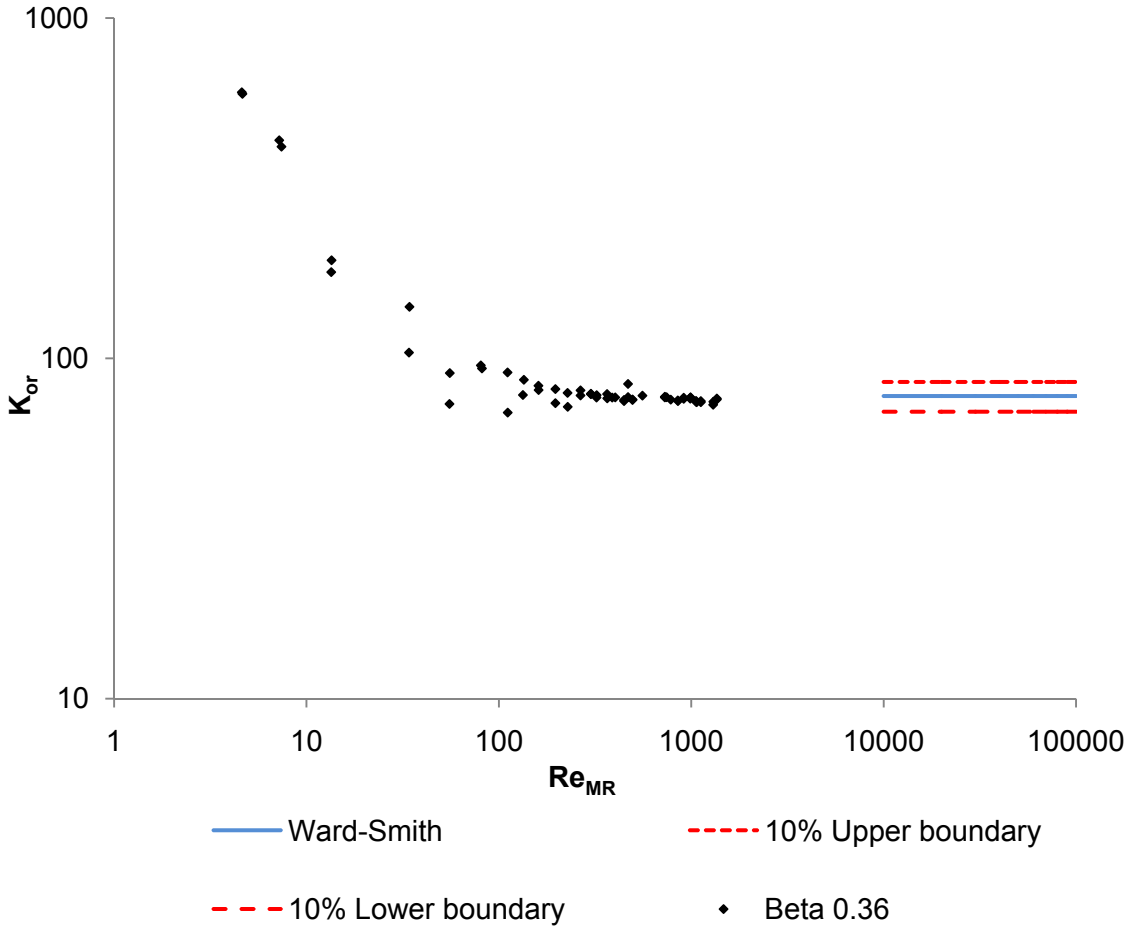

Figure 5.1 Comparison of β = 0.36 experimental data and Ward-Smith (1971)

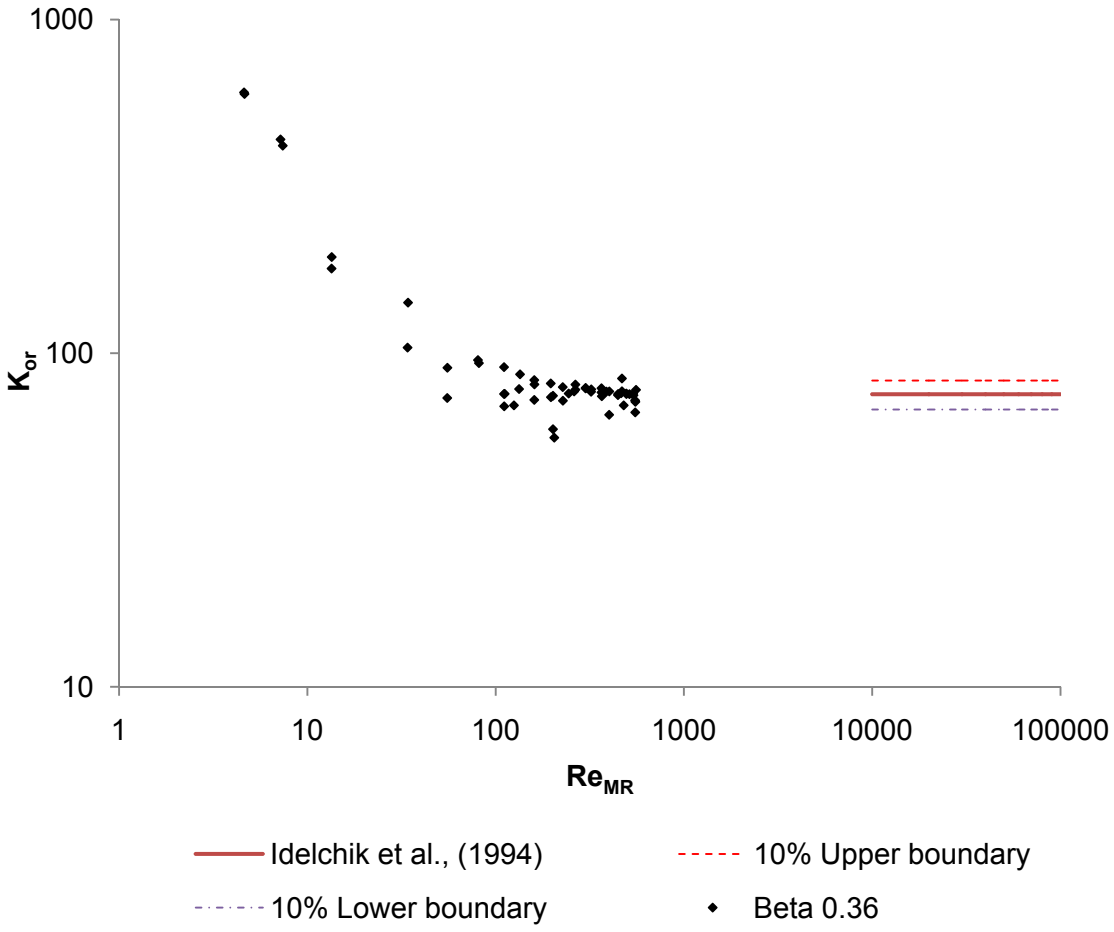

Figure 5.2 Comparison of β = 0.36 experimental data and Idel'chik (1994)

5.2.2 Comparison between literature and new data for β = 0.5 and t/d = 5

Figure 5.3 presents the comparison of the experimental pressure loss coefficient with Ward-Smith (1971) in the turbulent regimé for Re ≥ 1 x 10^4. Figure 5.4 presents the experimental loss coefficients with Idel'chik et al., (1994) for Re ≥ 5 x 10^4. The loss coefficients were found to be within 10% error margin compared to Equation 2.72 (Ward-Smith, 1971). Loss coefficients predicted by Idel'chik et al.,(1994) and the experimental data were found to be within 15% error margin. Table 5.3 presents the relative percentage error of the data compared against the two published models.

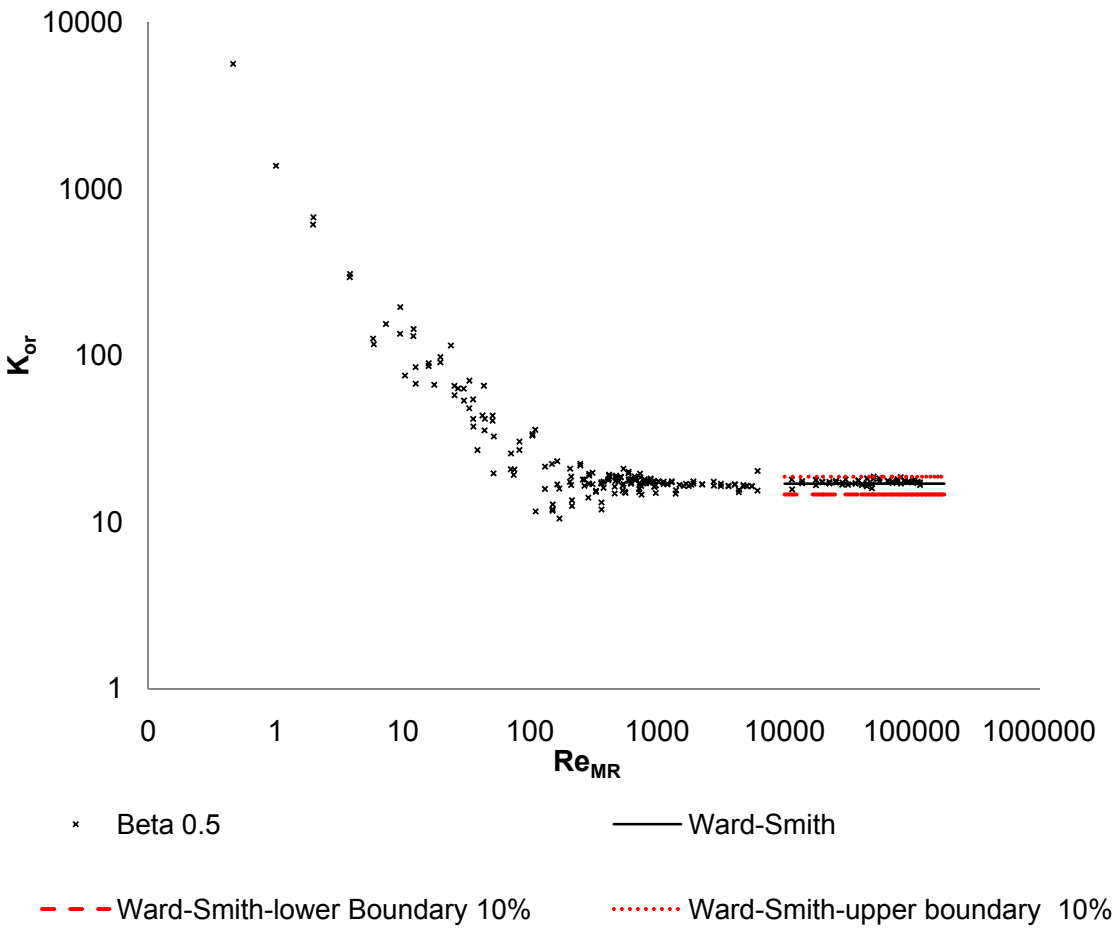

Figure 5.3 Comparison of β =0.5 experimental data and Ward-Smith (1971)

Average K_{or} values are presented in Table 5.1 and compared with literature.

Table 5.3 Comparison of K_{or} with literature for β = 0.5 and t/d = 5

Experimental	Idel'chik et al., (1994)	Ward-Smith (1971)	%error (Ward-Smith)	%error (Idel'chik et al.,)
17.70	16.60	16.99	± 4.5	± 7

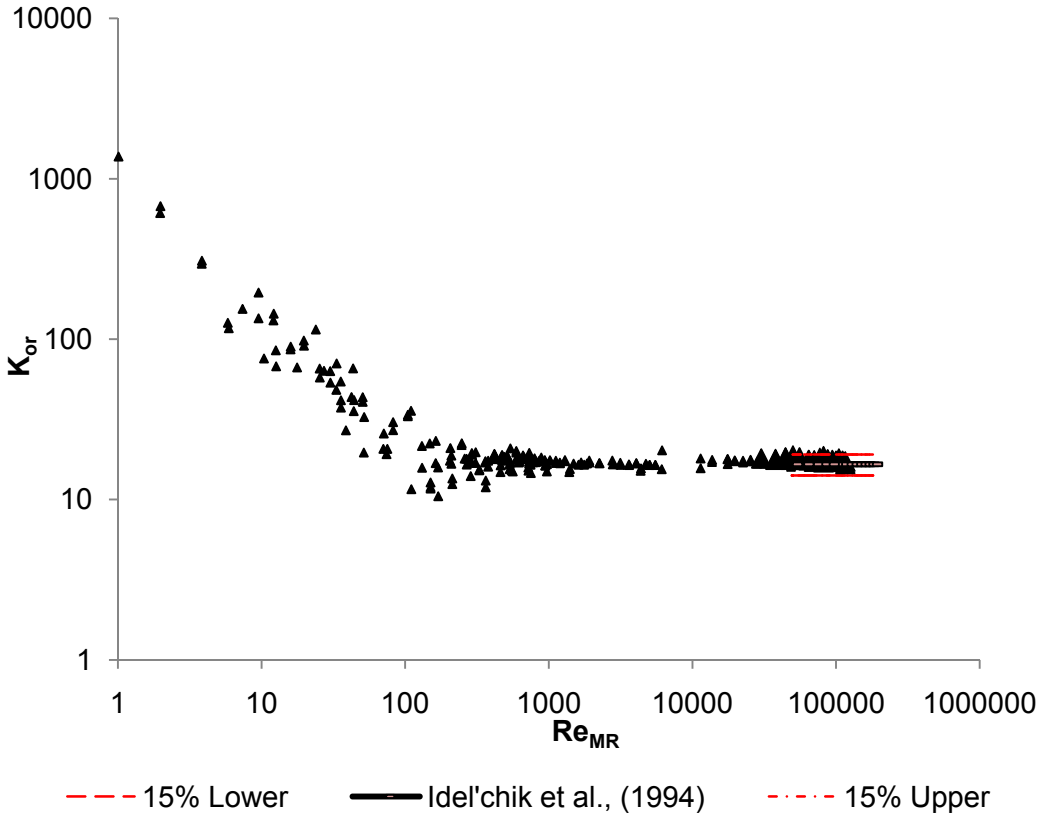

Figure 5.4 Comparison of β = 0.5 experimental data and Idel'chik et al., (1994)

5.2.3 Comparison between literature and new data for β = 0.7 and t/d = 5

The loss coefficients were found to be within 15% error margin when compared to Ward-Smith (1971) and 25 % compared to Idel'chik et al., (1994). Figure 5.5 and 5.6 presents the comparison between experimental data and literature. Table 5.4 gives the relative percentage error of the data compared to the two published models.

Table 5.4 Comparison of K_{or} with literature for β = 0.7 and t/d = 5

Experimental	Idel'chik et al., (1994)	Ward-Smith (1971)	%error (Ward-Smith)	%error (Idel'chik et al.,)
2.33	2.61	2.56	± 12	± 10

It can be seen from Table 5.4 that the relative percentage error margin for β = 0.7 is higher than that of β = 0.5 when compared to the literature. According to Husain and Teyssandier (1984) pressure fluctuation increases with β. As the beta ratio decreases

the dominant source of uncertainty shifts from measurement accuracy to turbulent flow fluctuations (Darin et al., 2001).

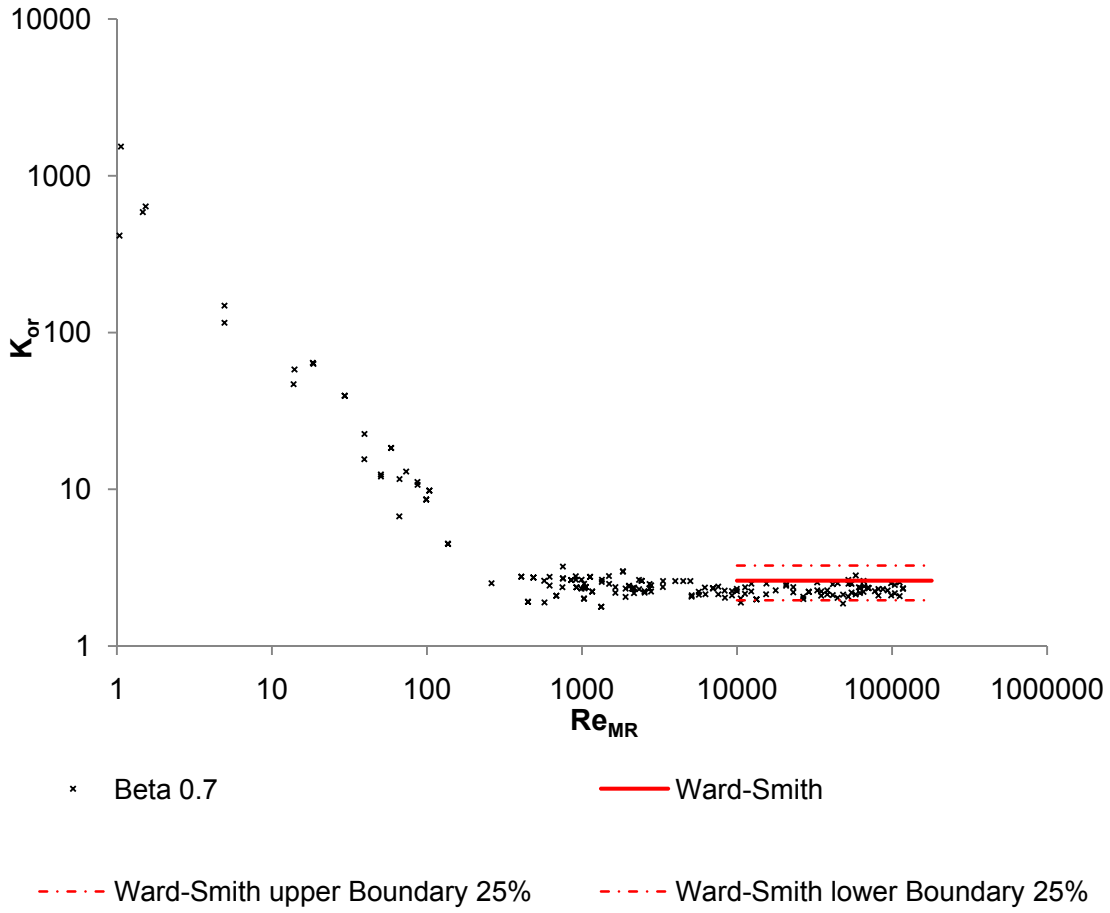

Figure 5.5 Comparison between β = 0.7 experimental data and Ward-Smith (1971)

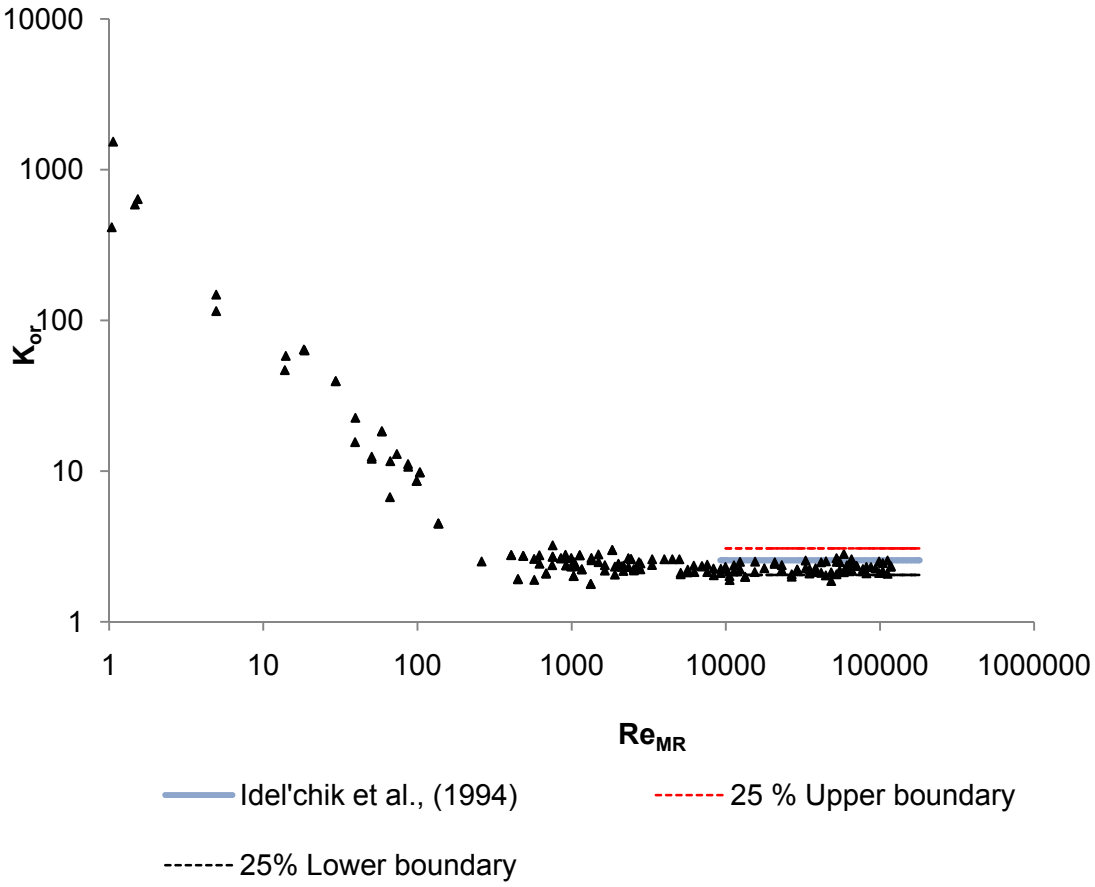

Figure 5.6 Comparison between experimental data β =0.7 and Idel'chik et al., (1994)

A comparison of numerical discrepancies between the two β ratios used in this work and the open literature are presented in Table 5.5.

Table 5.5 Comparison of numerical discrepancies between two β ratios

β	**Ward-Smith (1971)**	**Idel'chik (1994)**	**Experimental**	**%error (Ward-Smith)**	**%error (Idel'chik et al.,)**
0.5	16.99	16.60	177.7	± 4.5	± 7
0.7	2.61	2.56	2.33	± 12	± 10

5.3 Discharge coefficient comparison

The discharge coefficients for orifices with β ratios of 0.5 and 0.7 and an aspect ratio of 5 are compared with Equation 2.78 (Hall, 1963). The model published by Hall (1963) was based on data obtained using D & D/2 tapping arrangement. Data presented in this chapter was obtained using the Flange tapping method. However, it was shown in Figure 4.18 that no significant difference was observed between the two sets of data obtained using two different tapping locations. Hence, the use of Hall's equation to evaluate the experimental data is justified. Because of a lack of experimental data a direct comparison of the experimental data with literature, especially in laminar flow was not possible.

5.3.1 C_d comparison between literature and new data for β = 0.36 and t/d = 4

Experimental data was generated up to a Reynolds number of 1000 for a β = 0.36 orifice. The model published by Hall (1963) is valid for turbulent flow. No experimental data was found in the literature for β = 0.36, t/d = 4 orifice for direct comparison purpose. A plot of C_d values against Reynolds number in the range of 4 – 1000 is presented in Figure 4.14. Figure 2.23 and 2.24 presents the available discharge coefficient data in the literature.

5.3.2 C_d comparison between literature and new data for β = 0.5 and t/d = 5

Discharge coefficient values for β = 0.5 were compared with Equation 2.78 (Hall, 1963) in the turbulent régime. It was not possible to compare data in the laminar and transitional flow régimes for lack of experimental data and correlations. Figure 5.7 presents the comparison between experimental data and literature. The C_d value was found to be 0.8, which was within ± 0.5% error margin in the turbulent régime compared to Hall (1963).

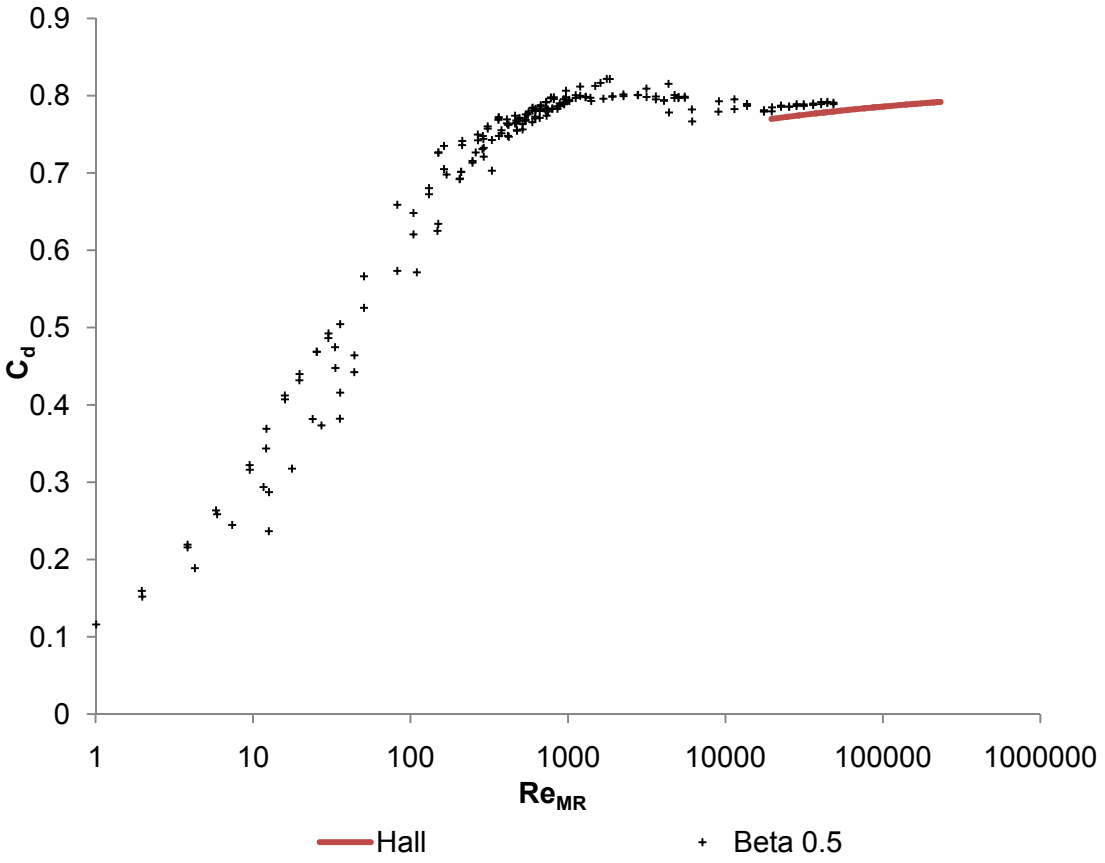

Figure 5.7 Comparison between experimental C_d and Hall (1963)

5.3.3 C_d comparison between literature and new data for β = 0.7 and t/d = 5

Once again, experimentally obtained C_d value was compared with Equation 2.78 (Hall, 1963). The C_d value was found to be within ± 2% error margin in the turbulent régime compared to Hall (1963). Figure 5.8 presents the comparison between Hall (1963) and experimental C_d data.

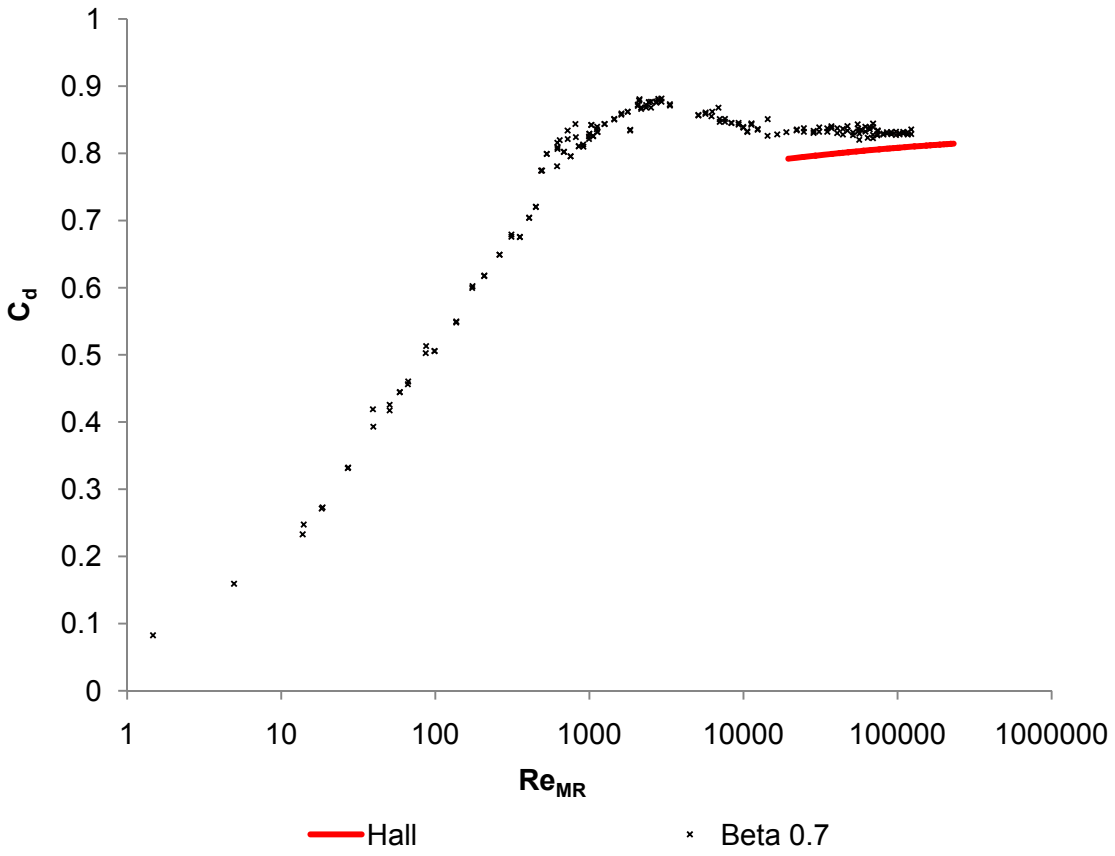

Figure 5.8 Comparison between experimental C_d and Hall (1963)

Table 5.6 illustrates numerical discrepancies found between Hall (1963) and the experimental data.

Table 5.6 Numerical discrepancies between the data and the open literature

β	Hall (1963)	Experimental	%error
0.5	0.788	0.792	0.50
0.7	0.829	0.813	2

In conclusion, it can be said that none of the experimental data and correlations found in the open literature or commercially available literature could be used to verify the

pressure loss coefficient and discharge coefficient data in the laminar or laminar to turbulent régime. Data and correlations found for turbulent flow was 0.5 and 2% respectively for beta ratio of 0.5 and 0.7 orifice for discharge coefficient and within a 25% error margin for pressure loss coefficients. All the data with its respective errors compared to the literature are highlighted in Tables 5.2 - 5.6. The percentage error was calculated using Equation 3.6.

5.4 Development of the correlation to predict pressure loss coefficients

There was a necessity to develop a correlation to predict pressure losses through square-edged long orifices because of a lack of an adequate correlation. With insight gained from the data analysis, a correlation was developed using 500 data points to predict the orifice pressure loss coefficient, given its geometry and Re_{MR}. The purpose of this section is to present the derivation of the new correlation and to compare it with the experimental data and other data sets in the literature. The correlation is plotted against the Metzner-Reed Reynolds number for the analysis.

5.4.1 New correlation

The shortcomings of different correlation presented in the open literature imposed the development of an empirical correlation. In 2003 Choi and his co workers developed a generalized correlation to predict refrigerant mass flow rate through adiabatic capillary tubes. The correlation was developed by generating dimensionless parameters for operating conditions, capillary tube geometry, and refrigerant properties using the Buckingham π theorem (Buckingham, 1914). A similar approach was followed in this work to develop a correlation for predicting long square-edged orifice pressure loss coefficients. The orifice pressure loss coefficients are a function of different variables as presented in Equation 5.1.

$$\frac{\Delta P}{\rho V^2} = K_{or} = f\left(\frac{\rho VD}{\mu_{eff}}, \frac{t}{d}, \frac{d}{D}\right) \qquad \text{Equation 5.1}$$

Equation 5.1 can also be written as:

$$K_{or} = f\left(Re, \frac{t}{d}, \beta\right) \qquad \text{Equation 5.2}$$

The roughness of the orifice wall was omitted as the orifice wall used was smooth. The generalized correlation can be presented explicitly in power law form to enforce dimensional homogeneity as:

$$K_{or} = CRe^{x}\left(\frac{t}{d}\right)^{y}\beta^{z} \qquad \text{Equation 5.3}$$

where, Re = Re_N or Re_{MR} depending on the type of fluid. According to Finnemore and Franzini (2002), dimensional analysis provides a qualitative relationship between the variable. The experimental results were used to obtain the constants to complete the qualitative relationship. Constants C, x, y and z are presented in Table 5.7, showing dependence on the orifice geometry only.

Table 5.7 Coefficients for equation 5.3

C	x	y	z
170.5	-1	0.2	-3.17

On this basis, a correlation equation describing Newtonian and non-Newtonian pressure loss coefficient is proposed and presented as:

$$K_{or} = \frac{170.5\beta^{-3.17}}{Re}\left(\frac{t}{d}\right)^{0.2} \qquad \text{Equation 5.4}$$

Figure 5.9 presents a comparison of the derived correlation and experimental data. The relative uncertainty of this correlation over a Reynolds number range of 1-100 was 49%. The correlation holds for the range:

- $0.2 \leq \beta \leq 0.7$
- $2 \leq t/d \leq 5$
- $1 \leq Re \leq 100$

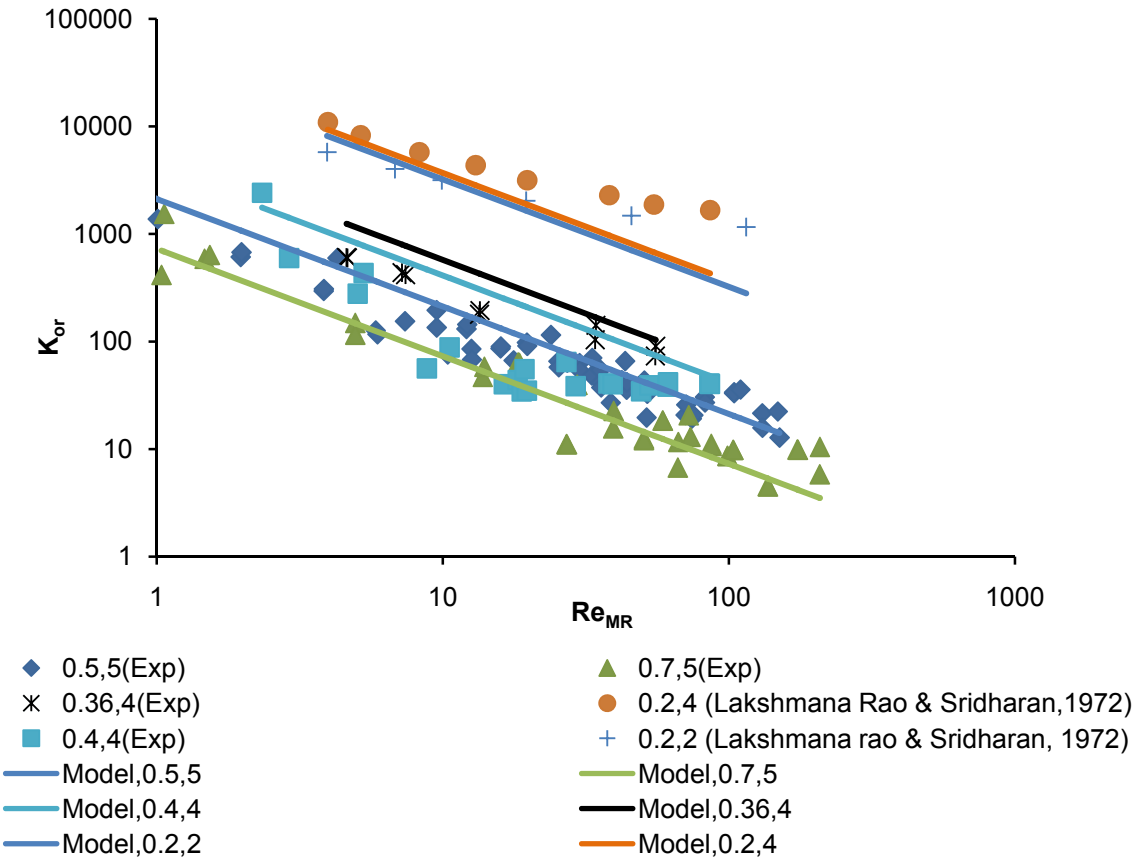

Figure 5.9 Comparison between the new correlation and the experimental data

The limitation of Equation 5.4 which is only applicable for laminar flow regime necessitated the development of a new correlation which is applicable from laminar to turbulent flow regimes. It can be seen from Figure 4.11 that in laminar flow the loss coefficient depends on Re and increases with decreasing Reynolds number. But, in turbulent flow the loss coefficient is dependent on the orifice geometry only. On the foundation of this observation, Equation 5.5 is proposed which is a simple combination of Equation 5.2 & 5.4 with an assumed physical mechanism between the dimensionless parameters.

$$K_{or} = \frac{170.5\beta^{-3.17}}{Re} + \left[C_1\beta + C_2\left(\frac{t}{d}\right)^{g_e} \right] \qquad \text{Equation 5.5}$$

Where, Re = Re_N and Re_{MR}

The first part of Equation 5.5 is strongly valid for viscous dominated region and the second part of the equation is only valid for inertia dominated region. The constants C_1, C_2 and g_e (geometry factor) are factors introduced for proper agreement in the transitional region. The factors are floating parameters and dependent on β and t/d ratios and to be determined through non-linear regression analysis.

The effect of aspect ratio, (t/d), ranging from 2 to 5 on K_{or} in turbulent flow, is evaluated. Table 5.8 presents different beta and aspect ratio and their respective pressure loss coefficient. It can be seen from Table 5.8 that a percentage difference was calculated between the maximum K_{or} and the K_{or} for smallest aspect ratio which is 2. The highest percentage different was found to be ± 8% in turbulent flow regime. So, it was assumed that the pressure loss coefficient, K_{or}, is nearly constant for aspect ratio range of 2-5. Experimental data obtained by Lakshmana Rao and Sridharan (1972) for two different aspect ratios was plotted to evaluate the effect of aspect ratio on K_{or} in laminar flow. Figure 5.10 presents the experimental data obtained by Lakshmana Rao and Sridharan (1972). It is noticeable from Figure 5.10 that the K_{or} value for two different aspect ratios does not vary by more than 10% in the Reynolds number range of 20 - 100 and the difference is insignificant in Reynolds number above 100; but the deviation is higher For Reynolds number below 20.

Table 5.8 Effect of aspect ratio on K_{or} in turbulent flow (ESDU, 2007)

		K_{or}					
Beta ratio	**Aspect ratio→**	**2**	**3**	**4**	**5**	**Maximum K_{or}**	**% Difference**
0.2		896	896	896	922	922	2.82
0.3		163	163	163	172	172	5.23
0.4		44	46	47	48	48	8.33
0.6		4.91	4.91	5.2	5.35	5.35	8.22

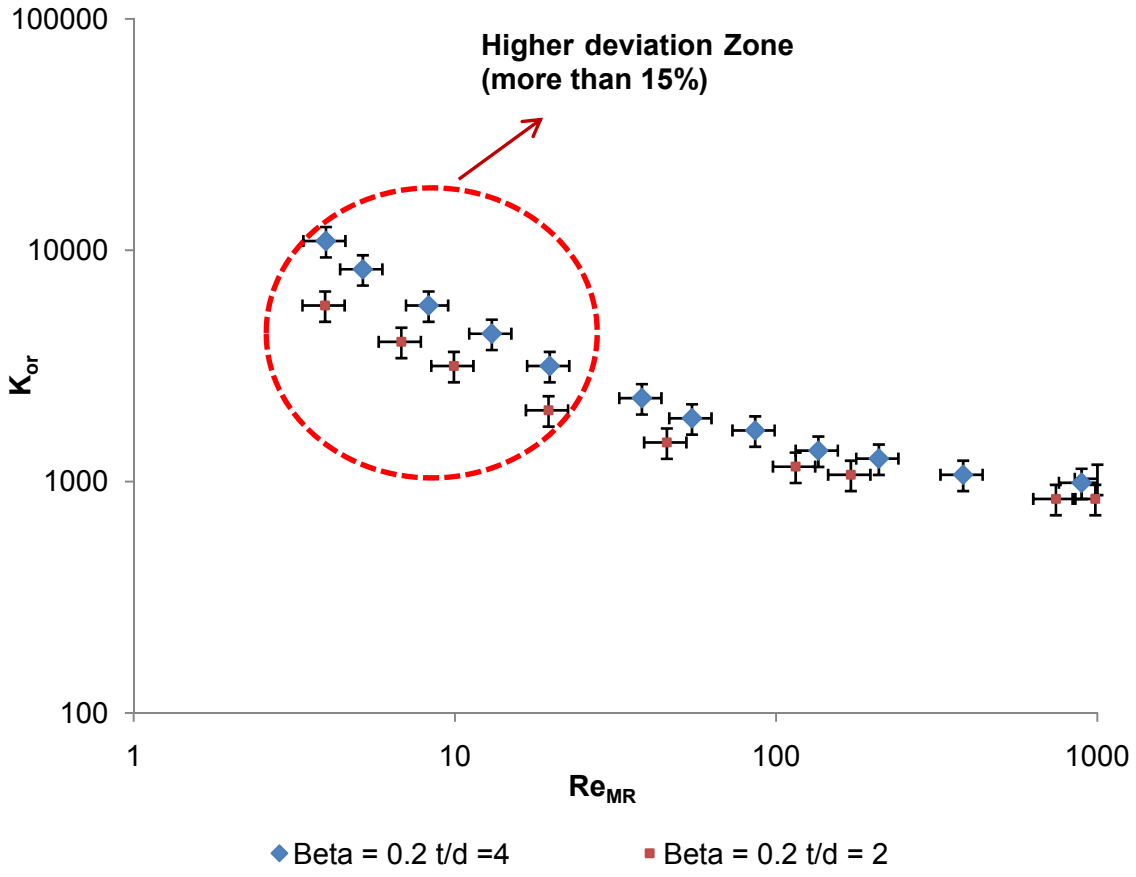

Figure 5.10 Comparison between K_{or} for different aspect and β ratio in laminar flow (Lakshmana Rao & Sridharan, 1972)

Multivariable non-linear regression analysis was performed to optimize the difference between the experimental data and Equation 5.5. Suitable values of -17 and 5 were obtained for constants C_1 and C_2 (Equation 5.5) respectively but different g_e values were used to correlate the experimental data within acceptable error margin. After replacing constants C_1 and C_2 with optimum values Equation 5.5 can be written as:

$$K_{or} = \frac{170.5\beta^{-3.17}}{Re} + \left[-17\beta + 5\left(\frac{t}{d}\right)^{ge}\right] \qquad \text{Equation 5.6}$$

The g_e values obtained were plotted against different aspect ratios to derive the functional relationship between g_e and t/d. A power law function was fitted to obtain the mathematical relationship between each g_e and t/d ratio for different β ratios. Figure 5.11 presents a plot of g_e against t/d for different β ratios.

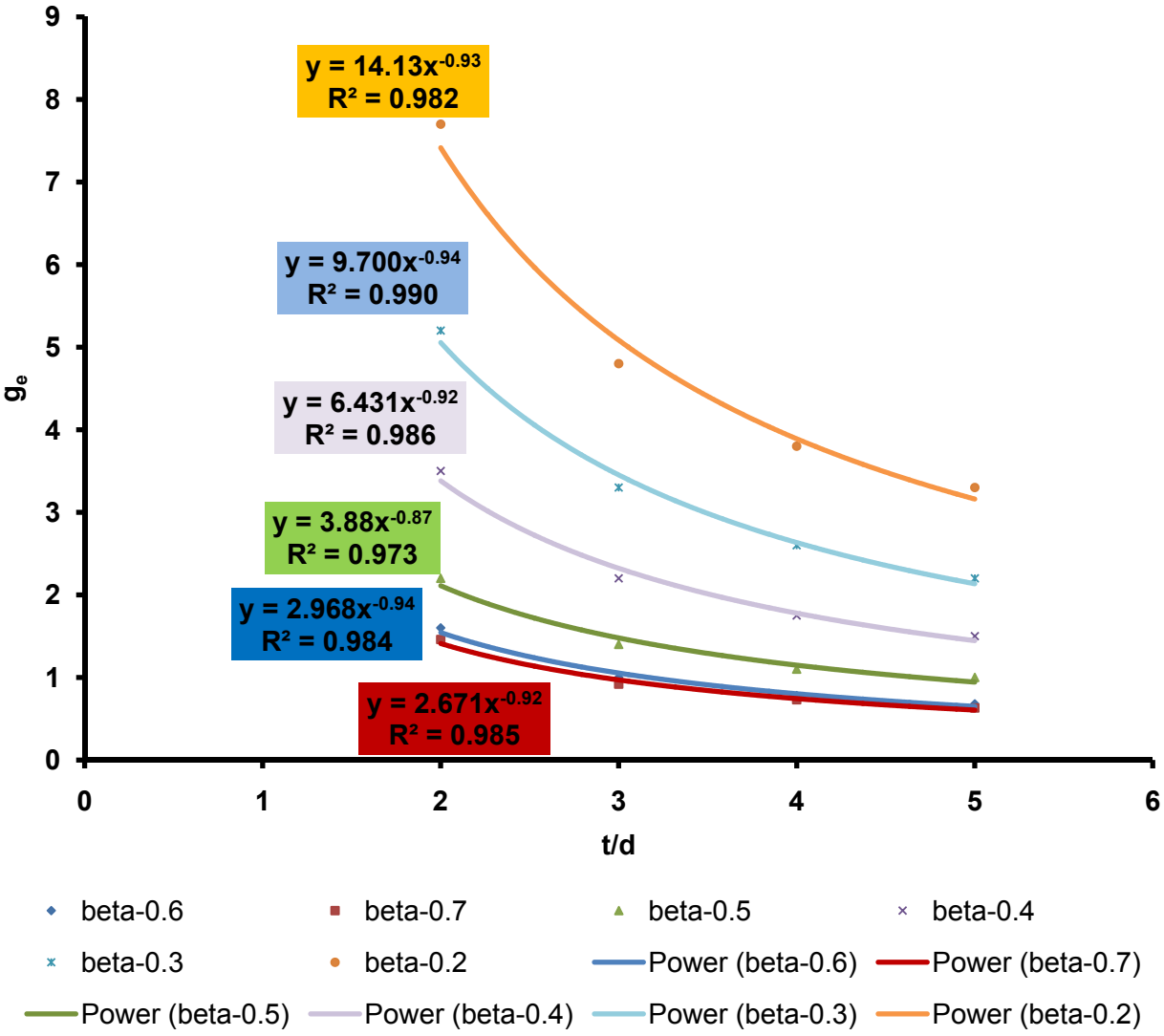

Figure 5.11 Functional relationship between β and geometry factor

According to Benziger and Aksay (1999) that a value of R^2 above 0.90 represents well fit of experimental data. All the power law fit in Figure 5.11 has a R^2 value above 0.95. It can be seen from Figure 5.11 that the different power law functions obtained possesses almost identical scaling component. So, the different scaling components can be minimized to one single value by taking the average of scaling components. The average scaling component was found to be -0.92. A single expression was derived for the different functions to describe the functional relationship between g_e and β including the aspect ratios by plotting the different power law constants obtained from Figure 5.11

against different beta ratios. Figure 5.12 presents the plot of different correlation constants against β ratios.

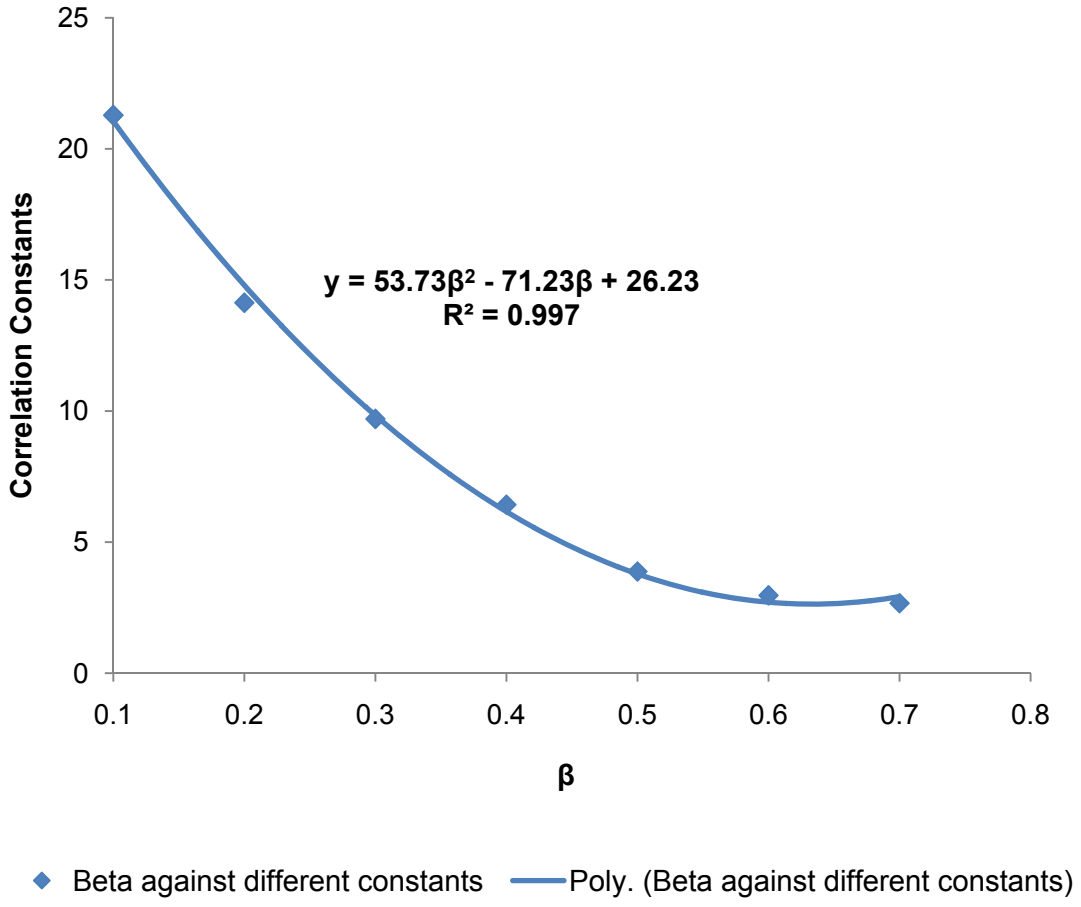

Figure 5.12 Functional relationship between β and correlation constant obtained from Figure 5.11

The term g_e can be expressed as:

$$g_e = \left(53.77\beta^2 - 71.23\beta + 26.23\right)\left(\frac{t}{d}\right)^{-0.92} \qquad \text{Equation 5.7}$$

Finally replacing g_e in Equation 5.6 with Equation 5.7:

$$K_{or} = \frac{170.5\,\beta^{-3.17}}{Re} + \left[-17\beta + 5\left(\frac{t}{d}\right)\left[\left(53.77\,\beta^{2} - 71.23\,\beta + 26.23\right)\left(\frac{t}{d}\right)^{-0.92} \right] \right]$$

Equation 5.8

Equation 5.8 has the following range of applicability:

- $0.2 \leq \beta \leq 0.7$
- $2 \leq t/d \leq 5$
- $1 \leq Re \leq 10^6$

5.5 Comparison between the experimental data and the newly derived correlation

The newly derived correlation, [Equation 5.8], is evaluated firstly against the experimental data obtained and secondly to data available in the literature given in Figures 5.13 – 5.16.

Figure 5.13 presents a comparison between experimental data and the new correlation for diameter and aspect ratio of 0.36 and 4 respectively. It can be seen from Figure 5.13 that 86% of the experimental data falls within 40% error margin. The agreement between the correlation and the experimental data is greater than 40% in the laminar flow régime of $Re_{MR} < 100$. The agreement in turbulent flow régime is fully matched.

It can be seen from Figure 5.14 that about 80% of the data falls within the ± 40%. This agreement is better in the turbulent flow régime compared with the laminar régime.

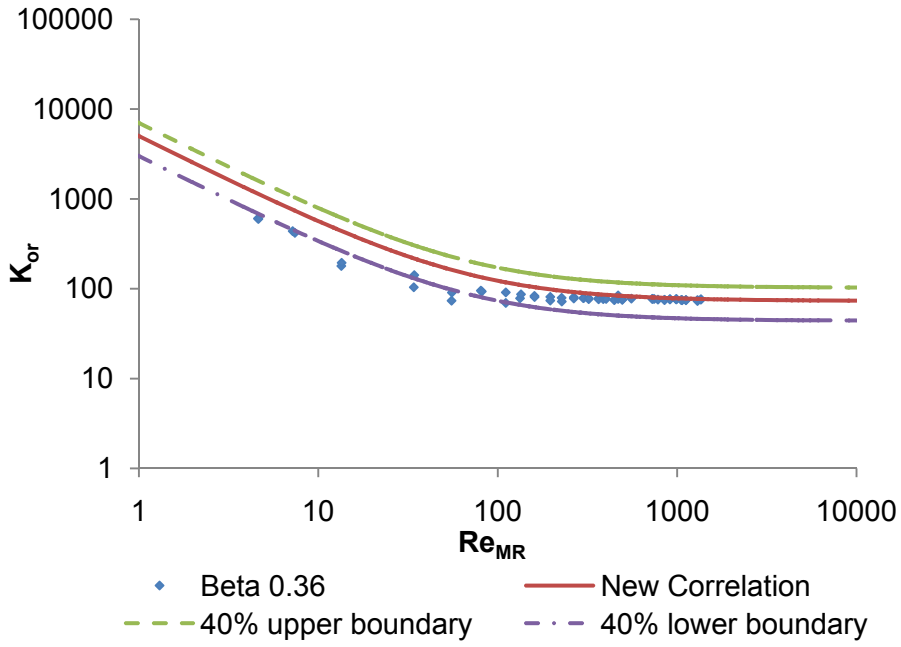

Figure 5.13 Comparison between new correlation and experimental data for beta = 0.36

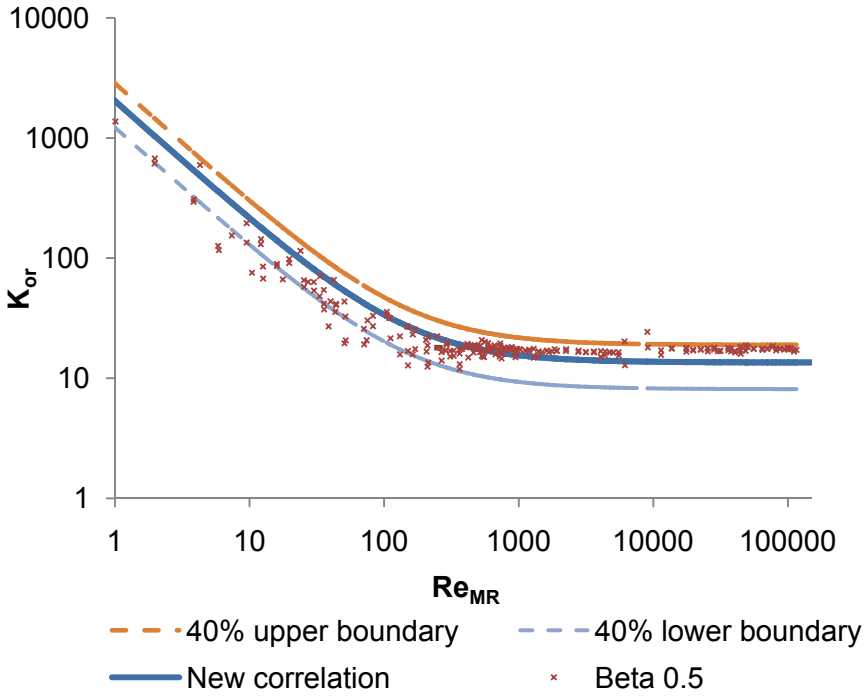

Figure 5.14 Comparison between the new correlation and experimental data for β =0.5

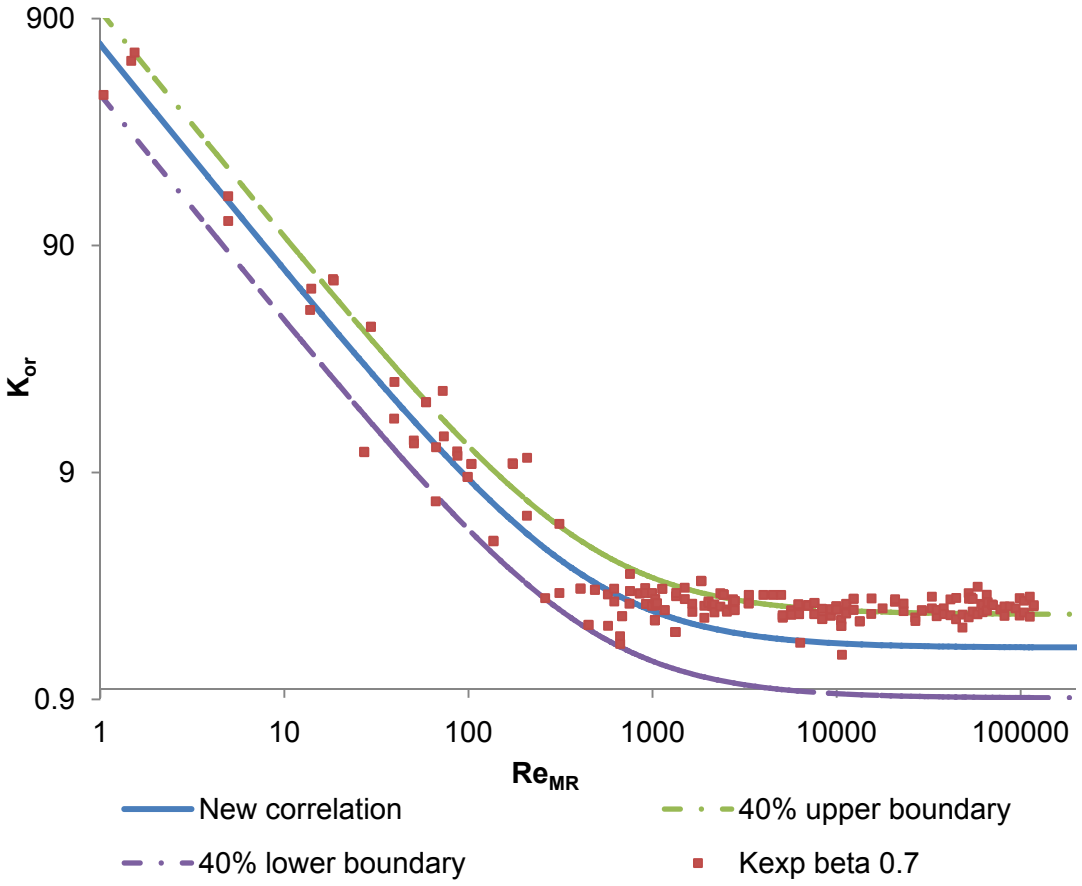

Figure 5.15 Comparison between the new correlation and experimental data for β = 0.7

It can be seen from Figure 5.15 that the fit between the experimental data and the correlation for β ratio is poor compared with β = 0.5. The fit is less in the turbulent region compared to the laminar flow régime. Approximately 50% of data falls within the ± 40% error margin compared to the correlation in laminar flow. In turbulent flow the correlation under predicts by about 40%.

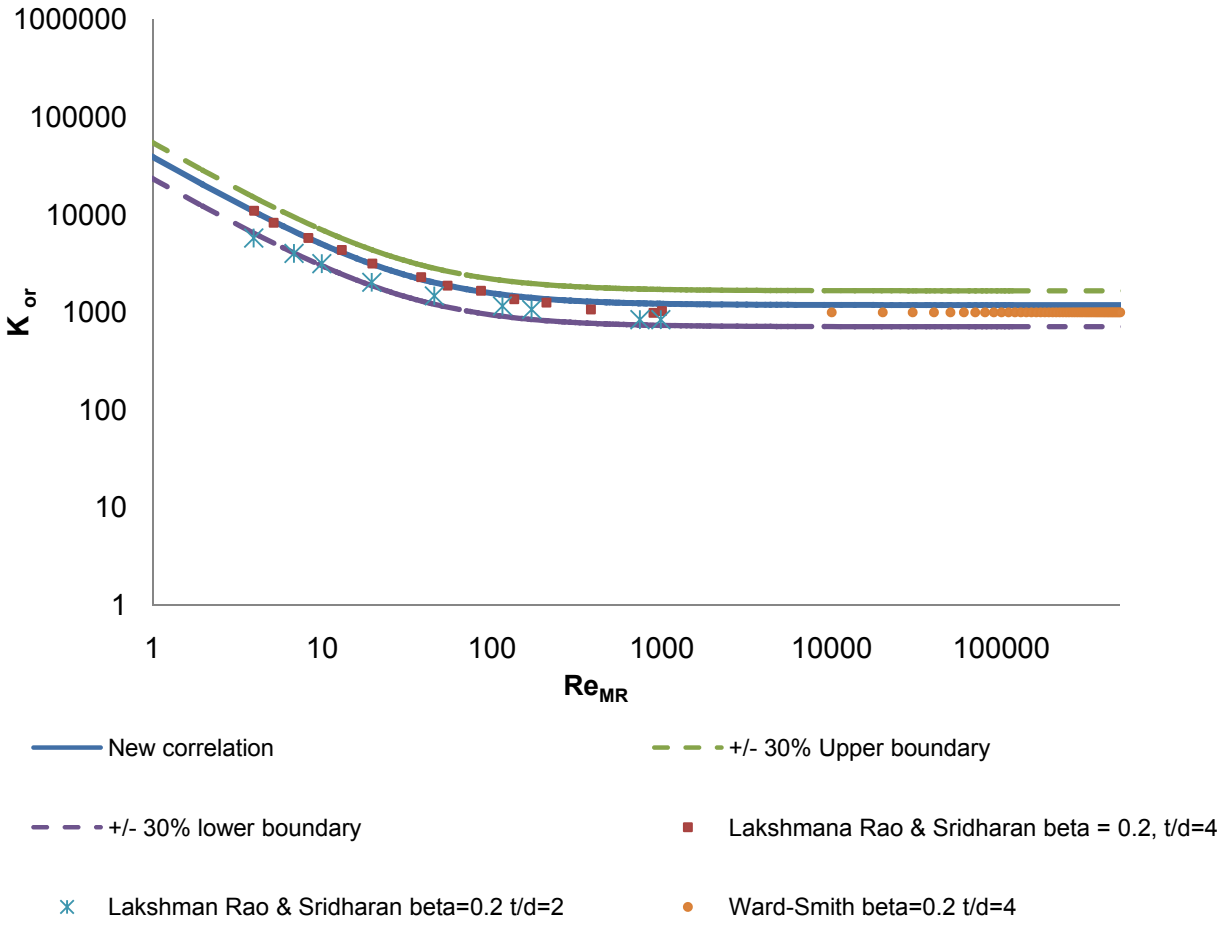

Figure 5.16 Comparison between the Correlation and the literature

It can be seen from Figure 5.16 that in the turbulent régime the correlation agrees well with the literature for different thicknesses to diameter ratios. In the laminar régime for Reynolds number, Re > 5, the correlation and literature agrees with each other within an error margin of ± 40 %.Table 5.9 presents the overall relative percentage uncertainty of the new correlation compared to the literature and experimental data.

Table 5.9 Overall relative uncertainty in the turbulent flow régime for the new correlation

Beta ratio	% Uncertainty
0.2	16
0.3	6
0.36	28
0.4	12
0.5	27
0.6	20
0.7	31
% Average	**20**

It can be seen from Table 5.9 that the correlation has an overall relative uncertainty of 20% compared to the literature and experimental data. This correlation with an overall uncertainty of 20%, should be deemed a good correlation considering the range of Reynolds numbers, beta ratios and aspect ratios.

5.6 Conclusions

A summary of the conclusions are presented:

- Pressure loss coefficient data for β ratios of 0.36, 0.5 and 0.7 have been determined in laminar, transitional and turbulent flow régimes using a range of Newtonian and non-Newtonian fluids.
- Discharge coefficient data for β ratios of 0.36, 0.5 and 0.7 have been determined in all the three flow régimes using a range of Newtonian and non-Newtonian fluids.
- A comparison of the experimental data obtained and the data found in the literature was completed for both K_{or} and C_d and discrepancies were quantified.
- It was found after the comparison study that the literature lacked correlations for predicting pressure loss coefficients from laminar to turbulent flow for certain flow geometries.
- A new correlation was derived from the experimental data and that found in literature to predict pressure loss coefficient within ± 40% error margin.

- A comparison between the correlation and the existing models showed good agreement.
- The correlation can be used to predict pressure loss coefficients from laminar to turbulent flow régimes for β and aspect ratios of 0.2 – 0.7 and 2 – 5 respectively.
- The new correlation can successfully be used to design fluid flow loops in hydraulic applications.

CHAPTER 6

6.1 Introduction

A description of the experimental study of long square-edged orifices (β = 0.36, 0.5 and 0.7) are presented in this thesis. This study has resulted in the formulation of an empirical correlation for predicting pressure loss coefficients from the laminar to turbulent flow régimes arising from a scarcity of correlation and experimental data in the literature. This section presents a summary of the work completed on orifice plates, contributions and recommendations for future research.

6.2 Summary

Three long square-edged orifices with dimensions of β = 0.36, 0.5 and 0.7 and aspect ratio of 4, 5 and 5 respectively were inserted horizontally in a pipe line and tested at the Cape Peninsula University of Technology. Pressure loss and discharge coefficients were determined experimentally for laminar, transitional and turbulent flow for these three long square-edged orifices. The data was compared with the experimental data and correlations available in the literature, such as Ward-Smith (1971), Idel'chik et al., (1994), ESDU (2007), Lakshmana Rao and Sridharan (1972) and Hall (1963). Evaluation of this work highlighted the following facts:

- The topic of orifice pressure losses especially large β and aspect ratios has been neglected at low Reynolds numbers;
- the loss coefficients in laminar flow are not constant as in turbulent flow;
- experimental data for pressure loss coefficient is scarce in laminar flow. No experimental K_{or} data were found for β = 0.36, 0.5 and 0.7 with aspect ratio of 4, 5 and 5 respectively;
- none of the available correlations found in the literature could be used to predict K_{or} for laminar to turbulent flow régime for β = 0.2 – 0.7. Available correlations could either predict in laminar or turbulent flow régime separately, but not in both regions and,

- the newly derived correlation is able to predict K_{or} within ± 40% error margin for β and aspect ratio range of 0.2 – 0.7 and 2 – 5 respectively in the laminar to turbulent flow régime.

6.3 Significant contributions

New pressure loss and discharge coefficient data have been reported to the open literature. A design correlation has also been reported to the open literature for long square-edged orifices. This correlation can successfully be used in designing pipe line system and flow circuits containing orifices as well as contributing to academic discourse and debate in this discipline. The Reynolds number range of models, published by Ward – Smith (1971) and Idel'chik et al., (1994) has also been extended through this work.

6.4 Conclusions

Experimental data for β = 0.36, 0.5 and 0.7 has been provided to open literature, and a new correlation has been derived to predict K_{or} in laminar – turbulent régime and proved to be successful.

6.5 Future research recommendations

At the end of this experimental study the following is recommended:

- More experiments should be conducted to obtain K_{or} and C_d data for β ratio range of 0.3 - 0.4;
- new correlation should be tested in laminar – turbulent zone but especially for laminar flow for β ratio of 0.6 and in between 0.2 - 0.4 and,
- if discrepancies are found the correlation should be modified to accommodate the changes.

List of references

1. ANSI/API. (1995). Manual of petroleum measurement standards. *AGA report no. 3 part1* . ANSI/API.
2. ASME. (2004). Measurement of fluid flow in pipes using orifice, nozzle and venturi. *American society of mechanical engineers standard, ASME MFC-3M-2004* . ASME.
3. Banerjee, T. K., Manas, D., & Das, S. K. (1994). Non-Newtonian liquid flow through globe and gate valve. *Canadian journal of chemical engineering , 72*, 207 - 211.
4. Barry, B. A. (1991). *Error in practical measurement in surveying, engineering and technology.* Rancho Cordova: Landmark Enterprises.
5. Baudouin, M. M. (2003). Contraction and expansion losses for non-Newtonian fluids . *Unpublished MTech thesis* . Cape Twon, South Africa: Cape Technikon.
6. Bechtold, J. (2006). *Jill Bechtolds home page*. Retrieved November 14, 2006, from Department of Astronomy, University of Arizona: http://boojum.as.arizona.edu/~jill/NS102_2006/Lectures/Lecture12/Turbulent.html
7. Benziger, J. B., & Aksay, I. A. (1999). *Notes on data analysis: Chemical engineering 346 spring term .* Princeton, Newjersey: Department of chemical engineering, Princeton university.
8. Bohra, L. K. (2004). Flow and pressure drop of highly viscous fluids in small aperture orifices. *MS thesis* . Georgia: Georgia Institute of Technology.
9. Bower, J. R. (1995). Backward orifice plate causes major gas flow measurement error. *Oil and gas , 93*, 43-44.
10. Brinkworth, B. J. (1965). *Introduction to experimentation.* London: English university press.
11. Buckingham, E. (1914). On physically similar systems: illustrations of the use of dimensional equations,. *Phys.rev.4(4)* , 345-376.
12. Chhabra, R. P., & Richardson, J. F. (2008). *Non-Newtonian flow and applied rheology.* Oxford: Butterworth - Heinemann.
13. Choi, J., Kim, Y., & Chung, J. T. (2003). An empirical correlation and rating charts for the performance of adiabatic capillary tubes with alternative refrigerants. *Applied thermal engineering , 24*, 29-41.
14. Coulson, J. M., & Richardson, J. F. (2008). *Chemical engineering volume 1.* Oxford: Pergamon press.

15. Darin, L. G., Lanasa, P. J., Morrison, G. L., & Morrow, T. B. (2001). Effects of orifice plates installed backwards and meter tube roughness on discharge coefficients. *Proc.Annual ACM-SIAM*, (pp. 403 - 415).
16. Durst, F., & Wang, A. B. (1989). Experimental and numerical investigations of the axisymmetric, turbulent pipe flow over a wall mounted thin obstacle. *Porceedings of the 7th sysmposium on turbulent shear flows*, *1*, pp. 10.4.1-10.4.6. Stanford CA.
17. Durst, F., Founti, M., & Wang, A. B. (1987). Experimental investigation of the flow through an axisymmetric constriction. *Proceedings of the sixth symposium on turbulrnt shear flows*, *6*, pp. 19.5.1-19.5.7.
18. Edwards, M. F., Jadallah, M. S., & Smith, R. (1985). Head losses in pipe fittings at low Reynolds number. *Chemical engineering res. des , 63*, 43 - 50.
19. ESDU. (2007). *Incompressible flow through orifice plates-A review of the data in the literature.* Engineering science data unit.
20. Fester, V. G., Kazadi, D. M., Mbiya, B. M., & Slatter, P. T. (2007). Loss coefficients for flow of Newtonian and non-Newtonian fluids through diaphragm valves. *Chemical engineering res. des: Transactions IChemE part A , 85*, 1314 - 1324.
21. Finnemore, E. J., & Franzini, J. B. (2002). *Fluid mechanics with engineering applications.* Boston: McGraw-Hill.
22. Haldenwang, R. (2003). Flow of non-Newtonian fluids in open channels. *Unpublished DTech thesis* . Cape Technikon.
23. Hall, G. W. (1963). Analytical determination of the discharge characteristics of cylindrical tube orifices. *Journal of mechanical engineering science , 5*, 91-97.
24. Hanks, R. W., & Ricks, B. L. (1975). Transitional and turbulent pipe flow of pseudo plastic fluids. *Journal of hydraulics , 9*.
25. Hasegawa, T., Suganuma, M., & Watanabe, H. (1997). Anomaly of excess pressure drops of the flow through very small orifices. *Physics of fluids , 9*, 1 - 3.
26. Heywood, N. I., & Brown, N. P. (1991). *Slurry handling: Design of solid - liquid systems .* Barking: Elsevier.
27. Ho, Y. S., & Leung, T. P. (1985). Performance of conical entrance orifice plates at low Reynolds number. *International journal of heat and fluid flow , 2*, 122 - 125.
28. Husain, Z. D., & Teyssandier, R. G. (1984). Effects of flow-induced disturbances and the frequency response of pressure transducers on the measurement of the differential pressure on the flange taps. *ASME/Winter annual meeting.* Washington D.C: ASME.

29. Idel'chik, I. E., Malyavskaya, G. R., Martynenko, O. G., & Fried, E. (1994). *Handbook of hydraulic resistance.* London: CRC press.
30. ISO. (2002). *Measurement of fluid flow by means of pressure differential devices inserted in circular-cross section conduits running full .* BS EN ISO 5167-2:2002(E).
31. Jog, M. A., Mandal, A., Xue, J., & Ibrahim, A. A. (2008). Flow of power law fluids in simplex atomizers. *International journal of heat and fluid flow , 29*, 1494-1503.
32. Johansen, F. C. (1930). Flow through orifice pipes at low Reynolds number. *Proceedings of Royal Society*, *126*, pp. 231-245. London.
33. Kazadi, D. M. (2005). Non-Newtonian losses through diaphragm valves. *Unpublished MTech dissertation* . Cape Town: Cape Peninsula University of Technology.
34. Kendrik, R. (1997). Effect of the latest revision of ANSI/API 2530/AGA 3 on orifice meter primary elements. Daniel measurement and control.
35. Kirkup, L. (2002). Data analysis with Excell: An introduction for physical scientist. Cambridge: Cambridge university press.
36. Kittredge, C. P., & Rowley, D. S. (1957). Resistance coefficients for laminar and turbulent flow through one-half-inch valves and fittings. *Transactions of the American society of mechanical engineering , 79*, 1759-1765.
37. Kotze, R. (2007). Rheological characterization of highly concentrated mineral suspensions using an ultrasonic velocity profiler. *Unpublished MTech dissertation* . Cape Town: Cape Peninsula University of Technology.
38. Lakshmana Rao, N. S., & Sridharan, K. (1972). Orifice losses for laminar approach flow. *Journal of the hydraulic division , 98*, 2014 - 2033.
39. Lakshmana Rao, N. S., Sridharan, K., & Alvi, S. H. (1976). Crirtical Reynolds number for orifice and nozzle flows in pipes. *Journal of hydraulic research , 15*, 167-178.
40. Lazarus, J. H., & Slatter, P. T. (1988). A method for the rheological characterization of the tube viscometer data. *Journal of pipe lines , 7*, 165-176.
41. Liu, H. (2003). *Pipeline engineering.* Lewis publishers.
42. Macosko, C. W. (1993). *Rheology: Principles, Measurement and applications.* New York, weinheim, Cambridge: VCH publishers, INC.
43. Malkin, A. Y. (1994). *Rheology fundamentals.* Ontario: Chemtech publishers.
44. Massey, B. S. (1990). *Mechanics of fluids.* Van nostrand reinhold.
45. Mbiya, B. M. (2008). Predicting pressure losses in straight-through diaphragm valves. *Unpublished DTech thesis* . Cape Town: Cape Peninsula University of Technology.

46. McKinley, G. H., & Rothstein, J. P. (1999). Extensional flow of a polystyrene Boger fluid through a 4:1:4 axisymmetric contraction/Expansion. *Non-Newtonian fluid mech* , 61-88.
47. Metzner, A. B., & Reed, J. C. (1955). Flow of non-Newtonian fluids-correlation of the laminar, transtition and turbulent flow regions. *Aiche journal , 1*, 434-440.
48. Mezger, T. G. (2002). *The rheology handbook: for users of rotational and oscillatory rheometers.* Hannover: Viencebtz Verlag.
49. Miller, D. S. (1996). *Internal flow.* Cranfield: BHR group.
50. Miller, D. S. (1990). *Internal flow systems.* Cranfield: BHRA.
51. Miller, R. W., & Kneisel, O. (1969). Experimental study of the effects of orifice plate eccentricity on flow characteristics. *ASME J. basic engng , 91*, 121-131.
52. Morrison, G. L., Deotte, R. E., Moen, M., Hall, K. R., & Holste, J. C. (1990). Beta ratio, swirl and Reynolds number dependence of wall pressure in orifice flow meters. *Flow measurement and instrumentation , 86*, 269 -277.
53. Morrow, T. B. (1999). Accuracy counts. How abnormal conditions affect orifice meter measurements. *Flow control network* .
54. Moseley, J., Charles, D. M., & Hal, L. (1975). *Patent No. 3894562.* United states.
55. Nally, B. M. (2010). *Pump, centrifugal pumps, PD pumps, seals & mechanical seals data*. Retrieved 2 14, 2010, from Mc Nally institute: http://www.mcnallyinstitute.com/13-html/13-12.html
56. Ohrn, T. R., Senser, D. W., & Lefebvre, A. H. (1991). Geometric effects on spray cone angle for plain-orifice atomizers. *Atomization and sprays , 1*, 253-268.
57. Paterson, A., & Cooke, R. (1999, March 24-26). The design of slurry pipeline systems. Cape Town: Paterson & Cooke.
58. Paterson, A., & Cooke, R. (2010, February). The design of slurry pipeline systems. Cape Town: Paterson & cooke.
59. Pienaar, V. G. (1998). Non-Newtonian fitting losses. *Unpublished MTech thesis* . Cape Town: Cape Technikon.
60. Pienaar, V. G. (2004). Viscous flow through sudden contractions. *Unpublished DTech thesis* . Cape Town: Cape Technikon.
61. Polizelli, M. A., Menegalli, F. C., Telis, V. N., & Telis-Romero, J. (2003). Friction losses in valves and fittings for power-law fluids. *Brazilian journal of chemical engineering , ISSN 0104-6632*.

62. Prabu, S. V., Mascomani, R., Balakrishnan, K., & Konnur, M. S. (1995). *Effects of upstream pipe fittings on the performance of orifice and conical flow meters.* Bombay: Elsevier Ltd.
63. Rabinowitsch, B. (1929). Uber die viskositat und elastiziat van solen . *Z.Ohisical chem.*
64. Ramamurthi, K., & Nandakumar, K. (1999). Characteristics of flow through small sharp-edged cylindrical. *Flow measurement and instrumentation , 10*, 133–143.
65. Reader-Harris, M. J., Sattary, J. A., & Spearman, E. P. (1995). Orifice plate discharge coefficient equation - further work. *Flow measurement and instrumentation , 6*, 101-114.
66. Sahin, B., & Akilli, H. (1997). Finite element solution of laminar flow through square edged orifice with a variable thickness. *International journal of computational fluid dynamics ,9,* 85-88.
67. Sahin, B., & Ceyhan, H. (1996). Numerical and experimental analysis of laminar flow through square-edged orifice with variable thickness . *Trans.institute of measurement and control* , *18,* 166-174.
68. Sahin, B., Tunay, T., & Akilli, H. (2004). Investigation of laminar and turbulent flow through an orifice plate inserted In a pipe. *Transactions of the CSME ,28,* 403-414.
69. Samanta, A. K., Banerjee, T. A., & Das, S. K. (1999). Pressure losses in orifice for the flow of gas-non-Newtonian liquids. *The canadian chemical engineering journal, 77, 579-583*.
70. Skelland, A. H. (1967). *Non-Newtonian flow and and heat transfer .* New York: Wiley.
71. Slatter, P. T. (1999). A new friction factor for yield stress fluids. *14th international conference on slurry handling and pipeline hydrotransport* (pp. 255-265). Masstricht: BHR group.
72. Slatter, P. T. (1994). Transitional and turbulent flow of non-Newtonian slurries in pipes . *Unpublished PhD thesis* . Cape Town, South Africa: univerity of Cape Town.
73. Swamee, P. K. (2005). Discharge equations for venturimeter and orifice meter. *Journal of Hydraulic Research , 43*, 417-420.
74. Turian, R. M., T, W. M., F, L. G., M, D. J., & Plackmann, G. W. (1998). Flow of concentrated non-Newtonian slurries:2 friction losses in bends, fittings, valves, Venturi meters. *International journal of multiphase flow , 24*, 243 - 269.
75. Ward – Smith, A. J. (1971). *Pressure losses in ducted flows.* Butterworths.

76. Ward-Smith, A. J. (1979). Critical flow metering: the characteristics of cylindrical nozzles with sharp upstream edges. *International journal of heat fluid flow , 1*, 123-132.

77. Zedan, M. F., & Teyssandier, R. G. (1985). The effects of recesses anjd protrusions on the discharge coefficient of a flange tapped orifice plate. *GPA Technical publication: TP 13 experimental studies* .

78. Zhang, Z., & Chai, J. (1999). Compromise orifice geometry to minimize pressure drop. *Journal of hydraulic engineering , 125*, 1150 - 1153.

Appendices

Water

Water test results for β = 0.5

Date:	12/22/2009	Test done by Mume & Faahad
Orifice Type:	Long	
Orifice thickness:	0.115	Area[m^2]
Orifice dimension[m]:	0.023	0.000415476
Pipe Diameter [m]:	0.046	0.001661903
Diameter ratio	0.5	
Aspect ratio	5	
Gravitational constant	9.81	
Material Type:	Water	
Density[kg/m^3]:	995.5	
Concentration:	100%	
K:	0.001	
n:	1	
PPT used:	110	
Range selected:	0-500	

1/n	**n/(n+1)**	**(n+1)/n**	**$K^{1/n}$**
1	0.5	2	0.001

Axial distances	-6.99	-4.69	-3.77	-2.40	-0.11	-0.09	0.08	2.39	4.69	6.99	9.29
ND distances incl.[L/D]:	-152.0	-102.0	-82.03	-52.10	-2.33	-1.85	1.72	51.89	101.89	151.89	201.89
Distances[m]:	0.00	2.30	3.22	4.60	6.89	6.91	7.10	9.38	11.68	13.98	16.28

Pod 1 (Pa)	**Pod 2 (Pa)**	**Pod 3 (Pa)**	**Pod 4 (Pa)**	**Pod 5 (Pa)**	**Pod 6 (Pa)**	**Pod 7 (Pa)**	**Pod 8 (Pa)**	**Pod 9 (Pa)**	**Pod 10 (Pa)**	**Pod 11 (Pa)**	**Average Q [l/s]**
95757	92669	91388	89476	86443	86512	10162	25947	24172	20442	16953	4.20
96424	92802	91333	89309	86517	86450	11101	25331	23818	20057	16892	4.20
88990	86057	84766	82939	80226	80220	10704	24558	22810	19568	16580	4.03
89045	86036	84778	82847	80211	80241	10354	24713	22755	19322	16710	4.02
80776	78085	76951	75022	72799	72806	10129	23035	21194	18293	15881	3.80
80634	77868	76693	75059	72688	72721	10461	23183	21069	18221	16013	3.79
74436	72079	70845	69460	67274	67181	10758	21780	20372	17584	15244	3.63
74552	72116	70927	69519	67412	67181	11404	21886	20361	17811	15328	3.63
67350	65157	64120	62950	60860	60829	10361	20555	18981	16477	14500	3.41
67481	65091	64161	62812	60824	60760	10356	19745	18951	16759	14406	3.42
59567	57533	56781	55572	53775	53842	10010	19016	17673	15432	13725	3.17
59570	57622	56807	55710	53895	53774	12434	19032	17673	15591	13911	3.17
53589	51724	50996	49991	48563	48376	9901	17839	16286	14774	13237	2.96

53528	51700	50946	49949	48366	48319	9754	17850	16550	14498	12661	2.97
48595	47011	46377	45485	44029	43977	9791	16885	15921	13906	12737	2.79
48618	47089	46400	45650	44088	44025	9868	16890	15607	14170	12680	2.79
42399	40975	40604	39735	38448	38416	9769	15615	14991	13488	12170	2.55
42368	41046	40504	39691	38588	38462	9782	15645	14950	13399	12264	2.55
36881	36129	35794	35087	34141	33937	10054	14631	13942	12667	11790	2.34
37271	36079	35684	35026	34036	33920	10719	14501	14085	12691	11772	2.34
30459	29604	29300	28869	27977	27887	11621	13393	12867	11975	11243	2.02
30363	29640	29248	28872	28035	27870	10585	13432	13005	11994	11277	2.02
26677	25926	25653	25323	24656	24519	10357	12712	12306	11660	11055	1.82
26664	25942	25661	25333	24707	24554	10179	12810	12366	11670	11015	1.82
23154	22665	22380	22045	21519	21410	9912	12138	11800	11133	10686	1.61
23222	22637	22411	22072	21488	21469	9938	12140	11826	11070	10697	1.61
19549	19178	18956	18722	18353	18211	10335	11361	11256	10785	10386	1.37
19458	19218	18986	18773	18390	18298	10093	11391	11294	10850	10454	1.37
19824	19650	19427	19301	19031	18943	13339	14267	14351	14011	13723	1.09
16665	16538	16434	16346	16213	16131	13247	13468	13596	13384	13237	0.80
16635	16526	16450	16332	16141	16132	13537	13696	13604	13409	13257	0.80
15009	14903	14865	14816	14699	14686	12928	13278	13203	13115	13007	0.60

Water test results for β = 0.7

Date:	2/20/2010	Test done by Faahad & Butteur
Orifice Type:	Long	
Orifice thickness:	0.161	Area[m^2]
Orifice dimension[m]:	0.0322	0.000814332
Pipe Diameter [m]:	0.046	0.001661903
Diameter ratio	0.7	
Aspect ratio	5	
Gravitational constant	9.81	
Material Type:	Water	
Density[kg/m^3]:	998.5	
Concentration:	100%	
K:	0.001	
n:	1	
PPT used:	110	
Range selected:	0-500	

1/n	**n/(n+1)**	**(n+1)/n**	**$K^{1/n}$**
1	0.5	2	0.001

Axial distances	-7.03	-4.73	-3.81	-2.43	-0.14	-0.10	0.10	2.33	4.62	6.92	9.23
ND distances incl.[L/D]:	-152.83	-102.83	-82.83	-52.94	-3.05	-2.29	2.29	50.66	100.59	150.59	200.81
Distances[m]:	0	2.3	3.22	4.595	6.89	6.925	7.135	9.455	11.75	14.05	16.36

Pod 1 (Pa)	Pod 2 (Pa)	Pod 3 (Pa)	Pod 4 (Pa)	Pod 5 (Pa)	Pod 6 (Pa)	Pod 7 (Pa)	Pod 8 (Pa)	Pod 9 (Pa)	Pod 10 (Pa)	Pod 11 (Pa)	Average Q [l/s]
52521	49227	47948	46042	43328	43419	27059	31483	28396	25059	21898	4.43
52566	49348	48097	45991	43354	43263	27141	31452	28422	24994	21938	4.43
49069	45979	44785	43069	40426	40500	25747	29697	26735	23545	20911	4.22
48991	45870	44763	43016	40567	40515	25627	29628	26905	23797	20677	4.22
44193	41636	40604	39023	36867	36814	24020	27367	25050	22118	19703	3.93
44324	41414	40664	39028	36740	36791	23968	27377	24690	22191	19492	3.92
41093	38529	37711	36378	34411	34436	22863	25784	23669	21073	18735	3.72
41148	38718	37782	36300	34401	34333	22834	25936	23487	21247	18845	3.72
38385	36208	35403	34104	32492	32122	21804	24510	22464	20327	18075	3.53
38802	36192	35449	34156	32194	32286	21820	24520	22377	20212	18238	3.53
35199	33076	32405	31300	29633	29620	20641	22926	20954	18985	17366	3.29
34908	33104	32484	31394	29660	29649	20602	22901	21112	19033	17314	3.295
32451	30664	30042	29047	27642	27590	19711	21630	20064	18274	16632	3.08
32429	30794	30073	29115	27649	27591	19677	21682	20158	18267	16626	3.08
30489	28965	28408	27612	26257	26094	18970	20793	19396	17725	16280	2.92
30866	29039	28433	27514	26227	26128	18971	20734	19412	17606	16283	2.92
27736	26408	25905	25193	24025	23976	17993	19449	18275	16795	15632	2.67
27733	26496	25887	25179	24023	23932	17978	19458	18169	16832	15792	2.67
26035	24960	24444	23838	22798	22723	17416	18690	17420	16432	15260	2.50
26188	24876	24457	23746	22702	22649	17409	18649	17655	16421	15286	2.50
24188	23267	22770	22238	21392	21270	16752	17828	16928	15808	14882	2.31
24207	23287	22768	22176	21312	21257	17290	17841	16789	15865	14891	2.31
21711	20940	20601	20139	19391	19434	15898	16715	15767	14858	14183	2.03
21658	20798	20545	20001	19305	19254	15781	16590	15837	14974	14232	2.04
20799	20011	19805	19312	18673	18680	15488	16236	15439	14824	14079	1.99
20965	19972	19818	19300	18747	18661	15748	16213	15518	14718	14023	1.98

CMC

CMC 5% test results for β = 0.36

Date:	5/14/2010	Test done by Faahad & Butteur
Orifice Type:	Long	
Orifice thickness:	0.06624	**Area[m^2]**
Orifice dimension[m]:	0.01652	0.000214343
Pipe Diameter [m]:	0.046	0.001661903
Diameter ratio	0.36	
Aspect ratio	4.0	
Gravitational constant	9.81	
Material Type:	CMC	
Density[kg/m^3]:	1033.013	
Concentration:	6%	
K:	0	
n:	1.08	

PPT used:	0.7
Range selected:	110

1/n	n/(n+1)	(n+1)/n	$K^{1/n}$
1.43	0.41	2.43	1.12

Axial distances	-6.96	-4.66	-3.77	-2.39	-0.10	-0.06	0.06	2.38	4.68	6.98	9.28
ND distances incl.[L/D]:	-151.27	-101.27	-81.92	-52.03	-2.14	-1.27	1.27	51.71	101.71	151.71	201.71
Distances[m]:	0.00	2.30	3.22	4.60	6.89	6.93	7.09	9.56	11.86	14.16	16.46

Pod 1 (Pa)	Pod 2 (Pa)	Pod 3 (Pa)	Pod 4 (Pa)	Pod 5 (Pa)	Pod 6 (Pa)	Pod 7 (Pa)	Pod 8 (Pa)	Pod 9 (Pa)	Pod 10 (Pa)	Pod 11 (Pa)	Average Q [l/s]
190549	180228	175881	169787	159498	158796	70915	75041	65395	54187	44671	2.22
190364	180065	175590	169333	159420	157705	70736	74861	64688	54115	43981	2.22
169419	159648	156108	150256	140844	139806	67490	69996	60452	50989	41891	2.01
169268	159783	155879	149610	141059	140168	67370	69996	60412	50554	41069	2.01
146298	137516	133907	128921	120717	119888	63709	64411	55498	47019	38621	1.79
145896	136962	134100	128681	119903	119704	63599	64448	56172	47023	38126	1.79
130997	122999	119643	114571	106895	106623	60873	60572	52429	44787	36999	1.60
130857	122958	119399	114547	106715	106539	60761	60556	52815	44358	36201	1.60
112834	106056	103303	98970	91682	91868	56866	55703	48614	41291	34906	1.37
113424	106262	103207	99297	91963	91728	56821	55716	48199	41365	33898	1.37
100371	94124	91359	87713	81568	80826	53441	51905	45168	39748	32821	1.20
100282	93999	91238	87408	81430	80950	53405	51889	45686	38979	32447	1.19
88648	82831	80645	77051	71257	71002	49526	48179	42070	36812	31026	1.03
88430	82629	80599	76926	71662	71009	49615	48227	42771	36491	30397	1.03
72885	67981	65827	62955	58053	57879	44415	42869	37689	33043	28501	0.80
72885	67981	65827	62955	58053	57879	44415	42869	37689	33043	28501	0.81
59276	55324	53627	51430	47972	47250	39523	37398	33485	29461	25848	0.60
59539	55539	53899	51606	47383	47317	39728	37523	33928	30019	25942	0.60
48923	46105	44901	43052	39828	39890	34109	31939	29105	25779	23161	0.42
48573	46159	44965	42947	39909	39687	34107	32145	28955	26047	22668	0.42
38112	36274	35433	34321	32656	32452	30172	28431	26812	24874	23004	0.20
38112	36406	35747	34529	32642	32427	30201	28449	26857	25005	23038	0.20
31398	30066	29571	28810	27467	27473	26115	24837	23617	22387	21106	0.13
31398	30066	29571	28810	27467	27473	26115	24837	23617	22387	21106	0.13
28615	27526	27198	26597	25675	25413	24466	23340	22442	20739	20320	0.09
28615	27526	27198	26597	25675	25413	24466	23340	22442	20739	20320	0.09
25698	25084	24687	24231	23414	23350	22819	22277	21084	20067	19397	0.06
25289	25012	24730	24221	23602	23444	22695	22060	21258	19359	19295	0.06
199139	188522	184211	177474	167733	166192	70357	75743	65942	56048	44664	2.33
198649	188238	183747	177684	168095	165392	70070	75599	65725	54963	44965	2.34
220916	210002	205733	198849	188042	185787	71397	79322	68064	57571	46531	2.57
220916	210041	205564	198653	188030	186106	71041	79158	68693	57086	46296	2.57
240192	229236	224431	217541	205678	204615	71780	81989	70633	59504	47668	2.77
262273	252207	247528	240029	228028	227002	71973	85231	72865	60897	48880	3.01
262273	252065	246679	239681	227412	226937	71583	84833	73239	61532	49013	3.01
289237	277107	271899	263852	251518	250821	70826	87361	75101	62286	50046	3.25

289237	276111	271968	263578	251203	250450	70152	86815	74760	62088	49547	3.25
190549	180228	175881	169787	159498	158796	70915	75041	65395	54187	44671	2.22
190364	180065	175590	169333	159420	157705	70736	74861	64688	54115	43981	2.22

CMC 4% test results for β = 0.5

Date:	1/13/2010	Test done by Mume & Faahad
Orifice Type:	Long	
Orifice thickness:	0.115	**Area[m^2]**
Orifice dimension[m]:	0.023	0.000415476
Pipe Diameter [m]:	0.046	0.001661903
Diameter ratio	0.5	
Aspect ratio	5	
Gravitational constant	9.80655	
Material Type:	CMC	
Density[kg/m^3]:	1010.5	
Concentration:	2%	
K:	0.436	
n:	0.746	
PPT used:	110	
Range selected:	0-500	

1/n	n/(n+1)	(n+1)/n	$K^{1/n}$
1.33	0.42	2.34	0.33

Axial distances	-6.99	-4.69	-3.77	-2.40	-0.11	-0.09	0.08	2.39	4.69	6.99	9.29
ND distances incl.[L/D]:	-152.03	-102.03	-82.03	-52.10	-2.33	-1.85	1.72	51.89	101.89	151.89	201.89
Distances[m]:	0.00	2.30	3.22	4.60	6.89	6.91	7.10	9.38	11.68	13.98	16.28

Pod 1 (Pa)	Pod 2 (Pa)	Pod 3 (Pa)	Pod 4 (Pa)	Pod 5 (Pa)	Pod 6 (Pa)	Pod 7 (Pa)	Pod 8 (Pa)	Pod 9 (Pa)	Pod 10 (Pa)	Pod 11 (Pa)	Average Q [l/s]
156200	146181	143586	137248	129615	129668	50350	62215	53016	43968	35772	4
155298	146283	142961	137308	128534	128829	49796	61730	52513	43679	34947	4
140349	133870	130900	125855	117524	117789	50458	58121	49829	41274	33877	4
141101	134008	130996	125642	117621	117810	48346	56646	49531	41289	33098	4
133765	125552	122633	117817	109974	110096	47046	55544	47857	39449	31778	4
133565	125629	122595	117835	109857	109947	47486	55400	47401	39462	31773	4
122441	115245	112268	107644	100210	100234	45338	52170	44838	37211	30049	4
122203	114857	111717	107292	100033	100112	45616	52094	45004	37235	30399	4
113411	106396	103620	99371	92401	92474	44079	49112	42481	35418	28511	3
113461	106494	103591	99290	92369	92518	44709	49235	42737	35608	28641	3
107977	101116	98216	94155	87408	87603	43170	47215	41139	34406	27698	3
107570	100942	98282	94202	87546	87720	43589	45881	41151	34416	28163	3
99150	92587	90122	86084	79934	80028	42178	44674	39278	32538	26668	3
99014	92614	90184	86086	79829	80027	42149	44694	39265	32816	26524	3
92604	86509	83838	80124	74358	74399	40997	42878	37316	31379	25908	3

92653	86613	84105	80347	74416	74472	40546	42493	37714	31395	25898	3
85564	79977	77664	73980	68389	68535	39482	40963	35673	29666	24109	3
85674	79770	77469	74004	68337	68542	40124	40517	35406	30018	24183	3
78861	73342	71255	67994	62624	62896	38056	38634	33736	28292	23432	2
78848	73369	71266	68174	62717	62932	39257	38652	33835	28350	23713	2
71264	66118	64179	61187	56288	56504	36580	36449	31821	26919	21956	2
71257	66139	64356	61227	56434	56511	36229	36489	31651	26676	21748	2
67190	62458	60182	57665	53119	53063	35274	35375	30706	26038	21360	2
67173	62500	60651	57797	53203	53147	35324	35392	30726	26066	21371	2
62043	57536	55844	53127	48859	48873	33787	33715	29246	24883	20495	2
61049	57070	55282	52770	48575	48434	33714	33537	29093	24764	20434	2
56210	52293	51099	48612	44593	44506	33353	32810	28436	24448	20462	2
56192	52162	50612	48203	44216	44313	33166	32547	28131	24141	20100	2
50461	46969	45577	43414	39933	39844	31126	30415	26570	23047	19500	1
50607	46976	45573	43450	39937	39964	30972	30439	26632	23076	19581	1
54927	51691	50442	48544	45454	45300	37949	37033	33116	29650	26349	1
48145	45247	44164	42562	39786	39787	34169	33702	30694	27967	25301	1
48319	45555	44468	42835	40176	40122	34556	34030	30951	28222	25343	1
42888	40748	39845	38476	36220	36247	32177	31445	28820	26521	24211	1
42057	40758	39876	38485	36220	36194	32158	31717	28996	26670	24333	1
38542	36854	36093	34919	32920	32625	29608	29187	26543	24685	22744	1
32467	32140	31128	30637	29675	29393	28888	28030	26217	25088	23956	0
32603	32308	31286	30831	29808	29510	28977	28128	26305	25190	24160	0
26093	26023	25507	25275	24910	24545	23989	23689	23019	22356	21844	0
26120	26024	25477	25265	24875	24542	24162	23821	22967	22281	21745	0
24354	24307	23833	23696	23399	23110	22888	22606	21984	21409	21066	0
23044	22985	22663	22528	22269	22065	21909	21660	21141	20742	20457	0
30917	29744	29435	28850	27876	27897	27251	26246	25263	24053	23201	0
29206	28388	28088	27637	26733	26703	25939	25360	24384	23363	22643	0
27819	26911	26641	26073	25313	25296	24702	23937	23084	22176	21471	0
26366	25534	25355	24906	24221	24203	23673	23107	22404	21551	20929	0
218495	207467	203482	197341	186985	187091	55695	79854	68719	58500	48765	6
206485	195844	192136	186422	176561	176262	54096	76515	66131	55759	46494	5
188278	178308	175259	169239	160438	160291	52996	72260	62166	52630	43466	5
174737	165703	162251	156374	147543	147729	52197	68526	59253	50329	41487	5

CMC 5% test results for β = 0.5

Date:	1/20/2010	Test done by Faahad & Butteur
Orifice Type:	Long	
Orifice thickness:	0.115	Area[m^2]
Orifice dimension[m]:	0.023	0.000415476
Pipe Diameter [m]:	0.046	0.001661903
Diameter ratio	0.5	
Aspect ratio	5	
Gravitational constant	9.81	
Material Type:	CMC	
Density[kg/m^3]:	1029.09	

Concentration:	5%
K:	1.38
n:	0.64
PPT used:	110
Range selected:	0-500

1/n	**n/(n+1)**	**(n+1)/n**	**$K^{1/n}$**
1.56	0.39	2.56	1.65

Axial distances	-6.99	-4.69	-3.77	-2.40	-0.11	-0.09	0.08	2.39	4.69	6.99	9.29
ND distances incl.[L/D]:	-152.03	-102.03	-82.03	-52.10	-2.33	-1.85	1.72	51.89	101.89	151.89	201.89
Distances[m]:	0.00	2.30	3.22	4.60	6.89	6.91	7.10	9.38	11.68	13.98	16.28

Pod 1 (Pa)	**Pod 2** (Pa)	**Pod 3** (Pa)	**Pod 4** (Pa)	**Pod 5** (Pa)	**Pod 6** (Pa)	**Pod 7** (Pa)	**Pod 8** (Pa)	**Pod 9** (Pa)	**Pod 10** (Pa)	**Pod 11** (Pa)	**Average Q** [l/s]
195566	181684	176168	167331	153656	154018	89338	92809	79193	64562	51956	4
195374	181396	176145	167382	153758	153822	89110	92714	78907	64538	52185	4
222732	207260	201285	192288	176834	177078	93856	101020	85502	70592	55218	4
222032	206959	201317	192050	177235	176985	93685	100996	85174	70054	55353	4
213962	198432	193466	184663	170331	170186	92233	98493	83135	69207	53989	4
213490	198827	193123	184636	169885	170588	91504	97956	82926	68379	53959	4
202746	188307	183050	174590	160775	161258	89237	94473	81394	66085	53661	4
202596	188667	183250	174695	161094	161051	89242	94497	80660	65950	52342	4
181389	168623	163217	155642	142803	143009	84616	87523	75086	61223	49354	4
181570	168463	163196	155639	143097	142889	84678	87364	75108	61299	50010	4
176180	163321	158388	150618	138337	138504	83386	85583	73012	59870	47856	3
175900	163342	158553	151001	137815	138324	83351	85288	72877	59852	48130	3
164517	152413	147719	140251	129609	128635	80564	81600	68992	57220	47123	3
163913	152423	147876	140833	128795	129018	80621	81603	69814	57294	45599	3
154782	142704	138791	132128	120765	120618	77916	78136	66289	54797	43692	3
154794	143084	138658	131675	120436	120589	77845	78215	66638	54792	43490	3
150201	138686	134293	127735	116594	116886	76581	76531	64863	53675	42721	3
150081	139146	134433	127678	116939	116653	76632	76547	65719	53831	43324	3
139535	128795	124720	118312	107834	107947	73589	72692	61802	51059	41210	3
139514	128776	124818	118342	107804	108203	73558	72707	62100	51319	41508	3
131023	121274	116928	111094	101262	101280	70866	69582	59900	49259	39666	2
131016	121149	117209	111036	100977	101149	70897	69431	60025	49144	39222	2
120744	111780	107598	101984	92821	92990	67521	65717	57172	46482	37553	2
120765	111230	107538	101904	92864	92922	64592	65568	57176	46761	37684	2
111334	102539	98965	93816	85308	85252	64023	61755	53870	44122	35355	2
102278	94080	91013	85935	78186	78283	60114	58042	49650	41906	34334	2
102278	94519	90892	85904	78159	78069	60213	57865	49831	41447	34336	2
93254	85569	82621	77918	70959	70955	56297	54221	46786	39013	31998	2
92816	85072	82398	77725	70801	70824	56153	54372	47370	39064	32538	2
81631	74915	72324	68340	61855	61760	51813	49342	42389	35988	29955	1
81120	74668	72211	68074	61315	61522	52084	49355	42503	35905	29493	1
73300	66946	64976	61567	55803	53048	47999	45164	39450	33089	27589	1
73607	67392	65416	61502	56046	55949	48074	45198	39608	33427	28219	1

68140	62646	60572	57410	51996	52363	45293	42294	36963	31614	26890	1
68108	62711	60641	57396	52313	52307	46169	42306	36988	32093	27033	1
61115	56553	54926	52229	47855	47819	42302	39238	34281	29741	25179	1
60944	56181	54775	51909	47322	47609	43110	39046	34871	29552	25823	1
50384	46479	45174	42923	39058	39338	35830	33026	29668	25295	22440	1
50321	47087	45056	42918	39297	39311	36517	33155	29644	25302	22324	1
43061	40588	38807	36990	34133	34128	31730	29175	26597	22956	20862	0
43111	40256	38948	36960	33967	34159	31840	29159	26712	23037	20761	0
35500	33540	32944	31954	30412	30253	29220	27515	26110	23924	22280	0

CMC 8% test results for β = 0.5

Date:	1/19/2010	Test done by Faahad & Butteur
Orifice Type:	Long	
Orifice thickness:	0.115	Area[m^2]
Orifice dimension[m]:	0.023	0.000415476
Pipe Diameter [m]:	0.046	0.001661903
Diameter ratio	0.5	
Aspect ratio	5	
Gravitational constant	9.81	
Material Type:	CMC	
Density[kg/m^3]:	1043	
Concentration:	8%	
K:	8.3	
n:	0.6	
PPT used:	110	
Range selected:	0-500	

1/n	n/(n+1)	(n+1)/n	$K^{1/n}$
1.81	0.35	2.81	46.39

Axial distances	-6.99	-4.69	-3.77	-2.40	-0.11	-0.09	0.08	2.39	4.69	6.99	9.29
ND distances incl.[L/D]:	-152.03	-102.03	-82.03	-52.10	-2.33	-1.85	1.72	51.89	101.89	151.89	201.89
Distances[m]:	0.00	2.30	3.22	4.60	6.89	6.91	7.10	9.38	11.68	13.98	16.28

Pod 1 (Pa)	Pod 2 (Pa)	Pod 3 (Pa)	Pod 4 (Pa)	Pod 5 (Pa)	Pod 6 (Pa)	Pod 7 (Pa)	Pod 8 (Pa)	Pod 9 (Pa)	Pod 10 (Pa)	Pod 11 (Pa)	Average Q [l/s]
290460	269714	259075	242053	214798	215091	204727	171818	142852	116154	88022	1.51
293779	268704	257670	240612	213722	213527	205622	170561	141668	115283	87396	1.52
275025	250716	239865	224448	199416	199269	172964	160770	134204	109319	83578	1.35
275247	251366	240096	224498	199811	199035	175683	159534	133826	109332	83797	1.35
254963	233666	221903	208210	184538	184981	158008	149158	125609	102184	79960	1.17
254505	233213	221984	207087	184150	184980	161602	148856	126320	102958	79533	1.17
240246	219520	209517	196403	175192	175067	162205	141923	119382	98527	76843	1.04
239777	217373	209192	195961	174503	174768	161783	141279	119129	98028	76044	1.04
226293	205395	197665	184460	164827	165208	153776	135155	113364	93061	73082	0.93

226048	204928	197621	185060	164802	165078	153691	135025	113411	94074	72920	0.93
208151	189381	182167	170204	152360	152752	143167	125620	105903	87437	69985	0.78
208071	188594	181918	170193	151604	152546	142729	125554	105717	87290	69523	0.78
194623	176896	170070	159803	142331	143312	134808	117809	100587	83088	66406	0.67
194354	176500	170263	159580	142449	143168	134709	117122	100073	82962	66000	0.67
179195	162801	156911	147302	131873	132654	125393	110268	93858	78287	63570	0.56
179417	163064	157711	147959	132661	132667	125248	110487	94105	78509	63531	0.56
166970	152120	146737	137791	124048	124187	117749	103844	88451	74403	60754	0.47
166736	151892	146572	137792	123448	123987	117387	102672	88569	74393	60053	0.47
145101	132507	127957	120819	108924	109268	104046	92503	80849	68447	56537	0.34
145870	133287	129329	121445	109456	110076	104860	93042	80911	68321	56398	0.34
131713	120606	116953	110380	99719	100328	95855	85516	75287	64105	54459	0.25
131942	121023	116985	110561	99732	100393	95999	85514	75025	63950	53944	0.25
112350	103794	100440	95321	86464	87096	83347	74591	66315	57929	49469	0.16
112553	103684	100792	95331	86677	87256	83867	74653	66765	57875	49854	0.16
97056	89964	87645	83281	76219	76880	74103	67027	60214	52924	46689	0.10
97352	90272	87769	83317	76214	76784	74193	67054	60375	52908	46204	0.10
85441	79626	77572	74107	68150	68708	66358	60762	55137	48963	43404	0.06
85377	80074	77628	74125	68399	68509	66326	60387	54744	48959	44039	0.06
75426	70484	68932	66152	61369	61607	59875	55503	50751	45950	41288	0.03
75480	70616	69141	66164	61408	61538	59814	54857	50389	46033	41674	0.03
308851	284156	273651	256007	228856	228914	213363	181382	150478	120918	93350	1.87
310356	284238	273516	255209	227218	226499	214186	179555	148486	120102	91538	1.88

CMC 5% test results for β = 0.7

Date:		2/27/2010	Test done by Faahad & Butteur
Orifice Type:		Long	
Orifice thickness:		0.161	Area[m^2]
Orifice dimension[m]:		0.0322	0.000814332
Pipe Diameter [m]:		0.046	0.001661903
Diameter ratio		0.7	
Aspect ratio		5	
Gravitational constant		9.81	
Material Type:		CMC	
Density[kg/m^3]:		1028.1155	
Concentration:		7%	
K:		0.84	
n:		0.7	
PPT used:		110	
Range selected:		0-500	

1/n	**n/(n+1)**	**(n+1)/n**	**$K^{1/n}$**
1.42	0.41	2.42	0.77

Axial distances	-7.03	-4.73	-3.81	-2.43	-0.14	-0.10	0.10	2.33	4.62	6.92	9.23
ND distances incl.[L/D]:	-152.83	-102.83	-82.83	-52.94	-3.05	-2.29	2.29	50.66	100.59	150.59	200.81
Distances[m]:	0	2.3	3.22	4.595	6.89	6.925	7.135	9.455	11.75	14.05	16.36

Pod 1 (Pa)	**Pod 2 (Pa)**	**Pod 3 (Pa)**	**Pod 4 (Pa)**	**Pod 5 (Pa)**	**Pod 6 (Pa)**	**Pod 7 (Pa)**	**Pod 8 (Pa)**	**Pod 9 (Pa)**	**Pod 10 (Pa)**	**Pod 11 (Pa)**	**Average Q [l/s]**
133375	121805	117097	110146	98668	98767	85891	80166	67988	56743	45084	3.72
133375	121805	117097	110146	98668	98767	85891	80166	67988	56743	45084	3.72
166340	153150	147395	138821	125139	124698	102781	97553	82468	68596	54726	5.07
166340	153150	147395	138821	125139	124698	102781	97553	82468	68596	54726	5.07
158435	146112	140856	132194	118692	118699	98605	93538	79881	65920	53028	4.82
157819	145749	140418	132012	118559	118666	98546	93360	79495	66104	52771	4.82
152647	139344	134285	126370	114008	113403	95112	89765	76946	63480	50792	4.59
152464	139122	133954	126048	113572	113335	94875	89639	76652	63542	50967	4.59
144487	131951	127254	119713	107456	107283	90775	85638	72542	60450	48116	4.30
143886	131485	126974	119721	107623	107239	90573	85373	72597	60815	48284	4.30
137270	126524	121659	114555	102934	102465	87497	82166	70094	57991	46858	4.08
137270	126524	121659	114555	102934	102465	87497	82166	70094	57991	46858	4.08
120697	109813	105814	99669	89564	89271	78392	72921	62665	51707	41668	3.44
120697	109813	105814	99669	89564	89271	78392	72921	62665	51707	41668	3.44
115747	105525	101738	95698	86344	86292	76453	71132	61502	51147	42196	3.19
115118	105249	101316	95694	86641	85505	76475	70990	61158	51285	41773	3.19
117498	107440	103614	97677	88546	87602	78161	72715	63213	51897	42916	3.28
102332	93485	90281	85354	77024	76620	69670	64652	56565	47411	39216	2.66
102483	93842	90417	85065	77009	76750	69802	64640	56710	47338	39330	2.65

100429	91633	88425	82951	74099	74216	67153	61760	53274	44213	35043	2.68
95373	87170	84073	79301	71480	70949	63878	59028	50832	42377	34216	2.49
95373	87170	84073	79301	71480	70949	63878	59028	50832	42377	34216	2.49
91279	83341	80364	75854	68139	67720	61379	56354	48658	39812	32894	2.309
91279	83341	80364	75854	68139	67720	61379	56354	48658	39812	32894	2.31
84877	77410	74684	70300	63188	63099	57527	52861	45663	38197	30730	2.07
84877	77410	74684	70300	63188	63099	57527	52861	45663	38197	30730	2.07
78353	71934	68955	65020	58692	58390	53815	49151	42919	35924	29633	1.88
78329	71756	69058	65096	59020	58328	53797	49154	42551	36162	29885	1.88
72129	65746	63635	60076	54540	53963	50187	45673	40008	33507	27701	1.64
72046	66039	63625	60078	54414	53974	50197	45639	40055	34082	28005	1.64
64999	59652	57661	54610	49615	49016	46072	41757	36560	31315	26207	1.37
65095	59900	57560	54502	49565	49040	46098	41767	36081	31234	26152	1.38
59353	54659	52742	49966	45232	45099	42738	38908	33573	28849	24473	1.20
59353	54659	52742	49966	45232	45099	42738	38908	33573	28849	24473	1.20
53869	49511	48030	45320	41451	41192	39237	35544	31566	26889	23097	0.99
53869	49511	48030	45320	41451	41192	39237	35544	31566	26889	23097	1.00
47070	43743	42174	40068	36749	36546	35147	31957	28546	25214	21662	0.77
47070	43743	42174	40068	36749	36546	35147	31957	28546	25214	21662	0.77
41155	38436	37481	35431	32959	32717	31797	29171	26524	24026	21099	0.57
41402	38885	37420	35732	32942	32901	31971	29015	26728	23210	21020	0.57

CMC 7% test results for β = 0.7

Date:	2/25/2010	Test done by Faahad & Butteur
Orifice Type:	Long	
Orifice thickness:	0.161	**Area[m^2]**
Orifice dimension[m]:	0.0322	0.000814332
Pipe Diameter [m]:	0.046	0.001661903
Diameter ratio	0.7	
Aspect ratio	5	
Gravitational constant	9.81	
Material Type:	CMC	
Density[kg/m^3]:	1041	
Concentration:	7%	
K:	3.85	
n:	0.61	
PPT used:	110	
Range selected:	0-500	

1/n	**n/(n+1)**	**(n+1)/n**	**$K^{1/n}$**
1.63	0.37	2.63	9.11

Axial distances	-7.03	-4.73	-3.81	-2.43	-0.14	-0.10	0.10	2.33	4.62	6.92	9.23
ND distances incl.[L/D]:	-152.83	-102.83	-82.83	-52.94	-3.05	-2.29	2.29	50.66	100.59	150.59	200.81
Distances[m]:	0	2.3	3.22	4.595	6.89	6.925	7.135	9.455	11.75	14.05	16.36

Pod 1 (Pa)	Pod 2 (Pa)	Pod 3 (Pa)	Pod 4 (Pa)	Pod 5 (Pa)	Pod 6 (Pa)	Pod 7 (Pa)	Pod 8 (Pa)	Pod 9 (Pa)	Pod 10 (Pa)	Pod 11 (Pa)	Average Q [l/s]
187143	169741	162486	152304	136139	135094	132168	113453	95525	79740	62585	1.38
186253	169383	162129	152672	134585	134804	131638	113412	96310	78816	62781	1.40
170112	153882	148308	139093	123814	123994	119693	104597	88302	73082	58160	1.19
170112	153882	148308	139093	123814	123994	119693	104597	88302	73082	58160	1.19
161126	146484	140916	132165	118093	117680	113911	99678	85154	70634	56393	1.07
161126	146079	140777	132309	117806	117702	113777	99762	85660	70853	57041	1.07
49098	46515	45436	44244	42675	41985	41480	38766	36959	34412	32114	0.05
48074	46480	45166	43836	41340	41406	40928	39332	36720	34280	31922	0.05
63162	59190	57175	54651	50623	50666	50298	45762	42047	38814	35509	0.12
63162	59157	57365	54942	50623	50666	50958	45933	42047	38814	35509	0.12
76041	70096	68516	65070	60295	59845	59279	53219	48492	43347	38168	0.20
75834	70788	68738	65633	59987	60198	59245	53531	48742	42983	38379	0.20
102199	93968	90431	85723	78383	77742	75980	67626	60273	51570	44479	0.42
102441	94266	91340	86488	79145	78493	76542	68155	60592	51841	44695	0.42
111853	102462	99092	93683	85006	84617	82449	73092	64151	54936	46656	0.52
111853	102462	99092	93683	85006	84617	82449	73092	64151	54936	46656	0.51
127007	116717	112258	105809	95073	94856	92317	81327	71080	59981	49463	0.68
127007	116717	112258	105809	95073	94856	92317	81327	71080	59981	49463	0.68
144363	131865	126357	118799	106858	106489	103373	90677	78481	65771	53895	0.89
144462	131747	126892	119455	107021	106325	103598	90780	78776	66195	53916	0.89
206101	187852	179007	166934	149089	147666	141702	123802	104594	84995	66924	1.79
206101	187852	179007	166934	149089	147666	141702	123802	104594	84995	66924	1.79
191904	173520	166424	155899	139022	138774	132873	116187	98137	81102	63456	1.58
191005	173685	166347	156214	139437	138433	132745	116001	98614	81021	64265	1.58
53806	50688	49348	47700	45528	45015	44785	41323	38842	36225	33338	0.08
53822	50965	49730	48084	45005	44957	44338	41277	38762	34638	32990	0.084
50506	47838	46622	45178	43175	42671	42431	39332	37257	34810	32542	0.06
50201	47570	46740	45346	42480	42544	42233	39351	37421	34807	32527	0.06

Kaolin

Kaolin 8% test results for β = 0.5

Date:	1/27/2010	Test done by faahad,Butteur & Koko
Orifice Type:	Long	
Orifice thickness:	0.115	Area[m^2]
Orifice dimension[m]:	0.023	0.000415476
Pipe Diameter [m]:	0.046	0.001661903
Diameter ratio	0.5	
Aspect ratio	5	
Gravitational constant	9.81	
Material Type:	Kaolin	
Density[kg/m^3]:	1133	

Concentration:	8%
K:	0.06
n:	0.50
PPT used:	110
Range selected:	0-500

1/n	**n/(n+1)**	**(n+1)/n**	**$K^{1/n}$**
1.98	0.33	2.98	0.0037

Axial distances	-6.99	-4.69	-3.77	-2.40	-0.11	-0.09	0.08	2.39	4.69	6.99	9.29
ND distances incl.[L/D]:	-152.03	-102.03	-82.03	-52.10	-2.33	-1.85	1.72	51.89	101.89	151.89	201.89
Distances[m]:	0.00	2.30	3.22	4.60	6.89	6.91	7.10	9.38	11.68	13.98	16.28

Pod 1 (Pa)	**Pod 2** (Pa)	**Pod 3** (Pa)	**Pod 4** (Pa)	**Pod 5** (Pa)	**Pod 6** (Pa)	**Pod 7** (Pa)	**Pod 8** (Pa)	**Pod 9** (Pa)	**Pod 10** (Pa)	**Pod 11** (Pa)	**Average Q** [l/s]
126243	121027	119587	115913	112966	112332	16116	39598	35198	30641	26144	4.42
126323	121266	119027	116302	112431	112637	16101	39474	36569	30733	26388	4.42
113555	109050	107459	104409	101232	101026	15953	36655	32849	28924	25031	4.16
112422	108645	107310	105201	101297	100782	15841	37253	33028	28814	24755	4.16
102411	98407	97141	95005	91504	91181	15991	34193	31163	27372	23820	3.92
102105	98368	97356	94809	91995	91119	15953	34214	30671	27235	23577	3.92
90088	87075	85817	83858	81118	80606	16074	31537	28477	25463	22458	3.63
90192	86584	85492	83515	81279	80919	16018	31588	28824	25654	22738	3.62
78408	75413	74655	73096	70829	70328	16336	29263	26760	24237	21340	3.31
78316	75368	74698	73016	70471	70512	16290	29529	26941	24000	21581	3.31
70053	67262	66671	65067	63517	63279	16212	27171	24829	22367	19928	3.08
69713	67395	66529	64906	62867	62802	15675	26779	24639	21575	20122	3.09
63287	61091	60345	59109	57097	57007	16102	25708	23736	21671	19892	2.86
63101	60779	60119	58921	57076	56811	16099	25583	23668	21604	19621	2.86
56286	54553	53904	52607	51024	50981	16153	24331	22503	20772	19087	2.64
56422	54415	53961	52983	51307	51141	16328	24285	22817	20966	19231	2.64
50820	49127	48617	47608	46171	45973	16499	23230	21777	20188	18646	2.42
50356	48781	47965	47308	45718	45699	16260	22927	21677	19953	18600	2.42
45871	44638	44121	43356	42291	42074	16842	22591	21225	20010	18748	2.24
45999	44598	44093	43225	41930	41796	16488	22280	21071	19653	18522	2.24
45779	44514	44020	43270	41970	41911	16515	22252	21369	19840	18522	2.24
37986	36855	36686	36104	35132	34978	17160	21138	20190	19240	18347	1.90
37956	36739	36595	35967	34945	34973	17145	21028	20195	19071	18183	1.89
32209	31644	31314	30992	30248	30047	16036	19090	18428	17845	17119	1.68
32410	31678	31220	30756	29972	29878	16202	19099	18795	17735	16986	1.68
28067	27351	27168	26890	26176	26131	15963	18165	17419	17826	17392	1.44
28361	27576	27447	26928	26569	26343	16094	19514	18610	17436	16877	1.43
25175	24735	24656	24487	24072	23595	17605	18860	18532	18209	17940	1.11
25180	24756	24683	24526	24104	24018	17920	19228	18995	18511	18094	1.10
22237	21893	21832	21682	21442	21317	17833	18303	18149	17819	17494	0.88
22136	21890	21846	21657	21430	21309	17441	18144	18088	17853	17495	0.88

Kaolin 14% test results for β = 0.5

Date:	1/30/2010	Test done by Faahad & Butteur
Orifice Type:	Long	
Orifice thickness:	0.115	Area[m^2]
Orifice dimension[m]:	0.023	0.000415476
Pipe Diameter [m]:	0.046	0.001661903
Diameter ratio	0.5	
Aspect ratio	5	
Gravitational constant	9.81	
Material Type:	Kaolin	
Density[kg/m^3]:	1239	
Concentration:	14%	
K:	3.91	
n:	0.18	
PPT used:	110	
Range selected:	0-500	

1/n	**n/(n+1)**	**(n+1)/n**	**$K^{1/n}$**
5.55	0.15	6.55	1949.26

Axial distances	-6.99	-4.69	-3.77	-2.40	-0.11	-0.09	0.08	2.39	4.69	6.99	9.29
ND distances incl.[L/D]:	-152.03	-102.03	-82.03	-52.10	-2.33	-1.85	1.72	51.89	101.89	151.89	201.89
Distances[m]:	0.00	2.30	3.22	4.60	6.89	6.91	7.10	9.38	11.68	13.98	16.28

Pod 1 (Pa)	**Pod 2 (Pa)**	**Pod 3 (Pa)**	**Pod 4 (Pa)**	**Pod 5 (Pa)**	**Pod 6 (Pa)**	**Pod 7 (Pa)**	**Pod 8 (Pa)**	**Pod 9 (Pa)**	**Pod 10 (Pa)**	**Pod 11 (Pa)**	**Average Q [l/s]**
121249	116296	114520	111781	108172	108028	12760	35775	31377	26623	22135	4.25
121587	116545	114893	111555	107723	107528	12837	35701	31332	26522	21832	4.24
111523	106669	105410	102287	99148	98786	13084	33642	29865	25258	21334	4.04
110998	106658	105022	102366	99237	98371	13023	33460	29707	25353	21322	4.03
105912	101966	100585	97975	94058	93988	13877	33106	29214	24999	21191	3.91
105779	101621	100102	97807	94587	93594	13816	32633	29123	25068	21389	3.90
99568	96181	95155	92596	89778	89676	20865	37191	33613	30385	26762	3.59
99722	96030	94924	93182	89751	88939	20953	37354	33662	30365	26891	3.59
90031	86828	86395	84220	81080	81043	21477	35398	32167	29142	25948	3.36
90391	87349	86355	84692	81516	81057	21215	35170	32449	29390	26070	3.37
78165	74270	73720	71802	68728	69016	18745	29932	27062	24452	21558	3.12
77389	74264	73482	71956	69044	69212	17606	29244	27154	24367	21549	3.12
71047	68242	67518	65529	63614	63759	19383	29093	26568	24400	22106	2.90
70832	68272	67397	65829	63310	63491	18697	29308	26040	23806	20869	2.92
65630	63177	62541	60948	58642	57688	23461	31113	28869	26658	24409	2.59
65398	62536	62007	60646	58468	58292	23001	31112	28379	26088	23844	2.60
60578	58164	57629	55973	53832	54002	24156	30606	28122	26117	24065	2.37
60372	58019	57362	55908	53918	53833	24242	30524	28257	26013	24068	2.37
56799	54491	53839	52313	50435	50228	24601	30050	28090	25885	24077	2.21
54144	52570	51627	49933	48317	48325	27379	31198	29337	26890	24710	1.99

54060	52096	51344	50004	47832	47637	26432	30432	28651	26311	24115	2.00
48218	45990	45486	44350	42469	42562	28673	30741	29080	26967	25070	1.63
48374	46325	45533	44369	42408	42380	28291	30413	28817	26663	25006	1.63
46076	43932	43337	42239	40606	40331	29629	30905	28977	26887	25137	1.41
45811	43700	43076	41937	40399	40080	29287	30676	29124	26838	25119	1.42
44001	42014	41381	40256	38414	38377	30373	30958	29323	27064	25436	1.20
43535	41497	40734	39799	38037	37920	29919	30508	28829	26644	24940	1.21
42627	40338	40040	39001	37315	37134	30524	30761	29171	27201	25434	1.09
42468	40675	39971	38860	36996	37071	30380	30575	28920	26985	25270	1.09
40426	38634	38037	36938	35256	35229	30139	30033	28435	26443	24659	0.95
40657	38790	38353	37143	35609	35465	30141	30042	28461	26456	24709	0.95
38917	37257	36862	36026	34483	34207	30177	29815	28054	26439	24850	0.84
39617	37852	37286	36155	34561	34492	30332	29935	28268	26421	24845	0.84
37663	35801	35327	34374	32904	32665	30197	29372	27845	25995	24516	0.63
37633	35824	35402	34236	32611	32587	30712	29473	27890	25872	24397	0.63
39065	37689	36967	35971	34906	34553	34367	32714	31211	29390	28249	0.28

Kaolin 20% test results for β = 0.5

Date:	4/02/2010	Test done by Faahad & Butteur
Orifice Type:	Long	
Orifice thickness:	0.12	Area[m^2]
Orifice dimension[m]:	0.02	0.00
Pipe Diameter [m]:	0.046	0.00
Diameter ratio	0.50	
Aspect ratio	5.00	
Gravitational constant	9.81	
Material Type:	Kaolin	
Density[kg/m^3]:	1324.00	
Concentration:	0.20	
K:	16.00	
n:	0.15	
PPT used:	110.00	
Range selected:	0-500	

1/n	**n/(n+1)**	**(n+1)/n**	**$K^{1/n}$**
6.67	0.13	7.67	106528681.31

Axial distances	-6.99	-4.69	-3.77	-2.40	-0.11	-0.09	0.08	2.39	4.69	6.99	9.29
ND distances incl.[L/D]:	-152.03	-102.03	-82.03	-52.10	-2.33	-1.85	1.72	51.89	101.89	151.89	201.89
Distances[m]:	0.00	2.30	3.22	4.60	6.89	6.91	7.10	9.38	11.68	13.98	16.28

Pod 1 (Pa)	Pod 2 (Pa)	Pod 3 (Pa)	Pod 4 (Pa)	Pod 5 (Pa)	Pod 6 (Pa)	Pod 7 (Pa)	Pod 8 (Pa)	Pod 9 (Pa)	Pod 10 (Pa)	Pod 11 (Pa)	Average Q [l/s]
119086	112136	108889	104370	97551	97110	74513	74599	66898	59815	52710	1.95
118833	112136	108800	104442	97663	97125	74302	74615	66898	59802	52873	1.95
112113	105129	102510	98532	91632	91022	74060	72935	65917	58578	52141	1.67
112113	105129	102629	98657	91647	91314	74224	72904	65445	58535	52255	1.67
110059	102990	100260	96159	89515	88840	74215	72372	65761	58173	52262	1.55
110059	102990	100223	96113	89632	88980	73983	72529	65666	58269	51859	1.55
106642	99733	97535	93654	86883	86390	74475	71879	65546	57978	51521	1.37
106642	99733	97535	93654	86646	88930	74409	71915	65284	58162	51390	1.37
102131	95484	92571	88732	82970	82476	74228	70659	64228	57382	50722	1.13
102368	95484	92365	88732	82623	82298	73876	70628	64525	57446	51103	1.13
98678	91543	89719	86060	79965	79976	73751	69611	63347	56469	50183	0.96
98991	92274	90317	86224	79707	79886	73747	69684	63416	56546	50400	0.96
95105	88707	86924	83571	76647	76837	72887	68353	61647	55688	49696	0.78
95348	89049	87078	83729	77448	77264	73400	68578	61881	55795	49805	0.77
91988	85957	84036	80291	74385	74286	71887	66737	60674	54382	48526	0.55
86404	81409	79255	75436	70099	70138	69307	63389	57748	52327	46963	0.27
131264	124242	120786	116322	108846	110205	59747	67196	59339	52805	44963	2.91
131603	124242	120878	116067	109023	107472	59507	67245	59339	52400	44653	2.91
135503	127637	124587	120154	112811	112417	59026	67954	60509	52821	45374	3.06
135194	127637	124587	120154	112847	111921	58713	67709	60259	52624	45122	3.06
123774	116328	113382	108870	101683	100017	60516	65992	59064	50925	43929	2.64
123289	116328	113340	108920	101513	101232	60484	66008	59030	51213	43674	2.64
118888	110512	107931	103996	97173	96078	61243	65305	57829	50446	43324	2.44
118272	110310	108353	104155	97017	95916	61292	65280	57690	50598	43506	2.44
113917	106140	104006	99480	92616	92296	62147	64604	57348	50023	42482	2.25
113784	106084	103764	99708	92593	91983	61839	64246	57500	50103	43187	2.24

Kaolin 8% test results for β = 0.7

Date:	2/16/2010	Test done by Faahad & Koko
Orifice Type:	Long	
Orifice thickness:	0.161	Area[m^2]
Orifice dimension[m]:	0.0322	0.000814332
Pipe Diameter [m]:	0.046	0.001661903
Diameter ratio	0.7	
Aspect ratio	5	
Gravitational constant	9.81	
Material Type:	Kaolin	
Density[kg/m^3]:	1140	
Concentration:	8%	
K:	0.06	
n:	0.5	
PPT used:	110	
Range selected:	0-500	

1/n	n/(n+1)	(n+1)/n	$K^{1/n}$
2	0.33	3	0.0036

Axial distances	-7.03	-4.73	-3.81	-2.43	-0.14	-0.10	0.10	2.33	4.62	6.92	9.23
ND distances incl.[L/D]:	-152.83	-102.83	-82.83	-52.94	-3.05	-2.29	2.29	50.66	100.59	150.59	200.81
Distances[m]:	0	2.3	3.22	4.595	6.89	6.925	7.135	9.455	11.75	14.05	16.36

Pod 1 (Pa)	Pod 2 (Pa)	Pod 3 (Pa)	Pod 4 (Pa)	Pod 5 (Pa)	Pod 6 (Pa)	Pod 7 (Pa)	Pod 8 (Pa)	Pod 9 (Pa)	Pod 10 (Pa)	Pod 11 (Pa)	Average Q [l/s]
84904	77888	75540	71434	65908	65740	34779	42682	36635	30445	23593	5.75
84904	77888	75540	71434	65908	65740	34779	42682	36635	30445	23593	5.75
78201	71969	69956	66187	60905	60927	33141	39970	34307	28114	22120	5.50
78583	71840	69964	66342	60988	61009	32915	39791	33845	28202	22255	5.50
74238	68075	66189	62895	57675	57728	31431	37999	32598	26544	21215	5.32
74087	68087	66000	62824	57963	57700	31547	37856	32716	26833	21097	5.31
68950	63877	61725	58753	53943	53905	29851	35809	30245	25286	20521	5.09
69361	63555	61697	58650	54303	53897	29828	35648	31266	25711	20467	5.09
65569	59776	57827	55034	50630	50725	28205	33729	29216	24322	19432	4.89
64904	59738	58010	54967	50729	50583	28330	33757	29641	24478	19720	4.89
61448	56842	55028	52257	48146	48144	27242	32401	27714	23423	18926	4.73
61012	56566	55200	52456	48347	48161	27214	32351	28182	23180	18750	4.73
56557	52096	50797	48450	44963	44584	25656	30245	26625	21816	17680	4.49
56772	52393	50885	48296	44789	44447	25643	30155	26465	22091	17797	4.50
52132	48240	46914	44499	41024	41157	24195	28217	24425	20553	16970	4.26
52265	48225	47029	44549	41385	41167	24299	28206	24812	20722	16805	4.26
48714	45073	43917	41780	38733	38509	22973	26676	23313	19801	16415	4.06
48591	44944	43856	41822	38375	38410	22924	26642	23559	19796	16347	4.06
44844	41570	40377	38443	35687	35628	21627	24891	21933	18633	15316	3.85
44935	41642	40412	38600	35530	35639	21744	24952	22089	18453	15582	3.84
40942	38317	36924	35300	32467	32592	20290	23069	20406	17361	14508	3.62
40974	38051	36897	35251	32529	32511	20270	23150	20586	17494	14627	3.62
38728	36050	35091	33420	31124	31039	19645	22341	19614	16860	14411	3.48
38731	36073	35203	33538	31041	31127	19700	22276	19898	16845	14526	3.48
34573	32165	31255	29968	27822	27783	18116	20247	18188	15678	13446	3.20
34084	32093	31333	29899	27710	27811	18128	20334	17926	15567	13282	3.21
32299	30140	29282	28027	26121	26105	17424	19192	17297	14935	12813	3.04
32005	29925	29240	27981	26084	25986	17321	19209	17424	15124	13065	3.041
28758	26932	26223	25152	23342	23444	16255	17678	16168	14084	12443	2.75
28359	26656	25982	24911	23265	23166	16090	17590	15941	14017	12391	2.75
26540	24930	24365	23501	21920	22027	15734	16907	15531	13848	12417	2.57
26437	24705	24312	23295	21878	21835	15685	16912	15430	13864	12310	2.56
24043	22881	22197	21339	20041	20044	14957	15887	14736	13623	12009	2.32
21821	20517	20102	19487	18703	18647	14241	14892	14087	13039	11776	2.11
21783	20792	20305	19637	18460	18367	14190	15116	14007	12764	11766	2.11
19826	18993	18688	18088	17372	17196	13842	14402	13644	12621	11749	1.92
19570	18790	18507	18017	17172	17093	13836	14098	13568	12590	11748	1.92
21865	21225	20906	20534	19819	19768	17649	18226	17542	16811	16126	1.65

18342	17949	17794	17703	16856	16717	15654	15677	15459	14867	14476	1.17

Kaolin 14% test results for β = 0.7

Date:	4/02/2010	Test done by Faahad Butteur & Koko
Orifice Type:	Long	
Orifice thickness:	0.16	Area[m^2]
Orifice dimension[m]:	0.03	0.00
Pipe Diameter [m]:	0.05	0.00
Diameter ratio	0.70	
Aspect ratio	5.00	
Gravitational constant	9.81	
Material Type:	Kaolin	
Density[kg/m^3]:	1242.09	
Concentration:	15.00	
K:	3.50	
n:	0.18	
PPT used:	110.00	
Range selected:	0-500	

1/n	**n/(n+1)**	**(n+1)/n**	**$K^{1/n}$**
5.71	0.15	6.71	1285.17

Axial distances	-7.03	-4.73	-3.81	-2.43	-0.14	-0.10	0.10	2.33	4.62	6.92	9.23
ND distances incl.[L/D]:	-152.83	-102.83	-82.83	-52.94	-3.05	-2.29	2.29	50.66	100.59	150.59	200.81
Distances[m]:	0	2.3	3.22	4.595	6.89	6.925	7.135	9.455	11.75	14.05	16.36

Pod 1 (Pa)	**Pod 2 (Pa)**	**Pod 3 (Pa)**	**Pod 4 (Pa)**	**Pod 5 (Pa)**	**Pod 6 (Pa)**	**Pod 7 (Pa)**	**Pod 8 (Pa)**	**Pod 9 (Pa)**	**Pod 10 (Pa)**	**Pod 11 (Pa)**	**Average Q [l/s]**
105381	97089	93946	89322	81386	81846	43459	52858	44778	36650	29185	6.11
105381	97089	93545	88847	81509	81193	43544	52684	45293	37097	29026	6.10
95911	88154	85818	81326	74536	74522	40823	48796	41934	34274	27148	5.80
95792	88227	85678	81352	74655	74573	40998	48806	41732	34176	27533	5.81
90498	83629	80977	77011	70927	70616	38575	46658	40267	33008	25813	5.61
90552	83715	80986	76810	70716	70627	38508	46506	39948	33040	25696	5.60
85641	79143	76816	73036	67244	67064	37404	44760	38025	31735	25189	5.43
85823	79168	76930	73094	67061	67285	37342	44836	37979	31899	25267	5.42
80538	74352	72073	68553	62847	63032	35744	42415	36424	30059	24153	5.22
80477	74438	72251	68784	62930	63098	35644	42278	36108	30093	24098	5.22
73159	67647	65916	62512	57680	58048	33644	39203	33780	28435	23151	4.91
73018	67613	65998	62662	57701	57755	33535	39390	33985	28518	23049	4.93
67599	62393	60876	57913	53382	53349	31984	36839	31774	27064	22343	4.67
67817	62642	60895	57894	53409	53373	31784	36880	32060	27214	22170	4.67
63683	58762	57350	54807	50390	50535	30565	35104	30672	26077	21851	4.47
63500	58919	57159	54728	50436	50272	30775	35122	30418	26009	21551	4.47
57736	53665	52269	49746	45972	46027	29067	33053	28892	24822	20908	4.20

57960	53698	52279	50007	46072	45959	29032	32977	28691	24585	20843	4.18
54017	50199	48998	46738	43279	43388	28043	31373	27640	23743	20255	3.98
53918	50185	49019	46754	43211	43180	27914	31268	27389	23640	20087	3.98
50872	47365	46232	44155	40841	41010	27160	30199	26622	23033	19730	3.76
50667	47369	46037	43929	40779	41007	27088	29840	26707	23099	19853	3.76
43913	41298	40330	39307	36925	36952	28652	29959	27647	25198	23264	2.98
43773	41181	40330	39187	36871	36852	28582	29918	27647	25268	23167	2.97
40276	38215	37529	36357	34225	34315	27530	28507	26399	24581	22549	2.70
40276	38199	37561	36357	34402	34379	27679	28476	26399	24621	22423	2.70
39247	37149	36453	35230	33300	33273	27499	28005	26060	24025	22311	2.50
39247	37149	36453	35230	33300	33273	27499	28005	26060	24025	22311	2.50
38575	36840	36059	34793	33124	33164	28183	28475	26545	24538	22896	2.32
38575	36840	36059	34793	33124	33164	28183	28475	26545	24538	22896	2.32
38270	36427	35627	34577	32708	32386	27997	27893	26287	24389	22779	2.15
38270	36427	35627	34577	32708	32386	27997	27893	26287	24389	22779	2.15
37244	35232	34617	33799	31929	31912	28955	28460	26869	24714	23269	1.80
37244	35232	34617	33799	31929	31912	28955	28460	26869	24714	23269	1.80
35868	33978	33434	32516	30957	30800	28503	27821	26355	24535	23045	1.56
35868	33978	33434	32516	30957	30800	28503	27821	26355	24535	23045	1.56

Kaolin 20% test results for β = 0.7

Date:	2/9/2010	Test done by Faahad & Butteur
Orifice Type:	Long	
Orifice thickness:	0.161	**Area[m^2]**
Orifice dimension[m]:	0.0322	0.000814332
Pipe Diameter [m]:	0.046	0.001661903
Diameter ratio	0.7	
Aspect ratio	5	
Gravitational constant	9.81	
Material Type:	Kaolin	
Density[kg/m^3]:	1324	
Concentration:	20%	
K:	15	
n:	0.15	
PPT used:	110	
Range selected:	0-500	

1/n	**n/(n+1)**	**(n+1)/n**	**$K^{1/n}$**
6.66	0.13	7.66	69280082

Axial distances	-7.03	-4.73	-3.81	-2.43	-0.14	-0.10	0.10	2.33	4.62	6.92	9.23
ND distances incl.[L/D]:	-152.83	-102.83	-82.83	-52.94	-3.05	-2.29	2.29	50.66	100.59	150.59	200.81
Distances[m]:	0	2.3	3.22	4.595	6.89	6.925	7.135	9.455	11.75	14.05	16.36

Pod 1 (Pa)	Pod 2 (Pa)	Pod 3 (Pa)	Pod 4 (Pa)	Pod 5 (Pa)	Pod 6 (Pa)	Pod 7 (Pa)	Pod 8 (Pa)	Pod 9 (Pa)	Pod 10 (Pa)	Pod 11 (Pa)	Average Q [l/s]
108029	99700	97649	93089	85857	86306	66020	67758	59936	52736	45240	4.50
107496	99811	97514	93173	85792	85795	65582	67235	59861	52542	44855	4.50
118925	111373	108298	103807	96440	96054	67005	71879	63913	56221	48362	5.46
119311	111249	108700	103957	96626	96250	66867	72127	63795	56023	48472	5.46
115938	107750	105466	101218	93336	93229	66111	70431	62705	54997	47206	5.23
115787	107750	105416	101059	93093	93213	66107	70353	62705	55075	47169	5.24
112549	104866	102137	97970	90495	90523	65193	68831	60835	53579	46341	5.02
112076	104759	102250	97842	90309	90170	65342	68784	61046	53851	46120	5.02
109624	102091	99822	95310	88502	88119	64980	67762	60308	52927	45733	4.82
109789	102202	99863	95390	88015	88095	64750	67792	60308	53475	45395	4.82
107170	100004	97474	93329	85960	86166	64508	66977	59181	52205	44908	4.63
107513	100095	97461	92901	86316	85940	64382	66946	59181	52315	44731	4.63
101514	94142	91907	87586	80473	80660	63073	64102	56998	49763	42814	4.15
101341	94446	91694	87832	80998	80662	63076	64018	56767	49795	42824	4.15
99297	91895	89715	85542	79083	78724	62684	63184	55708	49025	42407	3.94
99152	91703	89634	85227	79643	78596	62601	62987	55846	49040	42260	3.95
97190	89918	87650	83333	77117	76795	62267	62167	54998	48443	41674	3.73
96792	89918	87777	83689	76727	76891	62352	62243	54998	48611	41738	3.72
94754	87712	85415	81656	75186	74787	62110	61509	54689	47834	41267	3.45
94754	87712	85415	81656	75186	74787	62110	61509	54689	47834	41267	3.45
92944	86803	84398	80276	73497	73404	62091	61058	54306	47687	41256	3.24
93260	86803	84398	80276	73848	73801	62439	61198	54168	47857	41124	3.24
91276	84797	82670	78759	72298	72270	62053	60440	53491	47158	40600	3.04
91276	84797	82670	78759	72298	72270	62053	60440	53491	47158	40600	3.04
88974	82195	80287	76183	70178	70126	61797	59548	52752	46667	40642	2.73
89247	82982	80668	76748	70626	70309	62419	60076	53294	47102	40724	2.72
89304	82640	80864	76847	70983	70771	63426	60692	54196	47800	41425	2.56
89642	83480	81255	77203	71378	70825	63690	60810	54466	48049	41570	2.56
87960	81400	79402	75661	69610	69497	63056	59977	53479	47170	40887	2.36
87739	81264	79394	75730	69480	69409	62946	59980	53384	47259	41181	2.35
88223	81055	79007	75280	69534	69155	63619	60384	54087	47926	41824	2.16
88223	81055	79007	75280	69534	69155	63619	60384	54087	47926	41824	2.16
86502	80330	78389	74823	68961	68976	65209	61345	55467	49348	43415	1.81
86502	80330	78389	74823	68961	68976	65209	61345	55467	49348	43415	1.81
83996	78633	76713	73561	68050	67687	65467	61125	55187	49662	44151	1.27
83682	78435	76975	74014	68452	68415	67260	62400	57134	51732	46786	0.86
84651	79173	77598	74991	69190	68739	68119	62751	56945	51764	46388	0.85
81481	75743	73911	69964	65261	64886	64382	59255	54618	49935	44888	0.49
81481	75743	73911	69964	65261	64886	64382	59255	54618	49935	44888	0.49